DEVELOPMENT AND EVALUATION OF INSTRUMENTED SOCCER EQUIPMENT TO COLLECT ANKLE JOINT KINEMATICS IN THE FIELD

by

Jonathan Stephen Akins

Bachelor of Science in Mechanical Engineering, Oklahoma State University, 2003

Master of Science in Bioengineering, University of Pittsburgh, 2008

Submitted to the Graduate Faculty of

Swanson School of Engineering in partial fulfillment

of the requirements for the degree of

Doctor of Philosophy

University of Pittsburgh

2013

UNIVERSITY OF PITTSBURGH

SWANSON SCHOOL OF ENGINEERING

This dissertation was presented

by

Jonathan Stephen Akins

It was defended on

July 25, 2013

and approved by

Mark Redfern, PhD, Vice Provost for Research, University of Pittsburgh

Scott Lephart, PhD, Professor, Department of Sports Medicine and Nutrition

Patrick Loughlin, PhD, Professor, Department of Bioengineering

April Chambers, PhD, Research Assistance Professor, Department of Bioengineering

David Brienza, PhD, Professor, Department of Rehabilitation Science and Technology

Mita Lovalekar, PhD, Assistant Professor, Department of Sports Medicine and Nutrition

Dissertation Director: Timothy Sell, PhD, Associate Professor, Department of Sports Medicine and Nutrition

DEVELOPMENT AND EVALUATION OF INSTRUMENTED SOCCER EQUIPMENT TO COLLECT ANKLE JOINT KINEMATICS IN THE FIELD

Jonathan Stephen Akins, Ph.D.

University of Pittsburgh, 2013

Ankle sprains commonly occur during athletic competition and result in traumatic injury to the lateral ligament complex. Ankle ligament sprains are the most common injury type for intercollegiate soccer players and athletes that sustain lateral ankle sprains may lose game and/or practice time, have recurrent sprains due to ankle instability, incur proprioceptive deficits, and be at an increased risk of ankle osteoarthritis. The high rate of ankle injuries among soccer athletes demonstrates a need for novel and advanced data collection methodologies to reduce the incidence of lateral ankle sprains and improve injury prevention interventions.

The purposes of this study were to develop instrumented soccer equipment to collect ankle joint kinematics in the field; establish the reliability and validity of a kinematic assessment using instrumented equipment during athletic maneuvers; and identify laboratory maneuvers that elicited game-like demands from athletes. Wireless orientation sensors were integrated into soccer shin guards and turf shoes. The instrumented equipment collected ankle joint kinematics during simulated athletic maneuvers in the laboratory and field. The simulated athletic maneuvers in the laboratory are commonly performed by soccer players and have been previously studied. Maneuvers included drop landing, drop jump, stop jump, and jump-stop cut. Drop landing and drop jump maneuvers resulted in poor to excellent reliability and very good to excellent validity. The stop jump maneuver resulted in poor to fair reliability and excellent

validity. The jump-stop cut maneuver resulted in poor to excellent reliability and very good validity. The soccer-specific field maneuvers were jump header, moving jump header, and slalom. All maneuvers resulted in poor to good reliability.

To identify laboratory maneuvers that elicited game-like demands, laboratory maneuvers of varied demand were compared to field maneuvers. Drop landing and drop jump maneuvers from a 60 cm platform elicited a similar response to the jump header maneuver. A jump distance recommendation for the stop jump maneuver was not warranted because jump distance did not significantly alter landing biomechanics. The instrumented equipment collected reliable and valid ankle joint kinematics in the sagittal plane and are a promising technology for in-game data collection and injury prevention.

TABLE OF CONTENTS

LIST OF TABLES

LIST OF FIGURES

PREFACE

Thank you Nancy for your perpetual support throughout my graduate career. I also thank my committee, Dr. Timothy Sell, Dr. Mark Redfern, Dr. Scott Lephart, Dr. Patrick Loughlin, Dr. April Chambers, Dr. David Brienza, and Dr. Mita Lovalekar. This work was supported by the Freddie H. Fu, MD Graduate Research Award.

1.0 INTRODUCTION

Injuries are an unfortunate aspect of athletics and many sports have adopted protective equipment to reduce injury rates. Football helmets are used to prevent head injuries and have evolved from padded leather to instrumented equipment. Modern instrumented helmets are capable of recording real-time impacts during athletic competition that are valuable injury prevention tools. Data collected from these helmets quantify player collisions and are used to establish design criteria to prevent concussions. Musculoskeletal injuries are prevalent in most sports, yet football helmets remain as the only protective equipment integrated with sensors. Instrumenting sporting equipment with inertial sensors will allow kinematic measurements to be collected outside the laboratory and during athletic competition. The kinematic data could provide health professionals, researchers, and coaches useful information to prevent musculoskeletal injuries.

The current human motion analysis research paradigm is to collect data in a laboratory to obtain reliable and valid biomechanical measurements. Recently, low-powered microelectromechanical inertial and magnetic sensors have been used to collect kinematic data outside of the laboratory and are referred to as inertial based motion analysis systems. These sensors are affordable, compact, and not limited to small capture volumes. Data collection outside of the laboratory allows participants to be evaluated on their actual playing surfaces and

in sport specific environments. Additionally, the chaotic environments that athletes encounter during competition (teammates, opponents, crowds, etc.) can be included during data collection.

1.1 BACKGROUND

Acute lateral ankle sprains are common during athletic competition[1, 2] and result in traumatic injury to the lateral ligament complex in 85-95% of all ankle sprains.[3-5] Athletes that sustain lateral ankle sprains may lose play and/or practice time, have recurrent sprains due to ankle instability,[6, 7] incur proprioceptive deficits,[8-10] and be at an increased risk of ankle osteoarthritis.[11, 12] In intercollegiate soccer, ankle ligament sprains were the most common injury type for males (17.0%, 3.19 injuries per 1000 athlete-exposures (AE))[1] and females (18.3%, 3.01 injuries per 1000 AE).[2] For all injuries, men's soccer injury rates rank third (18.8 injuries per 1000 AE) and women's soccer ranks fourth (16.4 injuries per 1000 AE) behind men's football (35.9 injuries per 1000 AE) and men's wrestling (26.4 injuries per 1000 AE).[13] The high rate of ankle injuries among soccer athletes demonstrates a need for novel and advanced data collection methodologies to reduce the incidence of lateral ankle sprains and improve injury prevention interventions.

Multi-directional movement patterns are necessary to successfully perform dynamic soccer maneuvers. Several studies have compared movement patterns of pathological individuals to healthy controls to identify altered movement patterns.[14-20] Quantifying altered movement patterns may lead to improved injury prevention, therapeutic, and prophylactic interventions.[20] For example, individuals with ankle instability resulted in greater dorsiflexion,[16] greater inversion,[14, 17-20] and increased frontal plane movement variability[15] during dynamic tasks that

included gait, running, and landing. Interestingly, Demeritt et al.[21] found that functional performance, measured with shuttle run and agility hop tests, was not negatively impacted in individuals with chronic ankle instability. Without limitations in functional performance, athletes may not properly address ankle instability and be at an increased risk of severe injuries and long term disability.[11, 12] A limitation of these studies is the collection of data in the laboratory instead of the field. Laboratories provide a controlled environment, but are limited in the ability to create sport specific environments.

Literature comparing data collected in a laboratory to data collected in the field is scarce. For cycling, seven male cyclists performed one-minute tests at their maximal aerobic power in the laboratory and outdoors on level and uphill terrains[22]. Crank torque profiles were significantly different and higher rates of perceived exertion were reported in the laboratory as compared to outdoor conditions. For running, metabolic costs of nine male runners were compared between treadmill running and outdoor running[23]. A 1% treadmill grade at velocities between 2.9 and 5.0 m/s resulted in similar metabolic costs as compared to level outdoor running. This study identified a laboratory test that simulates actual athletic demand. Many researchers have studied ankle joint kinematics during dynamic tasks,[14, 18-20, 24, 25] including three during injury,[26-28] but no studies were identified comparing human joint kinematics between laboratory and field environments. The primary reason for limited studies comparing laboratory and outdoor data is the portability of instrumentation. Therefore, the purposes of this study are to develop instrumented soccer equipment to collect ankle joint kinematics in the field, establish reliability and validity of a kinematic assessment using instrumented equipment during athletic maneuvers, and to identify typical laboratory maneuvers that elicit game-like demands from athletes.

1.2 INNOVATION

Research laboratories provide a controlled environment to obtain reliable and valid biomechanical measurements, but are limited in the ability to create population/sport specific environments. For example, many sports are played outdoors on grass or artificial surfaces. These surfaces are difficult to simulate in a laboratory and limited capture volumes restrict the tasks that can be analyzed. Additionally, participants in a laboratory may consciously or subconsciously alter, for example, their landing biomechanics due to researchers 'eyeballing' their technique. Development of reliable and valid motion capture technology capable of collecting biomechanical data outside of the laboratory allows researchers to collect data in population specific environments. Furthermore, integrating motion capture technology into sporting equipment will eliminate the obtrusive nature of typical motion capture technology because sensors and/or markers attached to athletes may alter their natural mechanics.

The National Collegiate Athletic Association mandated the use of shin pads in 1991 and while there was no reduction in lower leg injuries,[1] the mandate provides equipment in which to integrate sensors. Previous studies have measured reliable[29, 30] and valid[31-36] ankle joint kinematics using inertial measurement systems; however, these technologies required participants to be tethered to a computer or to wear a data logging system. Data logging systems can be attached to the waist or worn in a backpack and wires run to the sensor modules. This setup is acceptable for gait applications, but does not provide the necessary portability for dynamic athletic maneuvers. The system used in this study had wireless and data logging capabilities for each sensor module, eliminating cumbersome wires and data logging systems.

Future directions of instrumented sports equipment may allow simultaneous data collection from one to several players during athletic competition. Coupling this technology with

smartphones and/or tablets could provide coaches real-time athlete data and provide spectators with additional information about their favorite athlete. For example, coaches and spectators could visualize a player's running speed and ball striking velocity. Instrumented sports equipment would also provide clinicians and researchers with biomechanical data collected during actual competition and possibly an injury event. This would be a revolutionary tool to study injury biomechanics. Previous studies have utilized biomechanical approaches to obtain quantitative data from ankle injuries,[26-28] but require extensive post-processing and would not be feasible on multiple players. A field based system has several applications and will provide new insight into the mechanisms of injury, assist in the development of improved sport equipment, and aid injury prevention techniques.

1.3 STATEMENT OF PURPOSE

The purposes of this study were to develop instrumented soccer equipment to collect ankle joint kinematics in the field; establish the reliability and validity of a kinematic assessment using instrumented equipment during athletic maneuvers; and identify laboratory maneuvers that are capable of eliciting game-like demands from athletes.

1.4 SPECIFIC AIM AND HYPOTHESES

Specific Aim 1: To develop instrumented soccer shin pads and cleats to measure and record ankle joint kinematics using wireless inertial and magnetic sensors

Specific Aim 2: To establish the reliability and validity of a kinematic assessment using instrumented equipment during athletic maneuvers (drop landing, drop jump, stop jump, and side-step cutting)

Hypothesis 2.1: Ankle joint kinematics collect by the instrumented equipment will have good test-retest reliability (ICC > 0.80) and standard error of measurement between $\leq 5°$ for plantar flexion/dorsiflexion and $\leq 3°$ for inversion/eversion

Hypothesis 2.2: Ankle joint kinematics collected by the instrumented equipment will have excellent concurrent criterion validity with excellent correlation coefficients ($r \geq 0.95$) and root mean squared errors $\leq 5°$ for plantar flexion/dorsiflexion and $\leq 3°$ for inversion/eversion as compared to a video-based motion analysis system

Specific Aim 3: To identify laboratory maneuvers that elicit game-like demands by comparing ankle joint kinematics collected in the field to ankle joint kinematics collected in the laboratory during athletic maneuvers of varied demand

Hypothesis 3: Ankle joint kinematics will be similar between the landing phase of the jump header and drop landing maneuver at a platform height of 20 cm, between the landing phase of the moving header and stop jump at 40% of the participant's height, and between the cutting phase of the slalom course and jump-stop cutting maneuver at 40% of the participant's height

This is the first study to integrate soccer equipment with sensors to measure ankle joint kinematics in the field. Furthermore, this is the first study to compare field and laboratory data to identify laboratory maneuvers that elicit game-like demands. Identification of these laboratory maneuvers provide justification for selecting platform heights and jump distances for landing biomechanics during athletic maneuvers.

1.5 ORGANIZATION OF DISSERTATION

The following chapters are arranged by Specific Aims: Chapter 2 details the development of instrumented equipment; Chapter 3 the reliability and validity; and Chapter 4 the identification of laboratory maneuvers that elicit game-like demands. Limitations of this work are provided in Chapter 5 and Chapter 6 provides concluding remarks and future work.

2.0 DEVELOPMENT OF INSTRUMENTED SOCCER EQUIPMENT

Three-dimensional (3D) ankle joint kinematics are traditionally measured using high speed video-based motion analysis systems in a laboratory. These systems use multiple cameras to track retro-reflective markers placed on anatomical landmarks. Marker trajectories are used with anthropometric measurements to calculate kinematic data. These system are considered the gold standard for collecting human kinematics.[37] However, video-based motion analysis systems are costly, require trained personnel, have a limited capture volume, and are limited in outdoor data collection. Recently, a new motion analysis technology has been developed that uses low-powered microelectromechanical systems to measure 3D human kinematics using 3D accelerometers and 3D gyroscopes.[37, 38] The addition of 3D magnetometers reduce sensor drift by continuous correction of the orientation obtained by integrating rate sensor data.[39] The sensor module is referred to as an inertial measurement unit (IMU) or magnetic field angular rate and gravity sensor (MARG). For the purposes of this study, the term MARG will be used. Three-dimensional orientation of MARGs attached to each segment of interest is used with predefined anatomical coordinate systems[40] to calculate joint kinematics.

Development of the instrumented equipment required appropriate sensor selection, utility, characterization, integration into soccer equipment, and metal mapping. Sensor selection details the design specifications for this project and commercially available sensors. Sensor utility was a pilot study to determine if the sensors were capable of measuring tibial orientation

during an athletic maneuver. Sensor characterization established the frequency response of the selected sensor. The design, fabrication, and sensor integration of the soccer equipment is explained. Metal mapping of the laboratory and indoor training facility was performed to determine the appropriate location to collect data.

2.1 SENSOR SELECTION

Devices are commercially available and design specifications were established to determine the most appropriate sensor for this project. Design specifications were: sensors, sensor algorithms, sampling frequency, size/weight, calibration, device communication, data logging, power management, synchronization capabilities, and software (Table 1).

Sensor requirements included accelerometer, gyroscope, magnetometer, and thermometer. The accelerometer, gyroscope, and magnetometer had to be triaxial and have the ability to measure data expected during athletic maneuvers. Accelerations during a drop landing ranged 2.2 to 42.2 g[41-43] and peak angular velocities during an ankle injury ranged 638 to 1752 °/s.[26, 28] A range of expected magnetic field data was not identified. A thermometer was also required to allow temperature compensation for the gyroscope. Sensor algorithms were available for post-processing, but on-board algorithms were preferred to provide real-time angle measurements to assist with data collection and to make data processing more feasible.

The sensors' size and weight had to be as small as possible so each could be integrated into the soccer equipment. Sensors that were able to be removed from their housing were preferred to allow for a housing redesign to meet the needs of this project. Factory calibration of the sensors was necessary because specific equipment is required to perform calibrations.

Wireless device communication was necessary to allow for data collection during athletic maneuvers. A wired connection prior to collection trials would be acceptable, but a completely wireless system was preferred. The device must be capable of on-board logging data or wireless streaming of data. On-board data logging was preferred because of sampling frequency limitations inherent with streaming data and potential loss of data. The device must have the option of powering with a battery and preferably a lithium polymer battery cell. A lithium polymer battery cell is rechargeable, small in size, and able to power similar devices for several hours.

Two devices were used for this study, one on the tibia and one on the foot, and the data from the devices had to be synchronized together and with the video-based motion analysis system. Therefore, the device must allow for synchronization via hardware or software. The last design specification is software. Software is highly preferred, but not necessary. Purchasing devices with software will make device communication, data collection, and data reduction much easier.

Table 1. Design specification of commercially available sensors

Specifications	x-IMU, x-io Technologies Limited	H3-IMU, MEMSense LLC	Micro IMU, MEMSense LLC	MTw, Xsens Technologies B.V	Ultimate IMU, SparkFun Electronics, Inc.
Sensors	Digital	Digital	Digital	Digital	Digital
Accelerometer	3D ± 8g	3D ± 10g	3D ± 10g	3D ± 16g	3D ± 16g
Gyroscope	3D ± 2000 $°s^{-1}$	3D ± 1200 $°s^{-1}$	3D ± 1200 $°s^{-1}$	3D ± 1200 $°s^{-1}$	3D ± 2000 $°s^{-1}$
Magnetometer	3D ± 8.1 G	3D ± 1.9 G	3D ± 1.9 G	3D ± 1.5 G	3D ± 4.0 G
Thermometer	Yes	Yes	Yes	No	No
Sensor Algorithm	IMU and AHRS on-board	Proprietary	Proprietary	Proprietary	None
Sampling Frequency	1-512 Hz	50-1000 Hz	50 Hz	20-120 Hz	Not specified
Size (mm)	33 x 42 x 10	51 x 28 x 16	ϕ58 x 24	35 x 58 x 15	36 x 36 x ??
Weight (g)	12	55	95	27	Not specified
Calibration	Factory calibrated	Factory calibrated	Factory calibrated	Factory calibrated	None
Device Communication	USB, Bluetooth, Auxiliary port	USB, RS422	Hirose HR-30	Wireless via software	LPC2148 processor
Data Logging	SD card, Wireless (Bluetooth), USB	USB	USB	Wireless (2.4 GHz) up to 20m	SD
Power Management	USB, LiPo battery, external	USB RS422	USB	Charging station	LiPo Battery
Synchronization Capabilities	Auxiliary port: 8 Channel analog i/o, digital i/o, or PWM i/o	Input: 2 analog, 3 digital Output: 2 digital	None	Via software	None
Software	x-IMU GUI	None	None	MT Manager	None

Design specifications were met by the x-IMU sensor from x-io Technologies and the MTw sensor from Xsens Technologies (Table 1). Sensor specifications were similar. The x-IMU had a lower linear acceleration range, but included a thermometer for gyroscope drift. The primary differences were sampling frequency, data logging, and size. The sampling frequency of the MTw devices is dependent upon the number of sensors used during data collection. The MTw collects data wirelessly and is limited to 20 m in an office environment which restricts the athletic maneuvers that can be performed. The x-IMU device can stream wirelessly up to 100 m, but also can log data on-board using a secure digital (SD) card. The size is similar between the two devices with the x-IMU being slightly shorter and thinner which is beneficial for integrating into the soccer equipment.

The x-IMU device was selected based on the device's ability to operate independent of a computer and the smaller size. In the case that wireless transmission is the limiting factor for the data collection, the x-IMU can record data on-board up to 512 Hz. The x-IMU was 16 mm shorter and 5 mm thinner, allowing the device to be more easily integrated into the soccer equipment easier as compared to the larger MTw devices.

2.2 SENSOR UTILITY

A pilot study was performed to determine the utility of MARGs to measure tibial kinematics during a drop landing maneuver.

2.2.1 Methods

One participant performed a drop landing maneuver from a height of 50 cm. This maneuver was selected because it applies large accelerations (2.2 – 42.2g)[41-43] on the sensor and would be used in this study (Chapters 3 and 4). The participant dropped from the platform with both feet and landed on the ground with both feet. Segmental kinematics of the right tibia were collected during three trials.

Segmental kinematics of the tibia were simultaneously collected using a 3D motion analysis system and a MARG. The motion analysis system collected marker data at 192 Hz and analog data at 592 Hz. The MARG data was collected at 64 Hz via Bluetooth on a separate computer. Data were synchronized by measuring an analog output signal from the MARG auxiliary port with the motion analysis system. The MARG analog output signal was a pulse-width modulation (PWM) signal that changed from 0% to 100% duty cycle immediately prior to logging data. The first data point of the PWM signal at 100% measured with the motion analysis system was aligned with the first recorded MARG data point.

A rigid plate of three markers (triad) was attached the MARG using a double-sided adhesive disc. The triad local coordinate system (LCS) was aligned with the MARG LCS. The MARG LCS was established by the manufacture and the triad LCS was defined using the triad markers (Figure 1). The x-axes (red) of the triad/MARG combination were aligned with the longitudinal axis of the tibia. It was secured using underwrap and athletic tape to limit excessive motion artifact.

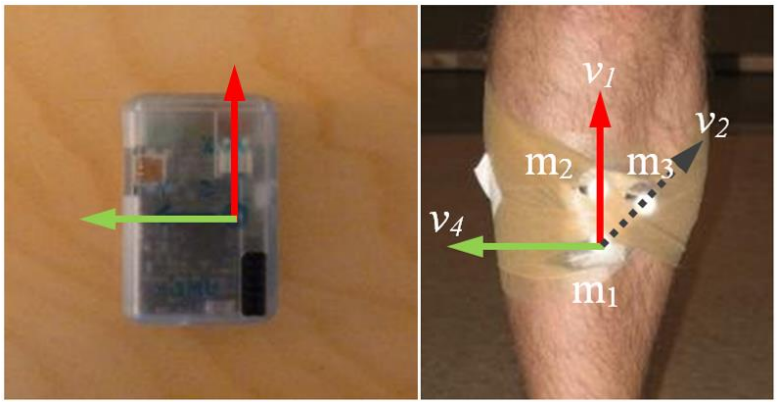

Figure 1. Local coordinate systems for the MARG and triad. The x-axis is vertical (red), the y-axis is to the left (green), and the z-axis is point out of the page (not pictured).

The triad LCS (Figure 1) was created using equations 1-5. The x-axis (red) was defined as the unit vector (v_1) from the inferior marker (m_1) to the superior marker (m_2). The z-axis (not pictured) was defined as the cross product of the unit vector (v_2, grey) from the inferior marker (m_1) to the medial marker (m_3) and the x-axis (v_1), pointing anterior or out of the page. The y-axis (v_4, green) was defined as the cross product of the z-axis and x-axis pointing to the right of the participant.

$$v_1 = \frac{m_1 - m_2}{|m_1 - m_2|} = x - axis \quad (1)$$

$$v_2 = \frac{m_1 - m_3}{|m_1 - m_3|} \quad (2)$$

$$v_3 = v_2 \times v_1 = z - axis \quad (3)$$

$$v_4 = v_3 \times v_1 = y - axis \quad (4)$$

Euler angle decomposition[44] was used to obtain tibial kinematics from the MARG and triad rotation matrices. Rotation matrices for the MARG were automatically calculated from the

sensor's software (x-IMU GUI, x-io Technologies Limited, United Kingdom) and rotation matrices for the triad (R_{triad}) were calculated using the previously defined unit vectors.

$$R_{triad} = [v_1' v_4' v_3'] \tag{5}$$

Using a ZX'Y'' rotation sequence

$$R = YXZ \tag{6}$$

$$R = \begin{bmatrix} \cos\gamma & 0 & \sin\gamma \\ 0 & 1 & 0 \\ -\sin\gamma & 0 & \cos\gamma \end{bmatrix} \cdot \begin{bmatrix} 1 & 0 & 0 \\ 0 & \cos\beta & -\sin\beta \\ 0 & \sin\beta & \cos\beta \end{bmatrix} \cdot \begin{bmatrix} \cos\alpha & -\sin\alpha & 0 \\ \sin\alpha & \cos\alpha & 0 \\ 0 & 0 & 1 \end{bmatrix} \tag{7}$$

$$R = \begin{bmatrix} \dots & \dots & \cos\beta\sin\gamma \\ \cos\beta\sin\alpha & \cos\alpha\cos\beta & -\sin\beta \\ \dots & \dots & \cos\beta\cos\gamma \end{bmatrix} \tag{8}$$

Solving for α, angle about the z-axis

$$\frac{R_{2,1}}{R_{2,2}} = \frac{\cos\beta\sin\alpha}{\cos\alpha\cos\beta} = \frac{\sin\alpha}{\cos\alpha} = \tan\alpha \therefore \alpha = \tan^{-1}\left(\frac{R_{2,1}}{R_{2,2}}\right) \tag{9}$$

Solving for β, angle about the x-axis

$$-R_{2,3} = \sin\beta \therefore \beta = \sin^{-1}\left(-R_{2,3}\right) \tag{10}$$

Solving for γ, angle about the y-axis

$$\frac{R_{1,2}}{R_{2,2}} = \frac{\cos\beta\sin\gamma}{\cos\beta\cos\gamma} = \frac{\sin\gamma}{\cos\gamma} = \tan\gamma \therefore \gamma = \tan^{-1}\left(\frac{R_{1,2}}{R_{2,2}}\right) \quad (11)$$

Tibial kinematic data from the triad and MARG were compared using correlation coefficients and root mean squared error (RMSE) for each axis of rotation. Correlation coefficients (*r*) were interpreted as moderate (0.65-0.74), good (0.75-0.84), very good (0.85-0.94), and excellent (0.95-1.00) based on previously published *r*-values.[33, 45-47] The RMSE was calculated using equation 12.

$$RMSE = \sqrt{\frac{1}{n}\sum_{i=1}^{n}\left[\theta(i)_{MARG} - \theta(i)_{V}\right]^2} \quad (12)$$

where *n* is the number of samples, $\theta(i)_{MARG}$ are the tibial segmental angles as measured by the MARG system and $\theta(i)_{V}$ are the tibial segmental angles as measured by the video-based motion analysis system.

2.2.2 Results and Discussion

Tibial kinematics calculated from triad and MARG data were very highly correlated and resulted in low error (Table 2). Correlations were excellent ($r \geq 0.957$) for all but the z-axis for drop landing 1 ($r = 0.863$), which was categorized as very good. The y-axis (approximately tibial flexion/extension) resulted in the lowest RMSE (0.003-0.063°), followed by the z-axis

(approximately tibial abduction/adduction) with 0.046-0.112°, and the x-axis (approximately internal/external tibial rotation) with 0.100-0.256°. Tibial kinematic data is plotted in Figure 2 and qualitatively show that the data is similar between the two systems.

Table 2. Correlation coefficient and root mean squared error of Vicon and MARG tibial kinematics (n = 1)

Trial	Axis	r	p-value	RMSE (°)
Drop Landing 1	Z	0.863	≤ 0.001	0.106
	X	0.967	≤ 0.001	0.100
	Y	0.969	≤ 0.001	0.003
Drop Landing 2	Z	0.963	≤ 0.001	0.112
	X	0.980	≤ 0.001	0.256
	Y	0.978	≤ 0.001	0.063
Drop Landing 3	Z	0.957	≤ 0.001	0.046
	X	0.974	≤ 0.001	0.220
	Y	0.996	≤ 0.001	0.022

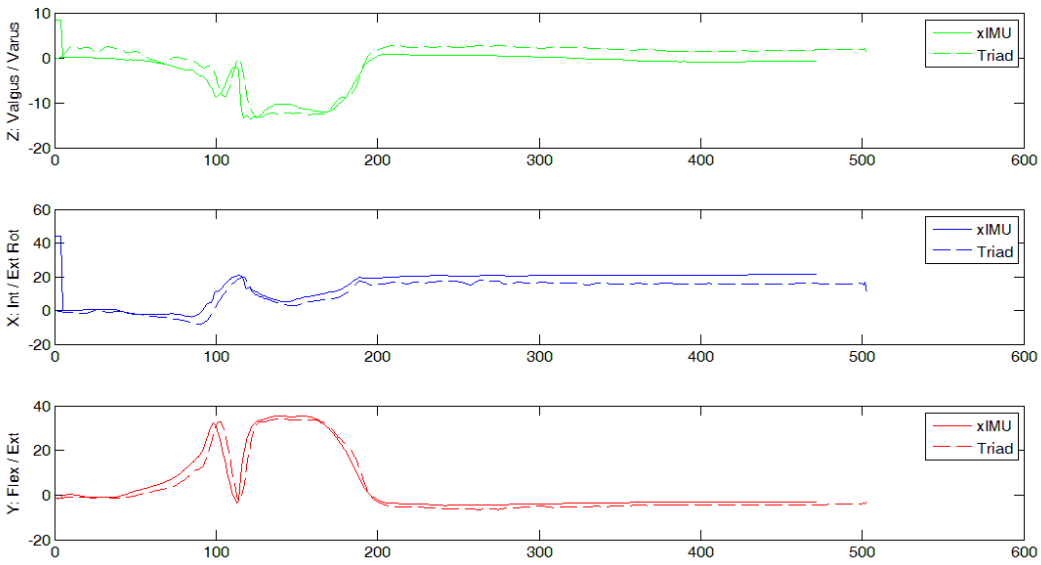

Figure 2. Tibial kinematics measured with triad and MARG (x-IMU) during the drop landing maneuver. This trial is representative of the other trials.

The purpose of the pilot study was to determine the utility MARGs to measure tibial kinematics. Tibial kinematic data were simultaneously collected with video-based motion

analysis and MARG systems during a drop landing maneuver. Tibial kinematics were highly correlated ($r \geq 0.86$) with little error (RMSE $\leq 0.26°$). These results provided evidence that the MARG was capable of measuring segmental kinematics during dynamic maneuvers with large impacts.

2.3 SENSOR CHARACTERIZATION

The purpose of characterizing sensors is to determine their behavior in response to a range of stimuli specific to the intended application. For this study, inertial sensors were used to measure segmental kinematics of human motion. The frequency response of a sensor can be used to fully characterize the sensor and is obtained by computing the transfer function. The transfer function of a linear, time-invariant system is defined as the ratio of the output signal to the input signal in Laplace or frequency domains, and can be calculated using experimental data. Therefore, the purpose of this study was to identify the frequency response of the MARG by estimating the transfer function using experimental data.

2.3.1 Methods

A test fixture was constructed to apply random signals to the MARG (Figure 3). A stepper motor was mounted to the fixture and a platform (15 x 15 cm) was attached to the motor. The stepper motor was a bi-polar NEMA 23 form factor motor with 1.8° step resolution and 90 N-cm torque. It was controlled with a microcontroller (Arduino, Italy) and Big Easy Driver (Schmalz Haus LLC, USA). Three retro-reflective markers (14 mm) were attached to the platform to measure

angular displacement of the stepper motor with the video-based motion analysis system at 256 Hz. Angular displacements of the motor were calculated by constructing a right-handed local coordinate system and using Euler angle decomposition. The MARG was attached to the platform with the test axis aligned with the stepper motor's axis of rotation. Data from the MARG were recorded to a SD memory card at 256 Hz. The MARG and video-based motion analysis data were synchronized using a synchronization pulse (1 Hz square wave) that was generated with the microcontroller. The pulse was measured with the MARG and triggered the remote start feature of the motion capture system. Data were manually synchronized after data collection.

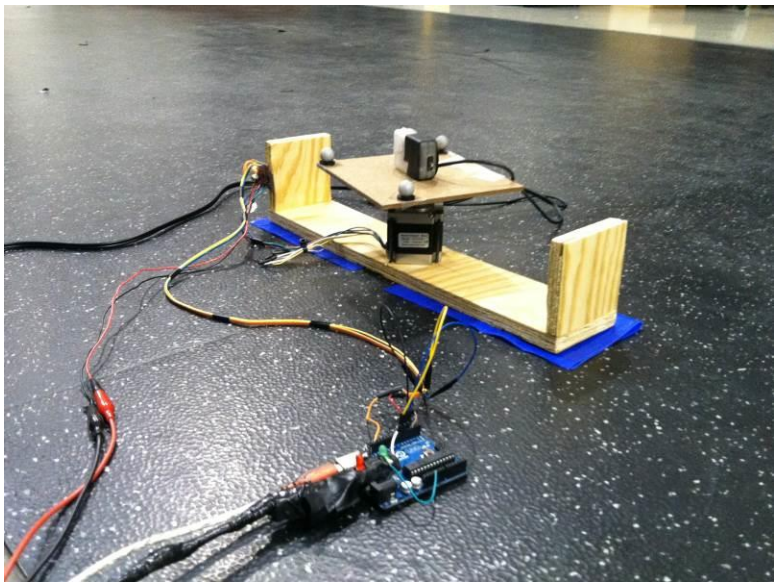

Figure 3. Sensor characterization test fixture. The MARG is shown with the y-axis aligned to the stepper motor's axis of rotation. The three retro-reflective markers on the platform were tracked using the video-based motion analysis system.

A pseudo-random signal was generated with the microcontroller and contained angles that ranged 10.8° to 59.4° and frequencies that ranged 0.5 Hz to 5 Hz. The range of angles were

selected based on ankle displacement angles during athletic maneuvers.[14] The range of frequencies were selected based on the maximum frequency that the motor was able to reliably reproduce a sinusoidal pattern. The random signal duration was 11.8 s and two cycles were recorded. The pseudo-random signal was collected for each axis of the MARG (x, y, and z) with the test platform at 0° and 30°.

Video-based motion analysis and MARG data were resampled to 64 Hz to remove high frequency content using an anti-aliasing finite impulse response filter. The signal measured with the video-based motion analysis system was defined as the input, $x(t)$, and the signal measured with the MARG was defined as the output, $y(t)$. The frequency response, $H(\omega)$, was calculated by taking the ratio of the cross-spectrum, $S_{yx}(\omega)$, to the input power-spectrum, $S_{xx}(\omega)$, as shown in equation 13.

$$H(\omega) = \frac{S_{yx}(\omega)}{S_{xx}(\omega)} \tag{13}$$

Magnitude (M) and phase (ϕ) responses were calculated, plotted, and used to assess the MARG performance. Magnitude responses were reviewed to identify the corner frequency, defined as the frequency where the magnitude began to roll-off at approximately -6 dB/octave. The phase response performances were assessed by calculating the time shift (delay or advance). Time shift, Δt, is illustrated in Figure 4 where input and output signals (equation 14) are plotted.

$$x(t) = \cos(\omega_0 t) \qquad y(t) = A\cos(\omega_0 t + \phi_0) \tag{14}$$

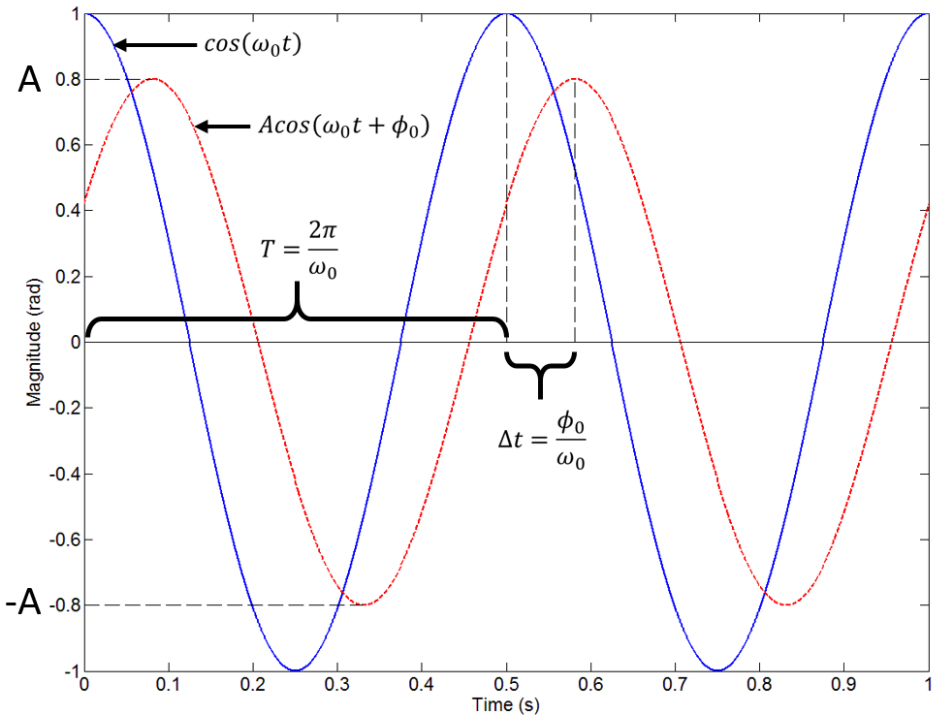

Figure 4. Time shift between two cosine curves

The time shift between equivalent phase points on the output, *y(t)*, relative to the input, *x(t)*, is related to the phase shift, ϕ, as

$$\frac{\Delta t}{T} = \frac{\phi}{2\pi} \tag{15}$$

where T is defined as the signal period

$$T = \frac{2\pi}{\omega_0} \tag{16}$$

where ω_0 is defined as the signal frequency. Combining equations 15 and 16, and solving for Δt gives the time shift

$$\Delta t = \frac{\phi}{2\pi}\frac{2\pi}{\omega_0} = \frac{\phi}{\omega_0} \quad (17)$$

The time shift was compared to time to peak angles during the landing phase of drop landing, drop jump, and stop jump maneuvers (Chapter 4) to determine if the phase shift could be tolerated.

2.3.2 Results and Discussion

Time and frequency domains of video-based motion analysis and MARG data were similar for all MARG axes (x, y, and z) and platform angles (0° and 30°). A representative time domain plot of the x-axis at a platform angle of 0° is shown in Figure 5a and the frequency domain is shown in Figure 5b. The frequency content of the pseudo-random signal (Figure 5b) illustrates the signal content was primarily below 1 Hz to 2 Hz. The frequency response of the MARG was also similar for all MARG axes and platform angles, and a representative plot of the x-axis at a platform angle of 0° is shown in Figure 6. The magnitude response (Figure 6a) illustrates that the video-based motion analysis system and MARG agreed up to approximately 10 Hz, where the roll-off occurred (Figure 6a). At frequencies greater than 10 Hz, the signal will be attenuated and not accurate. The phase response (Figure 6b) illustrates that the MARG has phase lead which indicates the MARGs signal will lead the video-based motion analysis signal. The phase response illustrates that the phase shift became greater at higher frequencies. The phase lead identified in this study may be a result of the sensor fusion algorithm and may also occur if the MARG is computing accelerations at higher frequencies not displayed in the frequency response

plots (Figure 6). The frequency response computation was confirmed and is detailed in Appendix A.

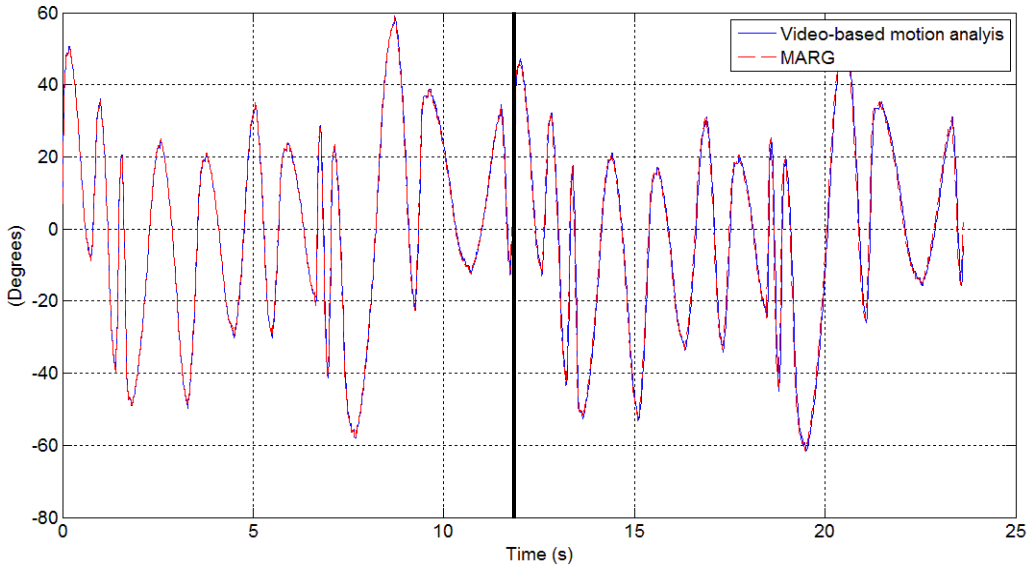

(a)

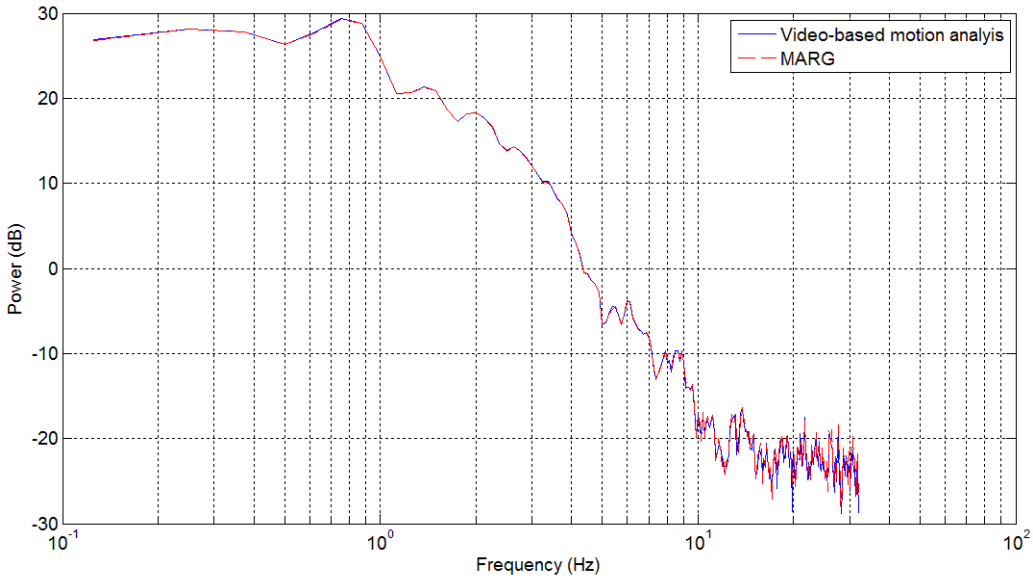

(b)

Figure 5. Pseudo-random signal in (a) time and (b) frequency domains. The vertical line in (a) illustrates the location where the signal repeats.

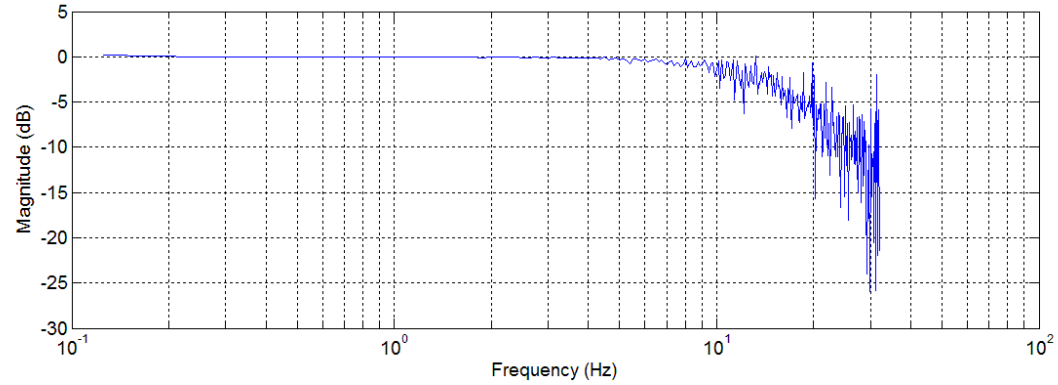

(a)

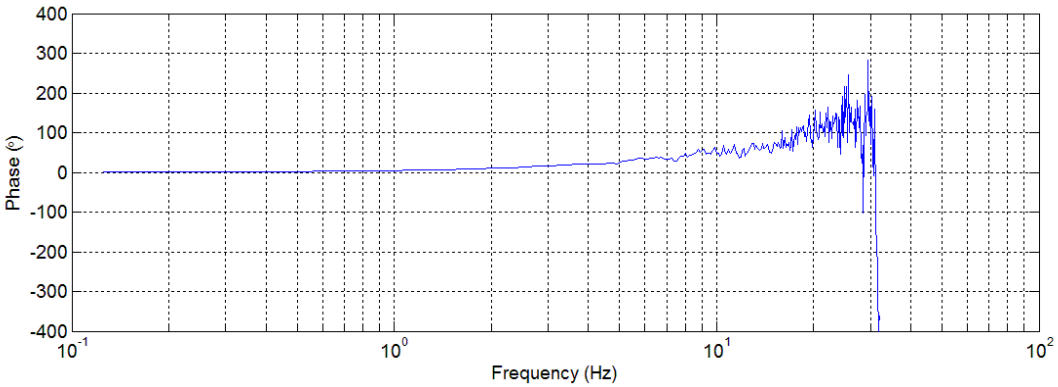

(b)

Figure 6. Frequency response, *H(ω)*, of the MARG. Video-based motion analysis data was defined as the input, *x(t)*, and MARG data was defined as the output, *y(t)*. (a) Magnitude response (b) phase response.

Time shift was calculated using phase angles and frequencies from the phase response (equation 17). The time shift resulted in a constant time advance of approximately 15 ms up to 8 Hz to 10 Hz, after which the time advance began to vary greatly (Figure 7a). The constant time advance is also illustrated by the positive linear relationship between frequency and phase angle in the Figure 7b. The phase response of the MARG was plotted with a linear x-axis instead of a logarithmic x-axis and the linear relationship can be seen up to approximately 10 Hz. (Figure 7b).

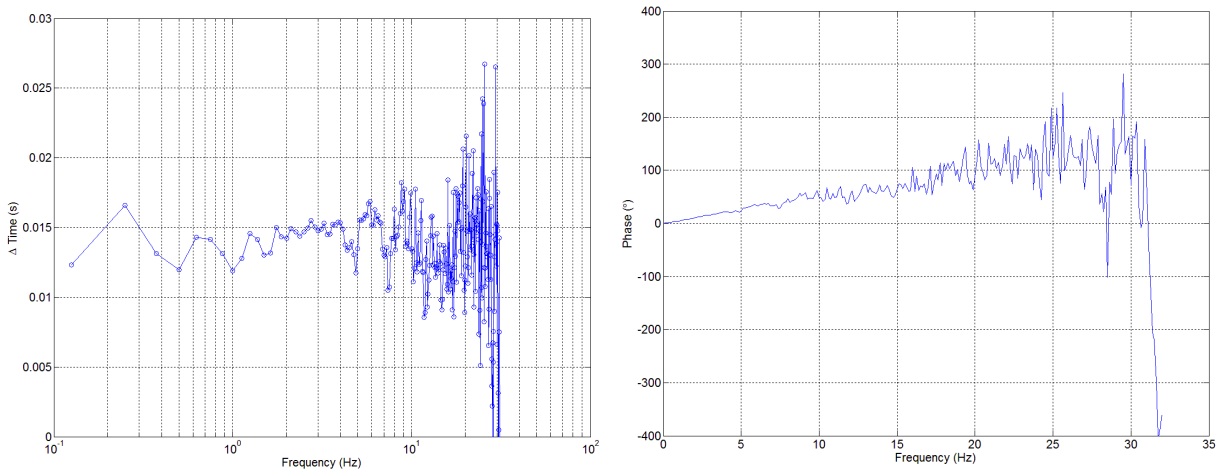

(a) **(b)**

Figure 7. Time advance of phase response. (a) Time advance due to phase response of the MARG. (b) Phase response of the MARG plotted with the linear x-axis.

Time to peak angle during the landing phase of the maneuvers is a variable of interest for this study and was used to determine if the time shift was tolerable. Average time to peak angle values for drop landing, drop jump, and stop jump maneuvers ranged from 140 ms to 230 ms and standard deviations ranged from 40 ms to 90 ms (Table 19, Chapter 4). With the time advance being less than 10% of the average time to peak angles and less than the standard deviations, a 15 ms time advance is not likely to affect the measurements. Therefore, the MARG is capable of collecting data comparable to the video-based motion analysis system without significant signal attenuation or phase shift up to 10 Hz.

2.4 INSTRUMENTED EQUIPMENT

The design goal for the instrumented equipment was to integrate sensors into soccer cleats and shin guards to wirelessly collect and record ankle joint kinematics. Additionally, the sensors must not interfere with the athlete's ability to perform the selected tasks.

2.4.1 Device

The x-IMU was selected for this study because it met the design specifications, performed well during the sensor utility pilot study, and sensor characterization analysis detailed above. Two x-IMU devices were purchased with a 1000 mAh battery and a plastic housing that enclosed the x-IMU and battery. The assembly was 57 x 38 x 21 mm and 49 g (Figure 8). The MARG contained a 3D accelerometer (± 8 g), 3D gyroscope (± 2000 °/s), 3D magnetometer (± 8.1 Gauss), and thermometer to account for temperature effects on the gyroscope.[48] Sensor data can be collected up to 512 Hz and recorded using an on-board SD memory card or streamed wirelessly using Bluetooth. Memory and battery capacities of the MARGs allowed data to be measured and recorded for up to 10 hours.

Figure 8. x-IMU with plastic housing and 1000 mAh lithium polymer battery.

Images from http://www.x-io.co.uk

Measuring joint kinematics requires a MARG to be attached to each segment that makes up the joint. For the ankle, MARGs must be attached to the tibia and foot. The anterior-medial aspect of the tibia provided a flat surface to secure the MARG to the tibia. However, the foot was more difficult. Previous studies measuring the foot have secured devices to the dorsal aspect of the foot and calcaneus.[29, 32, 34, 35, 49] These locations were not feasible for this study because the MARG would interfere with soccer performance. Soccer athletes use the dorsal aspect of the foot and heel to strike the ball. The plantar aspect of the foot was an attractive option because the MARG could be integrated into the insole, similar to insole pedometers. An insole pedometer, such as the NIKE+ device (NIKE, Inc., Beaverton, OR), is an electromechanical sensor that is inserted into specially design shoes. The sensor counts steps taken by the user and estimates distance, speed, and calories. Placing the MARG into the insole provides relative segmental motion of the foot since it was not attached directly to the foot surface. However, the tight fit of soccer shoes allowed the MARG to be in contact with the plantar surface of foot, providing foot segmental motion.

The foot is defined by three zones: forefoot; midfoot; and rearfoot. During athletic maneuvers, the athletes commonly landing on the forefoot and rearfoot.[50-52] To reduce the potential for sensor damage, the MARG should be placed at the midfoot. Therefore, the plantar aspect of the midfoot was selected to obtain segmental motion of the foot. This position did not interfere with soccer performance and reduced the potential for sensor damage.

2.4.2 Soccer Cleats and Shin Guards

There are three basic types of soccer shoes: cleats; turf; and indoor (Figure 9). Cleats have 8-12 large studs that protrude 10-16 mm from the outsole of the shoe. Studs allow the shoe to dig into soft natural grass and long synthetic surfaces to increase traction. Turf shoes have a uniform tread that protrudes 2-5 mm from the outsole. Turf shoes are used on firm natural grass and all types of synthetic surfaces. Indoor shoes are typically flat and the tread is created using a recessed design similar to tennis and basketball shoes. Indoor shoes are used on short synthetic and indoor surfaces. Turf shoes were selected for this study because their tread allowed sufficient traction on the sport court flooring in the laboratory and long synthetic field surface.

(a) **(b)** **(c)**

Figure 9. Type of soccer shoes. Adidas adiPower Predator TRX (a) cleats, (b) turf, and (c) indoor shoes. Images from www.adidas.com

Several turf shoe designs from different manufacturers are commercially available. To determine the best shoe for this study, midsole thickness was measured. The shoe with the thickest midsole allowed the most room for the MARG to be integrated. Midsole thickness of a men's size 10.5 was measured using small anthropometer (Model 01291, Lafayette Instrument Company, Lafayette, IN, USA). Midsole thickness ranged from 15-22 mm (Table 3) and the Adidas Predator shoes were the thickest. Therefore, the Adidas Predator TRX turf shoes were purchased in a range of sizes (9-12) to accommodate the majority of participants.

Table 3. Midsole thickness of soccer turf shoes

Manufacturer	Style	Midsole Thickness (mm)
Nike	Nike5 Bomba	16
Nike	CTR360 Libretto	15
Puma	King	17
adidas	adiNova IV TRX	17
adidas	Puntero VI TRX	19
adidas	Predator TRX	22
adidas	adi5 X-ite TRX	20

Plastic molded shin guards were selected for this study because they are popular among soccer players (Figure 10). Several designs from different manufacturers were examined and all consisted of a plastic shell backed with cushioning material to provide comfort. The Adidas 11Lesto shin guards were selected. These shin guards were composed of molded polypropylene and backed with ethylene-vinyl acetate (EVA) for cushioning. The large size was purchased because they are designed for a wide range of players (height: 5'4"-5'11"). Knee-high soccer socks and elastic straps were used to secure the shin guards to the tibia.

Figure 10. Adidas 11Lesto shin guards. Image from www.adidas.com

2.4.3 Design and Manufacturing

The turf shoes and shin guards were modified to integrate and secure the MARGs. Several modifications were made to the shoes. A portion of the midsole was milled out for a custom sensor housing, a portion of the rearfoot was milled out for a battery, a hole was cut through the lateral side of the upper for a rigid triad, and a hole was cut through the bottom of the outsole to allow for a synchronization cable to pass through. For the shin guards, a portion of the molded plastic and EVA cushioning was cut out for a custom sensor housing.

2.4.3.1 Turf Shoes and Custom Housing

A manual vertical milling machine was used to mill out a portion of the midsole to allow the sensor to be recessed (Figure 11). The midsole consisted of a rigid, fibrous layer, a rubber honeycomb layer, and the high density rubber outsole layer. The plastic housing that was purchased from the MARG manufacturer stacked the sensor and battery together. The height of the assembly was 21 mm and the height on the sensor alone was 10 mm. To reduce thickness of

the MARG, a custom housing was designed (Figure 12). The custom housing was designed to enclose only the x-IMU with the battery placed outside of the housing. A 400 mAh lithium polymer (LiPo) battery was used because it was smaller in size (35 x 25 x 5 mm) as compared to the 1000 mAh LiPo battery (51 x 34 x 6 mm). The reduced capacity restricted data collection to 4 hours which was acceptable for this study. A separate portion of the insole posterior to the MARG pocket was milled out for the battery (Figure 13a). The housing redesign reduced the thickness from 21 to 13 mm.

The housing redesign also allowed a rigid triad to attach directly to the housing (i.e. sensor). The rigid triad allowed for the video-based motion capture system to track the position of the MARG within the housing. A branch of the housing protruded through the lateral side of the upper and the rigid triad was attached (Figure 13). A rectangular socket design was used to eliminate rotation of the triad and reduce excessive bouncing during athletic maneuvers. The custom housing was designed in Solidworks (Dassault Systèmes SolidWorks Corp., Waltham, MA, USA) and fabricated using a fused deposition modeling (FDM) machine. The FDM machine is a rapid prototyping, or 3D printing, technology that layers molten engineering-grade thermoplastics to create plastic parts. The turf shoe and MARG assembly is shown in Figure 13b.

Figure 11. Milling of turf shoe insole to integrate the MARG

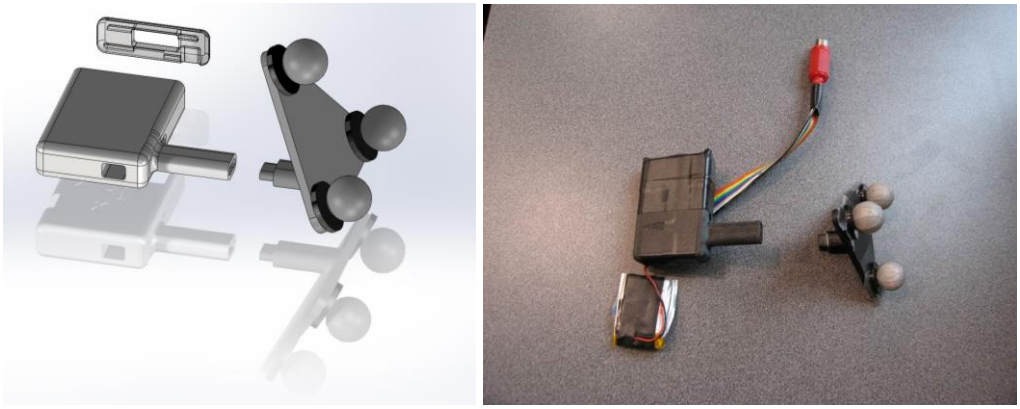

(a) **(b)**

Figure 12. Custom housing for placement of MARG into the turf shoe: (a) computer-aided design; (b) custom housing with x-IMU installed

(a)

(b)

Figure 13. Instrumented soccer turf shoes (a) without and (b) with the MARG

2.4.3.2 Shin Guards

A portion of the molded plastic and EVA cushioning was cut out for the sensor housing (Figure 14). The hole allowed the MARG to be positioned on the flat aspect of the tibia and the shin guard fit over around the housing. A rigid triad could be placed directly on the housing to allow the video-based motion analysis system to track its position. Similar to the turf shoes, the original sensor housing was too thick. A custom housing was designed with the same dimensions of the original sensor except the thickness. Thickness was reduced from 21 to 13 mm (Figure 15). The battery was placed adjacent to the MARG in between the molded plastic and EVA cushioning. Knee-high soccer socks and elastic straps secured the shin guards to the tibia. The shin guard housing was also designed in Solidworks and fabricated using the FDM machine.

(a) **(b)**

Figure 14. Instrumented shin guards (a) without and (b) with the MARG

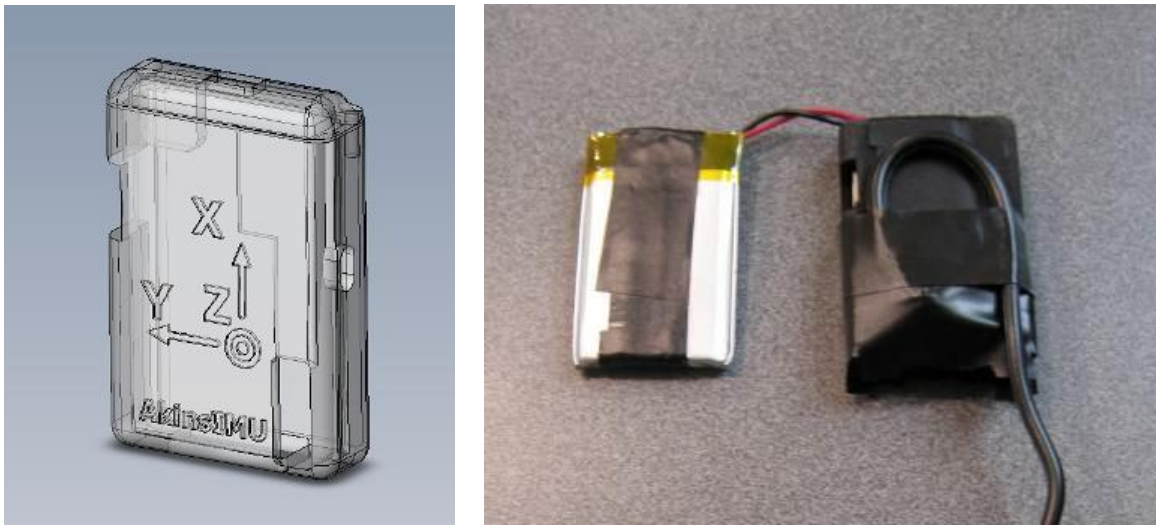

(a) **(b)**

Figure 15. Custom housing for shin guards: (a) computer-aided design; (b) custom housing with x-IMU installed

2.4.4 Synchronization

Data from the MARGs and the video-based motion analysis system must be synchronized to allow for comparisons. One of the design specifications for the devices was synchronization capabilities. The x-IMU device had an auxiliary port that could be setup to read analog signals (analog in). The video-based motion analysis system had a remote start feature to collect data using a trigger. Specifically, the system looks for the trailing edge of a square wave. An independent trigger was designed using an Arduino Uno microcontroller (Arduino, Ivrea, Italy). An Arduino Uno is a programmable microcontroller with multiple analog/digital inputs and outputs. The Arduino Uno microcontroller was selected because it can accurately create square waves and is small in size (75 x 53 mm). For field testing the compact size allowed the trigger to be a hand-held device.

The microcontroller was programmed using the Arduino integrated development environment (IDE) application (Arduino, Italy). The program produced two 1 Hz square waves of sufficient amplitude (~3 V) to trigger the video-based motion analysis system. The trigger was wired with all devices in parallel to allow all to measure the same signal. The devices included the remote start (video-based motion analysis system), one analog in for the video-based motion analysis system, two MARGs, and a light emitting diode (LED). When the trigger was activated the MARGs would recorded both waves (Figure 16) and the video-based motion analysis would begin recording on the trailing edge of the first square wave. The purpose for two square waves was to have a waveform measured with the motion analysis system and each MARG. The LED provided a visual signal for the investigator to know when the trigger was activated.

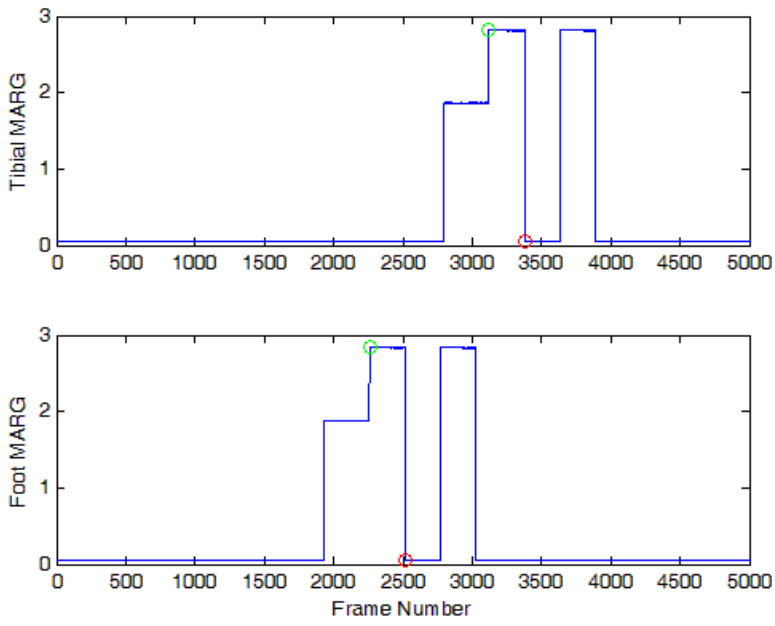

Figure 16. Synchronization pulse from trigger as measured by the MARGs. The green circle identifies the first pulse and the red circle identifies the trailing edge of the wave.

Figure 17 shows the instrumented equipment connected with the trigger. The trigger was connected to synchronization cables coming off each MARG and connected with RCA connections.

Figure 17. Instrumented equipment with synchronization trigger

2.5 METAL MAPPING OF THE INDOOR TRAINING FACILITY AND LABORATORY

The indoor training facility and laboratory were assessed to identify locations of high ferrous content prior to collecting data. The MARGs assume a homogenous earth magnetic field and distortion due to ferrous material will result in erroneous measurements. Distortion of the earth magnetic field can occur due to ferrous building material and other laboratory equipment. De Vries et al. moved MTx sensors, which are similar to the MARGs selected for this study, at various heights throughout the capture volume of their motion analysis system. They found

standard deviations in the heading of the earth magnetic field were 29° at a height of 5 cm above the floor level.[53]

The metal mapping protocol developed for this study was based on the work of de Vries et al.[53] and manufacturer's guidelines from the electromagnetic tracking system.[54] A MARG was systematically moved throughout a portion of the indoor training facility and the capture volume of the video-based motion analysis system at the laboratory. Measurements were used to identify locations of minimal earth magnetic field distortion that would allow optimal MARG measurements.

2.5.1 Indoor Practice Facility

The indoor practice facility of the UPMC Sports Performance Complex is a 125,000 square-foot building with a 70 foot ceiling. The facility contains a regulation size FieldTurf (Tarkett, Inc., Calhoun, Georgia, USA) American football field, surrounding track, and other athletic amenities. The indoor training facility provided a climate controlled environment that allowed for consistent ambient conditions and turf surface. The facility is used by collegiate and professional football teams therefore there are two sets of hash marks. The outer set of hash marks are collegiate (40 feet apart) and the inner set of hash marks are professional (18 feet, 6 inches apart).

The MARG was attached to a wood plank (6" x 48" x 1") to allow it to be slid across the field. Planar magnetometer measures (x- and y-axes) were measured as 128 Hz with the MARG. A digital camcorder (Sony, Japan) recorded movement of the sensor because it was not feasible to transport the motion analysis system to the indoor training facility. Magnetometer and video data were synchronized using a 1 Hz square-wave generated by the microcontroller. The synchronization pulse was measured using the analog input capability of the MARG (128 Hz).

An LED was simultaneously illuninated with the synchronization pulse and recorded with a digital camcorder. Magnetometer and video data were analyzed using Dartfish Software 6 TeamPro Data (Dartfish, Fribourg, Switzerland). Dartfish was founded in 1998 and is an image and video processing software package. It has many capabilites that range from biomecahnical research to televised broadcast footage.

Video data was compressed from AVCHD (Advanced Video Coding High Definition) 1080i format to high quality (3000 kbps, 640 x 480 pixels) Windows Media Video file type to reduce computation load. Compressed video data was imported into Dartfish and magnetometer data was linked to the video file. The synchronization pulse was aligned with the first frame of LED illumination (Figure 18). The synchornization time point was verified by ensuring the LED turned off as the pulse went to zero. Additionally, a second synchronization pulse was recorded to verify correct synchronization.

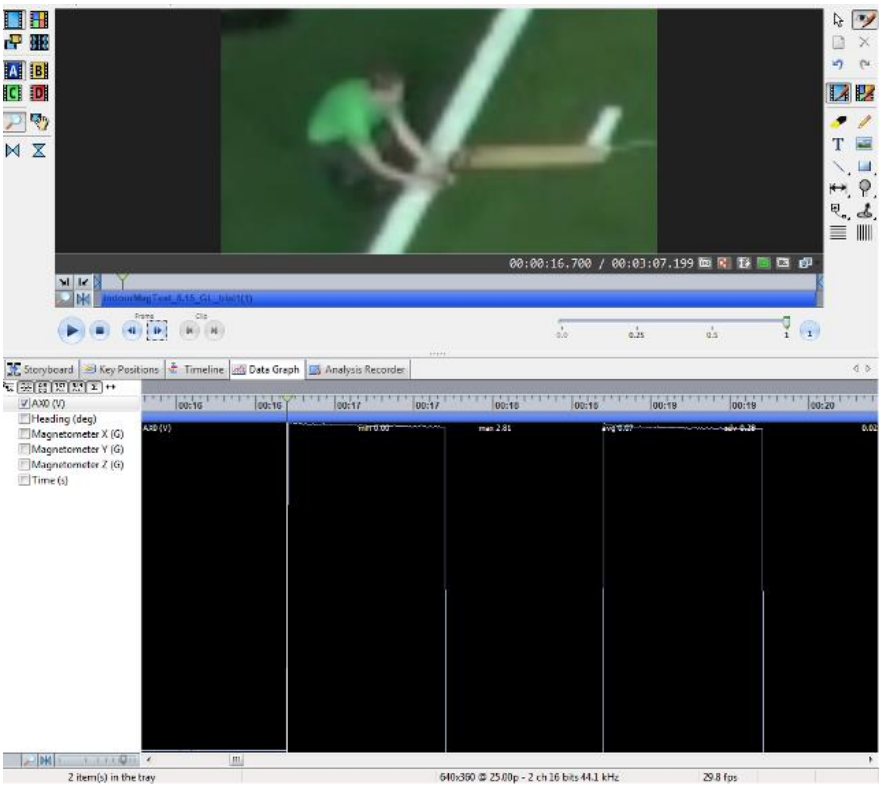

Figure 18: Synchronization of magnetometer and digital video data. The top pane of the image is the digital video data showing the wood plank and illuminated LED. The bottom pane is analog data collected with the MARG.

The MARG was slid across the field in between the outer hash marks (40 feet apart) from the goalline to the 20 yard line as shown by the red box in Figure 19. Two trials of multiple passes were performed to cover the entire area. The sensor was slid down the field (goalline to 20 yard line) for the first trial and sideways (hash-to-hash) for the second trial. Raw magnetometer and heading measurements were reviewed to determine acceptable locations. Heading measurements were calculated as

$$Heading = \tan^{-1}\left(\frac{Y}{X}\right) \tag{17}$$

where Y and X are planar measurements

Data were reviewed in Dartfish and the near-side professional hash mark on the five yard line was selected (Figure 19). This location was selected because there was minimal ferrous distortion and it was permenantly marked on the field. This location was identified as a good location in both trials. To further analyze this location, magnetometer and video data were aligned in the Dartfish software. Figure 19 shows the two trials with the video data transposed in the top pane and the magnetometer data in the bottom pane.

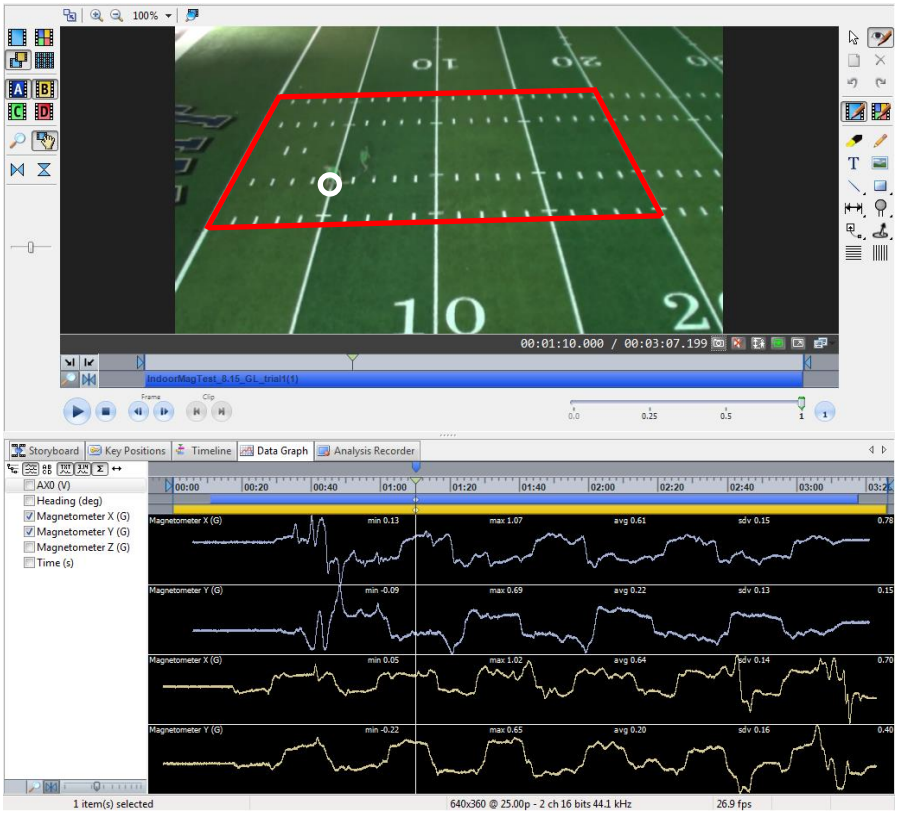

Figure 19: Metal mapping of the indoor training facility. The red box illustrates the area that measure assessed. Video from both trials are transposed in the top pane and magnetometer data from both trials are shown in the bottom pane. The selected location of minimal ferrous distortion was the hash mark of the five yard line as shown by the white circle.

2.5.2 Neuromuscular Research Laboratory

The laboratory floor was metal mapped to determine a location to obtain optimal magnetometer measurements. The capture volume of the video-based motion capture system can be seen in Figure 20 by the black flooring. The black flooring is composed of 24” x 24” tiles and the MARG was pulled along the edge of the tiles. The MARG position was simultaneously measured with a retro-reflective marker in the video-based motion analysis system and using the digital camcorder. Data were synchronized and processed as described previously for the indoor training facility.

Dartfish software was used to determine the location of minimal ferrous distortion. Position data collected with the video-based motion analysis system was used with the magnetometer data to map the ferrous distortion location. A temperature scale was used to illustrate high (red) and low (dark blue) values with respect to the mean value across the trial. This data was manually transposed onto an image of the Dartfish data to provide a spatial location of the measurements (Figure 20). The selected location of minimal ferrous distortion is shown by the white circle in Figure 20.

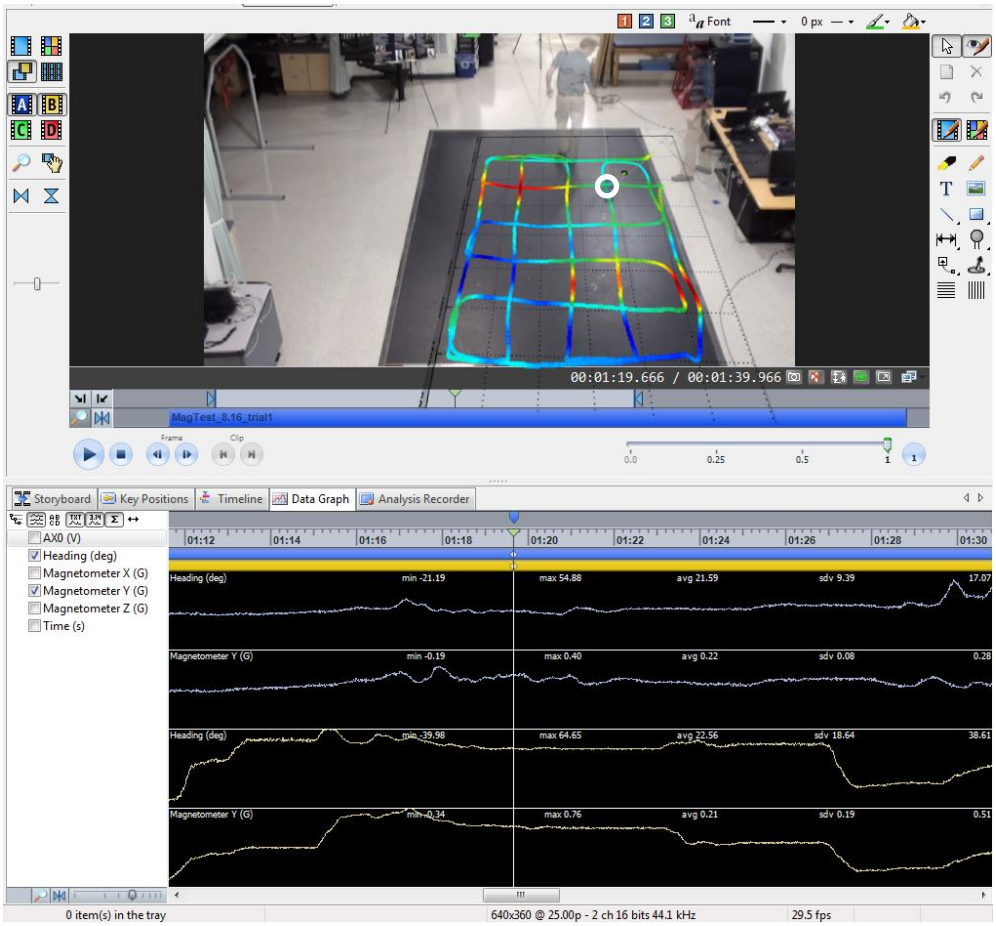

Figure 20. Metal mapping of the laboratory. Video from both trials are transposed in the top pane and magnetometer data from both trials are shown in the bottom pane. The selected location of minimal ferrous distortion is shown by the white circle.

Metal mapping of the indoor training facility and laboratory identified locations of minimal ferrous distortion to collect data. At the indoor training facility, the nearest professional hash mark at the five yard line was selected. At the laboratory, the location was marked on the floor.

2.6 SUMMARY

Commercially available inertial based sensors were reviewed. The x-IMU device was selected based on its ability to operate independently and small size. The x-IMU communicates wirelessly and records data on-board at a sampling frequency up to 512 Hz. The x-IMU was the smallest device and was further reduced by designing a custom housing. The final dimensions were 57 x 38 x 13 mm. The smaller size allowed the device to be easily integrated into the soccer turf shoes and shin guards.

A pilot study was conducted to determine the utility of the sensor to measure tibial kinematics. Tibial kinematic data were simultaneously collected with motion analysis and MARG systems during a drop landing task. Tibial kinematics were highly correlated ($r \geq 0.86$) with little error (RMSE $\leq 0.26°$). Results provided evidence that the MARG is capable of measuring segmental kinematics during dynamic maneuvers.

The magnetometer sensor of the MARG is sensitive to ferrous materials. To prevent erroneous measurements, the laboratory and indoor training facility were analyzed. Location of minimal ferrous distortion were identified. In the laboratory, the location was within the capture volume of the video-based motion analysis system and was marked on the floor. In the indoor training facility, the nearest professional hash mark at the five yard line resulted in minimal ferrous distortion and was selected.

3.0 RELIABILITY AND VALIDITY OF INSTRUMENTED EQUIPMENT

The purpose of this study was to establish the reliability and validity of a kinematic assessment using instrumented equipment during athletic maneuvers. It was hypothesized the instrumented equipment would have good test-retest reliability (ICC > 0.80) and standard error of measurement $\leq$ 5° for plantar flexion/dorsiflexion and $\leq$ 3° for inversion/eversion. Ankle joint kinematics collected by the instrumented equipment were hypothesized to be valid with excellent correlation coefficients ($r \geq 0.95$) and root mean squared errors $\leq$ 5° for plantar flexion/dorsiflexion and $\leq$ 3° for inversion/eversion as compared to a video-based motion analysis system.

3.1 INTRODUCTION

Prior to incorporating new devices into research, reliability and validity of the assessment must be established to ensure accurate measurements can be obtained. The laboratory gold standard for collecting human kinematics is a video-based optoelectronic motion analysis system.[37] Multiple cameras track retro-reflective markers attached to anatomical landmarks. Three-dimensional marker trajectories are used with anthropometric measurements and biomechanical models to calculate three-dimensional kinematics. These systems are typically limited to indoor laboratory environments and are prone to data loss due to line-of-sight difficulties.[55] Inertial

based motion analysis system are gaining popularity because the systems are portable and not limited to small capture volumes. Sensor modules are used with algorithms to measure segmental kinematics, and the segmental kinematics are used to calculate two- and three-dimensional joint kinematics. Previous studies have established reliability[29, 30] and concurrent criterion validity[31-36] of measuring ankle joint kinematics using inertial based motion analysis systems.

3.1.1 Reliability

Reliability of ankle joint kinematics using inertial sensors has been assessed in two studies that performed gait, a slower maneuver than the maneuvers in the proposed study, and used different statistical analyses to calculate reliability.[29, 30] Cloete and Scheffer[29] assessed the reliability of an off-the-shelf inertial motion capture system (Xsens, Enschede, The Netherlands) to measure ankle, knee, and hip kinematics during gait. Data were collected on young, healthy males (n = 30) on three different days, at least one week apart. Joint angles from three strides of each day were used for analysis. The coefficient of multiple determination and coefficient of multiple correlations were used to assess reliability of joint kinematics. All joints were highly reliable and in some cases performed better than values in the literature. Mariani et al.[30] used data from an inertial sensor attached to the calcaneus to estimate gait parameters of young (n = 10) and elderly (n = 10) persons during U-turn and 8-turn gait paths. Data were collected during one test session. Participants performed all maneuvers, instrumentation was removed, and then reattached to collect the retest data set. The gait parameters selected were stride length, foot clearance, stride velocity, and turning angle. Test-retest reliability was assessed using intraclass correlation coefficients (ICC) and were reliable with ICC(1,1) = 0.91-0.96. The authors did not calculate separate reliability statistics for the young and elderly population, but pooled the data from both

groups. Reliability statistics for each population are preferred especially if significant differences between groups are expected.

A limitation of the previous studies was the statistical analyses employed to calculate reliability. Cloete and Scheffer[29] used coefficients of multiple determination and coefficients of multiple correlation to calculate reliability. Coefficient of multiple determination is a statistical measure used to evaluate the similarity between two waveforms[56, 57] and coefficient of multiple correlation is the positive square root of the coefficient of multiple determination.[56] Both measures range from 0.0 to 1.0, with 1.0 signifying complete agreement between waveforms. While both measures are commonly reported, they are limited in establishing reliability because correlations do not provide information about the difference between the two waveforms. Mariani et al.[30] used ICC(1,1) to calculate reliability instead of the recommended ICC(2,1).[58] The ICC is a reliability coefficient that ranges from 0.0 to 1.0, with 1.0 being the best. Six types of ICC are described by Shrout and Fleiss[59] and include three models (1, 2, 3) and two forms (1, *k*). Model 1 assesses each subject by a different set of *k* raters and raters are randomly selected from a larger population of raters. Model 2 assesses each subject by the same raters, and raters are randomly selected. The selected raters are expected to be representative of their population and allow the results to be generalized to the population. Model 3 assesses each subject by the same raters of interest and the results cannot be generalized to the population. The two forms are single measurement (1) and the mean of multiple measurements (*k*). The type of ICC used for analysis is designated by combining the model number (1, 2, 3) and form (1, *k*) in parentheses. The ICC(2,1) is recommended to demonstrate the reliability of a measurement tool[58] and was used in this study.

3.1.2 Validity

Validity of ankle joint kinematics using inertial sensors has been assessed with differing results in six studies that employed maneuvers slower than the proposed study and used different statistical analyses (Table 4).[31-36] O'Donovan et al.[34] measured ankle joint kinematics during lower leg exercises and gait (n = 2). The lower leg exercises consisted of 12 open- and closed-chain ankle movements while seated. Root mean squared error (RMSE) between the inertial motion analysis system and a 3D video-based motion analysis system were calculated and averaged over all exercises and gait trials. Sagittal plane kinematics resulted in the smallest error (0.49°) followed by frontal and transverse planes (Table 4). Picerno et al.[35] assessed gait (n = 1) and found excellent validity using correlation coefficients ($r \geq 0.94$) and good sensor accuracy using RMSE (1.2° to 1.8°). Ferrari et al.[33] also assessed gait (n = 4) using coefficients of multiple correlations and found good validity in sagittal and frontal planes (CMC = 0.98), and moderately validity in the transverse plane (CMC = 0.68). Conversely, Cloete and Scheffer[32] assessed gait (n = 8) and found poor validity using correlation coefficients for all three planes of motion (r = 0.08 to 0.17) and poor sensor accuracy (RMSE = 9.1° to 11.6°). Bergmann et al.[31] assessed sagittal plane kinematics during stair ascent/descent (n = 14) and found good validity using correlation coefficients (r = 0.93) and moderate sensor accuracy (RMSE = 4.0°). Young et al.[36] also assessed sagittal plane kinematics during stair ascent and found good sensor accuracy using mean error (0.51°).

The results of these studies are limiting because multiple statistical methods were used to quantify valid and accurate measurements from the inertia based system. Validity measures included correlation coefficients[31] and coefficients of multiple correlations,[33] and resulted in values that ranged 0.08 to 0.98.[31-33] Correlation coefficients and CMC measure the level of the

linear relationship (or shape) between the two time histories and ranges between -1 to +1. The disadvantages of this measure include its sensitivity to phase differences and inability to distinguish between magnitudes. Sensor accuracy was assessed using root mean squared error,[31] mean absolute error,[35, 36] and standard deviations.[36] Sensor accuracy ranged 0.26 to 18.8° across all planes of motion. Root mean squared error takes the square root of the sum of the square difference between time histories. The advantages of RMSE includes that it removes any cancelling effect of positive and negative differences and provides a value with the same unit of measure (ex. degrees). Mean absolute error is calculated by taking the average unsigned error. Absolute error is advantageous because errors with the same magnitude and opposite signs do not cancel each other out. However, the direction of the error is lost with this measurement. Correlation coefficients and RMSE were selected to assess concurrent criterion validity for this study because together they provide a comprehensive analysis of the agreement. Additionally, the Sprague and Geers metric[60] was selected because it calculates magnitude and phase error for time histories. The magnitude and phase error are then combined to provide an overall error measure.

Inertial based systems have been used to measure reliable and valid ankle joint kinematics, but not during athletic maneuvers. Therefore, the purpose of this study was to establish the reliability and validity of a kinematic assessment using instrumented equipment during athletic maneuvers. The athletic maneuvers were common sports medicine research maneuvers and soccer specific maneuvers. Good test-retest reliability (ICC > 0.80) and standard error of measurement between $\leq$ 5° for plantar flexion/dorsiflexion and $\leq$ 3° for inversion/eversion were hypothesized for laboratory and field data. Ankle joint kinematics collected by the instrumented equipment were hypothesized to be valid with excellent correlation

coefficients ($r \geq 0.95$) and root mean squared errors $\leq 5°$ for plantar flexion/dorsiflexion and $\leq 3°$ for inversion/eversion as compared to a video-based motion analysis system.

Table 4. Sensor accuracy and validity

							Sensor Accuracy					Validity				
Study	Participants	Joint(s)	Sensor Type	Sensor Size	Maneuver	Gold Standard	Method	Joint	Sagittal	Frontal	Trans-verse	Method	Joint	Sagittal	Frontal	Trans-verse
O'Donovan et al., 2007	n = 2 (male) Age: 23, 25	Ankle	Accel: ADXL210E (± 10 g) Gyro: ADXRS150 (± 300 °s^{-1}) Mag: HMC2003 (± 2 Gauss)	60 x 40 x 24 mm	Lower leg exericise and gait	Optoelectric system (Evart 3D)	RMSE	Ankle	0.49	~1.65	3.33					
Picerno et al., 2008	n = 1	Ankle, Knee, Hip	MTx (Xsens, Enshede, The Netherlands)	30g, 38 x 53 x 21 mm	Gait	Optoelectric system (Vicon, Centennial, CO, USA)	MAE	Ankle Knee Hip	4.5 2.4 3.0	3.6 4.8 5.5	4.5 9.4 21.7	Correlation	Ankle Knee Hip		0.942 - 1.000	
							RMSE	Ankle Knee Hip	1.2 1.9 0.8	1.5 2.8 2.2	1.8 3.6 3.5					
Cloete and Scheffer, 2008	n = 8	Ankle, Knee, Hip	MTx (Xsens, Enshede, The Netherlands)	30g, 38 x 53 x 21 mm	Gait	Optoelectric system (Vicon, Centennial, CO, USA)	RMSE	Ankle Knee Hip	11.6 7.6 5.7	9.1 10.2 7.9	18.8 6.4 6.5	Correlation	Ankle Knee Hip	0.08 0.92 0.94	0.17 0.26 0.53	0.16 0.25 0.72
Bergmann et al., 2009	n = 14 (M = 9, F = 5) Age: 27 Height: 175 ± 8 cm Mass: 69 ± 10 kg	Ankle, Knee, Hip	MTx (Xsens, Enshede, The Netherlands)	30g, 38 x 53 x 21 mm	Stair Ascent	Optical Motion Tracker (CODA, Charmwood, UK)	RMSE	Ankle Knee Hip	4 4 5	N/A	N/A	Correlation	Ankle Knee Hip	0.93 0.98 0.96	N/A	N/A

Table 4 Continued

							Sensor Accuracy					Validity				
Study	Participants	Joint(s)	Sensor Type	Sensor Size	Maneuver	Gold Standard	Method	Joint	Sagittal	Frontal	Trans-verse	Method	Joint	Sagittal	Frontal	Trans-verse
Ferrari et al., 2010	n = 4 Age: 28.5 ± 1.8 BMI: 22.8 ± 2.0	Ankle, Knee, Hip	MTx (Xsens, Enshede, The Netherlands)	30g, 38 x 53 x 21 mm	Gait	Optoelectric system (Vicon, Centennial, CO, USA)						Coefficient of Multiple Correlations (CMC)	Ankle Knee Hip	0.98 1.00 0.99	0.98 0.88 1.00	0.68 0.80 0.95
Young et al., 2010	n = 3 (male) Age: mean = 30, range = 26-35 Height: 183 ± 1 cm Mass: 72.5 ± 5 kg	Ankle, Knee	MicroStrain 3DM-GX2 Accel: ± 10 g Gyro: ± 600 $°s^{-1}$	29g, 41 x 63 x 32 mm	Gait	Optoelectric system (Vicon, Centennial, CO, USA)	Mean error	Ankle Knee	0.26 0.15							
							SD	Ankle Knee	2.6 4.8							
					Stair Ascent		Mean error	Ankle Knee	0.51 0.12							
							SD	Ankle Knee	5.7 5.2							
					Stair Descent		Mean error	Ankle Knee	-0.56 -0.15							
							SD	Ankle Knee	4.1 4.9							

3.2 METHODS

3.2.1 Participants

Power calculations were performed using G*Power 3[61] to determine the necessary sample size. The power calculation was based on a correlation test used to assess concurrent criterion validity. A total of 12 participants were required using a power of 0.90, alpha of 0.05, a null hypothesis of $\rho_0 = 0.65$, and an alternative hypothesis of $\rho_1 = 0.95$. To account for participant attrition and potential loss of data, 17 participants were recruited.

Seventeen healthy male soccer players were recruited and enrolled in the study. Inclusion criteria for participants were no history of injury or joint instability of the ankle. Additionally, all participants engaged in organized, competitive soccer matches a minimum of once a week and participated in physical activity for a minimum of 30 minutes, 3 times per week. Participants were excluded if they had a recent (3 months) lower extremity musculoskeletal injury that could affect their performance of the maneuvers, history of an allergy to adhesive tape, major ligamentous injury or surgery of the knee or ankle, concussion or mild head injury within the previous year, or any neurological, balance, metabolic, cardiovascular, or pulmonary disorder.

3.2.2 Subject Recruitment

Subjects were recruited using flyers posted throughout the universities of the greater Pittsburgh region. Subjects that telephoned in response to the recruitment flyers were screened for

inclusion-exclusion criteria. Those eligible for the study were enrolled into the study and scheduled for testing. Written informed consent approved by the University of Pittsburgh Institutional Review Board was obtained prior to participation.

3.2.3 Instrumentation

Soccer turf shoes and shin guards were instrumented with magnetic angular rate and gravity sensors (MARG). The MARGs contained a 3D linear accelerometer (±8 g), 3D angular rate sensor (gyroscope) (±2000 $°s^{-1}$), and 3D magnetometer (±8.1 G) to measure ankle joint kinematics at 256 Hz (x-IMU, x-io Technologies Limited, United Kingdom). Ankle joint kinematic data were also collected using a 3D motion analysis system with eight high-speed cameras at 256 Hz (Vicon Motion Systems, Centennial, CO, USA). Data were synchronized using an Arduino Uno programmable microcontroller (Arduino, Italy). Maximum vertical jump height was measured using a Vertec Vertical Jump tester (Sports Imports, Columbus, OH, USA).

3.2.4 Procedures

Participants reported to the laboratory for two sessions, one week apart to minimize fatigue or memory bias effects.[58] Participants wore spandex shorts and shirt for laboratory testing and put athletic shorts and shirt over the spandex for field testing. Height, mass, and anthropometric measurements of leg length (anterior superior iliac spine to medial malleolus), knee width (medial to lateral femoral epicondyle), and ankle width (medial to lateral malleolus) were recorded. Participants wore instrumented soccer turf shoes and shin guards for all laboratory and field testing. Equipment on the dominant limb were instrumented and equipment on the other

limb were not. Limb dominance was determined by asking the participant which leg they would use to kick a ball maximally. Retro-reflective markers were adhered bilaterally to the anterior superior iliac spine, posterior superior iliac spine, lateral femoral epicondyle, lateral aspect of the thigh, lateral malleolus, and second metatarsal head (Figure 21). Additional markers were placed on the medial femoral epicondyle and medial malleolus of the test leg. These markers are shown on the right leg of the participant in Figure 21. Rigid triads of markers were attached to each MARG. For the tibial MARG, the triad was secured to the MARG using double-sided tape and underwrap. For the foot MARG, the triad was attached directly to the MARG housing. Anthropometrics measurements, instrumented equipment placement, and marker placement were performed by the same investigator on all participants.

Figure 21. Modified Plug-in-Gait Marker Set. Additional to the lower extremity Plug-in Gait marker set were medial epicondyle, medial malleolus, tibial sensor triad, foot sensor triad of the dominant leg.

Participants performed a 5 minute warm-up on a stationary bicycle at a self-selected pace. After the warm-up, maximum vertical jump height was assessed. Standing reach height was

measured with participants reaching the highest point with their feet flat on the ground. Three maximal two-footed jumps were performed and the highest point reached was measured. Maximum vertical jump height was calculated as the difference between the maximum height reached and the standing reach height. Maximum vertical jump height was used to determine the soccer ball height during the jump and moving header maneuvers in the field. Soccer ball height was 50% of the participant's maximum vertical jump height.[62]

Participants performed four athletic maneuvers in the laboratory: drop landing; drop jump; stop-jump; and jump-stop cut maneuver (Figure 22). The drop landing maneuver (Figure 22a) was a landing from a 40 cm platform. Participants dropped with both feet and landed on the ground with both feet. The drop jump maneuver (Figure 22b) was the same as the drop landing maneuver, except participants performed a maximal vertical jump immediately after landing. The stop-jump maneuver (Figure 22c) was a 2-footed jump from 40% of the participant's height to a marked landing location. Immediately after landing with both feet, participants performed a 2-footed vertical jump for maximum height. The jump-stop cut maneuver (Figure 22d) was a 2-footed jump from 40% of the participant's height to a marked landing location, followed by a 45° cutting maneuver with the dominant leg and run in the cut direction. Participants ran past a cone placed 2.5 m from the marked landing location. All maneuvers were described and demonstrated prior to data collection. Participants were provided verbal and visual instruction of how to perform each maneuver. Participants performed practice trials to become comfortable with the protocol. After participants and the investigators were comfortable with the maneuver, three trials were collected. Participants rested for 60 seconds in between maneuvers and trials to prevent fatigue.

Participants performed three soccer specific maneuvers in the field: jump header; moving header; and slalom course (Figure 23). For the jump header maneuver, participants were instructed to maintain a stiff neck by keeping their neck muscles tight and to bend at the waist when striking the ball. Prior to striking the ball, participants extend the torso backward and then flexed the torso forward to strike the ball. No instructions were provided on landing technique.

For the jump header maneuver[63] (Figure 23a), participants performed a vertical jump, struck the ball with their forehead, and landed with both feet. The landing phase of this maneuver was used for analysis. For the moving header maneuver[63] (Figure 23b), participants took a three step approach, jumped vertically, struck the ball with their forehead, and landed with both feet. The landing phase of this maneuver was used for analysis. The slalom course[64] (Figure 23c) began at the goal line and participants followed the illustrated path (Figure 24) as fast as possible. The cutting phase of the dominate foot was used for analysis.

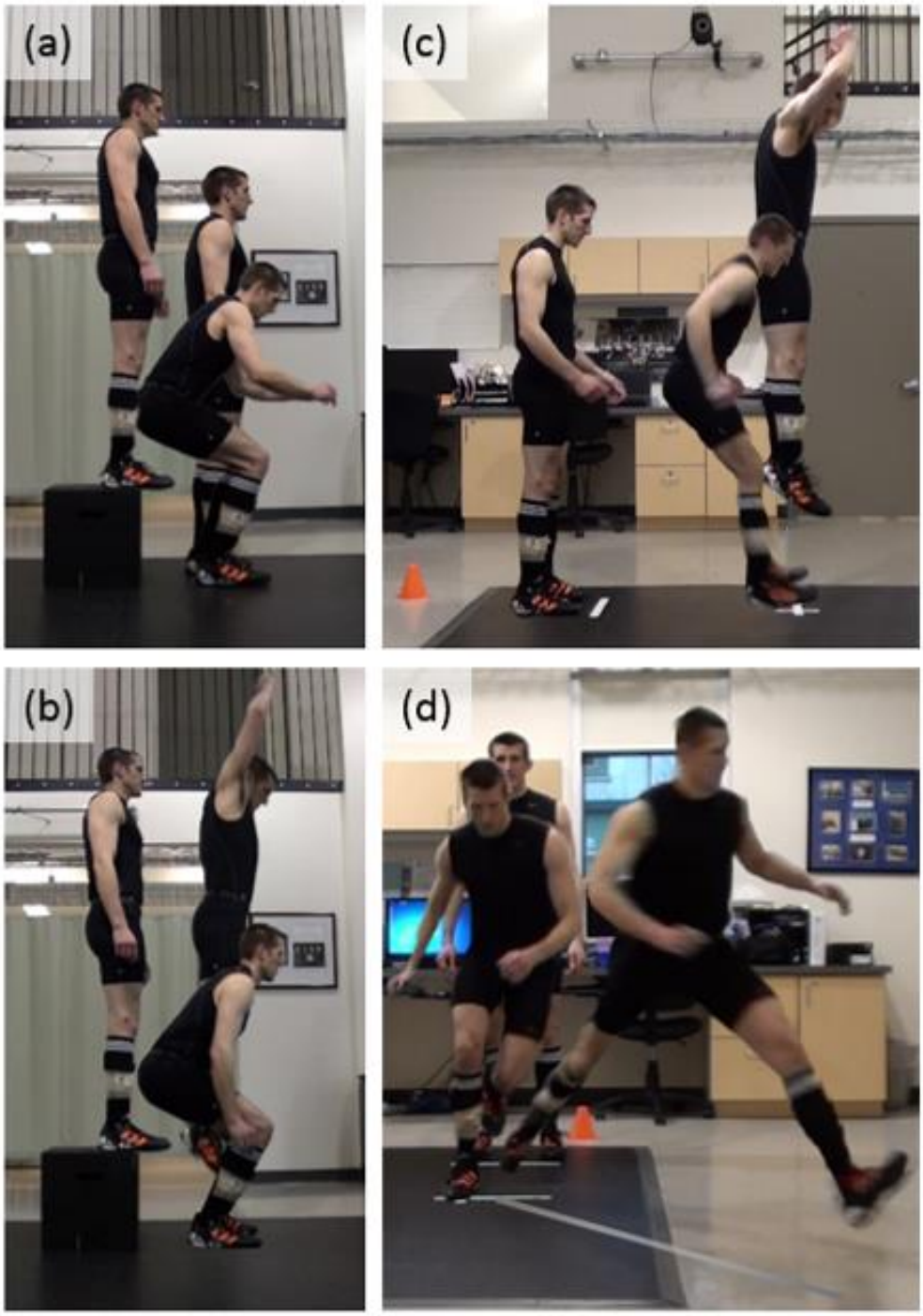

Figure 22. Laboratory maneuvers. (a) Drop landing (b) Drop jump (c) Stop jump (d) Jump-stop cut

Figure 23. Field maneuvers. (a) Jump Header; (b) Moving Header; and (c) Slalom

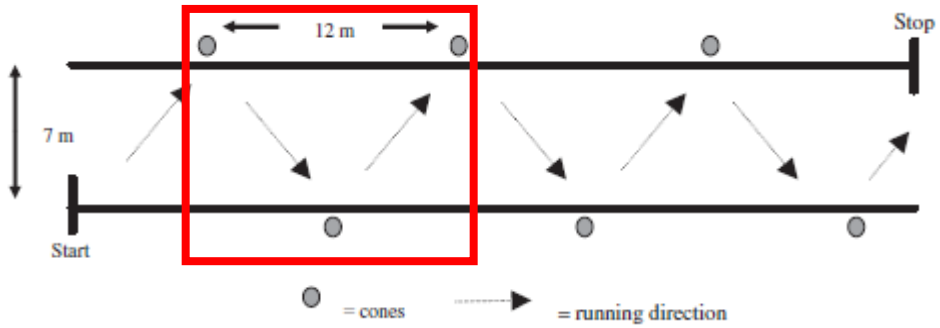

Figure 24. Slalom course schematic from Eils et al., 2004.[64] Red rectangle highlights the portion of the slalom course used in this study.

3.2.5 Data Reduction

3.2.5.1 Synchronization

Data from the MARGs and the video-based motion analysis system were synchronized using the programmable microcontroller that produced a synchronization pulse, two square waves at 1 Hz. The synchronization pulse was recorded with the auxiliary port (analog-in) of the MARGs and used to remotely start recording of the video-based motion analysis system. Data were synchronized after data collection by aligning the pulses of the two MARGs and the video-based motion analysis system.

3.2.5.2 Ankle Joint Kinematics using Video-Based System

Ankle joint kinematics were calculated using two biomechanical models: Plug-in Gait (PIG) and modified Plug-in Gait (mPIG). The conventional gait model (PIG) was selected because it is commonly used in human motion analysis research. The PIG model contained seven rigid segments: pelvis; two femurs; two tibia; and two feet.[65] Each segment was defined by an

anatomical coordinate system (ACS). Anatomical coordinate systems consisted of an origin and three orthogonal axes. For all segments except for the feet, the z-axes were pointed superior, y-axes to the left of the participant, and x-axes anterior. The foot segments were defined with the z-axes pointed anterior along the length of the foot, y-axes to the left, and x-axes pointed inferior. Ankle joint angles were calculated using Euler angle decomposition[44] with a YX'Z'' rotation sequence. Joint angles were offset using mean joint angles from the static trial.

The mPIG model contained the same seven segments and used additional markers to define knee and ankle joint centers and to track MARG orientations. The PIG model defined knee and ankle joint centers using chord functions.[65] The mPIG used additional markers placed on the medial femoral epicondyle and medial malleolus. The knee joint center was calculated as the midpoint between the medial and lateral femoral epicondyle markers; and the ankle joint center was calculated as the midpoint between the medial and lateral malleolus markers. The ACSs were defined the same as the PIG model using the modified calculation of joint centers. Triads of markers were attached to the MARGs and were used to track segmental motion of the tibia and foot segments.

Ankle joint kinematics were calculated using the method described by Winter.[44] Measurement coordinate systems (MCS) were defined for the tibia and foot as described in Chapter 2.2, equations 1-5. The MCSs were 3 x 3 orientation matrices, ${}^{G}R_{M}$, and were calculated for tibia and foot segments. The superscript *G* refers to the global coordinate system (GCS) and the subscript *M* refers to the MCS. Anatomical coordinate systems were defined as 3 x 3 orientation matrices, ${}^{G}R_{A}$, for each segment where the subscript *A* refers to the ACS. Transformation matrices were calculated for each segment (equations 18-19) to define the

relationship between MCS and ACS. These matrices were calculated during the static trial because the relationship was constant.

$$^{A:tib}R_{M:tib} = {}^{G}R_{M:tib}^{-1}\ {}^{G}R_{A:tib} \tag{18}$$

$$^{A:foot}R_{M:foot} = {}^{G}R_{M:foot}^{-1}\ {}^{G}R_{A:foot} \tag{19}$$

For each frame of the dynamic trial, the relationship between each segment's ACS and GCS, ${}^{G}R_{A}$, were calculated to using the respective MCS and transformation matrix (equations 20-21).

$$^{G}R_{A:tib} = {}^{G}R_{M:tib}\ {}^{A:foot}R_{M:tib}^{-1} \tag{20}$$

$$^{G}R_{A:foot} = {}^{G}R_{M:foot}\ {}^{A:foot}R_{M:foot}^{-1} \tag{21}$$

The relationship of each segment in the GCS allowed ankle joint kinematics to be calculated. The relationship of the foot with respect to the tibia, ${}^{foot}R_{tib}$, was calculated using equation 22. Euler angle decomposition[44] was used to calculate ankle joint kinematics from ${}^{foot}R_{tib}$ using a rotation sequence of YX'Z'' (equations 23-26). Mean ankle joint angles from the static trial were used to zero joint angles.

$$^{foot}R_{tib} = {}^{G}R_{A:foot}^{-1}\ {}^{G}R_{A:tib}^{-1} \tag{22}$$

$$R = YXZ \tag{23}$$

$$R = \begin{bmatrix} \cos\gamma & 0 & \sin\gamma \\ 0 & 1 & 0 \\ -\sin\gamma & 0 & \cos\gamma \end{bmatrix} \cdot \begin{bmatrix} 1 & 0 & 0 \\ 0 & \cos\beta & -\sin\beta \\ 0 & \sin\beta & \cos\beta \end{bmatrix} \cdot \begin{bmatrix} \cos\alpha & -\sin\alpha & 0 \\ \sin\alpha & \cos\alpha & 0 \\ 0 & 0 & 1 \end{bmatrix} \tag{24}$$

$$R = \begin{bmatrix} \cdots & \cdots & \cos\beta\sin\gamma \\ \cos\beta\sin\alpha & \cos\alpha\cos\beta & -\sin\beta \\ \cdots & \cdots & \cos\beta\cos\gamma \end{bmatrix} \tag{25}$$

$$\begin{bmatrix} \phi \\ \theta \\ \psi \end{bmatrix} = \begin{bmatrix} atan2(R_{2,1}, R_{2,2}) \\ -a\sin(R_{2,3}) \\ atan2(R_{1,3}, R_{3,3}) \end{bmatrix} \tag{26}$$

where atan2 is the four quadrant inverse tangent with imaginary parts ignored, asin is the inverse sine, and ϕ, θ, ψ are the ankle joint angles

Ankle joint kinematic data from PIG and mPIG models were used to identify discrete angles. Angles at initial contact, peak angles after initial contact, time-to-peak angles after initial contact, and overall angular displacements were identified in sagittal, frontal, and transverse planes using a custom Matlab (The MathWorks Inc., Natick, MA) script.

3.2.5.3 Ankle Joint Kinematics using Instrumented Equipment

Ankle joint kinematics were estimated using the orientation of both MARGs with a biomechanical model.[39, 48] Orientation of the MARG was calculated using sensor fusion. Sensor fusion is a technique that combines multiple sensor signals to overcome limitations of individual sensors and is able to reduce errors in angle data.[66] Sensor drift (error) due to signal integration and magnetic interference leads to inaccurate orientation estimation. The gradient descent algorithm[67] was selected for this study because it was developed specifically with the x-IMU device and performed better than a Kalman-based algorithm. The gradient descent algorithm resulted in 0.6° - 1.1° dynamic RMS error as compared to 0.8° – 1.3° dynamic RMS error of the Kalman-based algorithm.[67]

After the instrumented equipment was attached to the participant, a static calibration pose (T-pose) was used to determine initial sensor-to-sensor orientation and was followed by dynamic calibration motions. Dynamic calibration motions were used to establish orientation matrices to transform from the MARGs coordinate system to the segment's anatomical coordinate systems.[34] Three dynamic calibration motions were performed: whole body rotation; heel lifts; and squat.

The first calibration motion was rotation of the whole body about the longitudinal axis. Participants placed the test leg on the center of a turn table and placed their contralateral leg adjacent to the test leg. Participants used their arms to rotate to the left and then back to the starting position (1 rotation). A mechanical stop was placed to allow approximately 120° of rotation. After a practice trial, participants performed three rotations. This dynamic calibration motion was used to define the vertical anatomical axis for the tibia and foot MARGs. The second dynamic calibration motion was heel lifts to obtain the joint axis of rotation for the foot. Participants stood with the feet approximately shoulder width apart and lifted their heels up,

paused, and lowered back down flat footed. This was repeated two times for a total of three heel lifts. The third dynamic calibration motion was a squat to obtain the joint axis of rotation for the tibia. Participants stood in the same position and performed three squats, lowering their thighs parallel with the ground, pausing, and then returning to the original position. Three squats were performed.

The MARG orientation during each dynamic calibration motion was used to define the anatomical coordinate system for each segment. MARG orientation was obtained in quaternion representation from the gradient descent algorithm and then decomposed into the angle of rotation and unit vector. The angle of rotation and unit vector components were plotted and the corresponding anatomical vector was selected graphically (Figure 25). Figure 25a illustrates the whole body rotation dynamic calibration motion for the foot MARG. The top plot is of the angle of rotation and is approximately 120 degrees (2.1 radians). The lower plot is of the unit vector components that define the axis of rotation. Three rotations were performed and the unit vector components illustrate that the majority of axis of rotation was primarily about the z-axis (near 1.0) and little rotation about the x- and y-axes (near 0.0). Figure 25b illustrates the heel lift dynamic calibration motion for the foot MARG. Three heel lifts were performed with the majority of the rotation occurring about the y-axis and small contributions about the x- and z-axes.

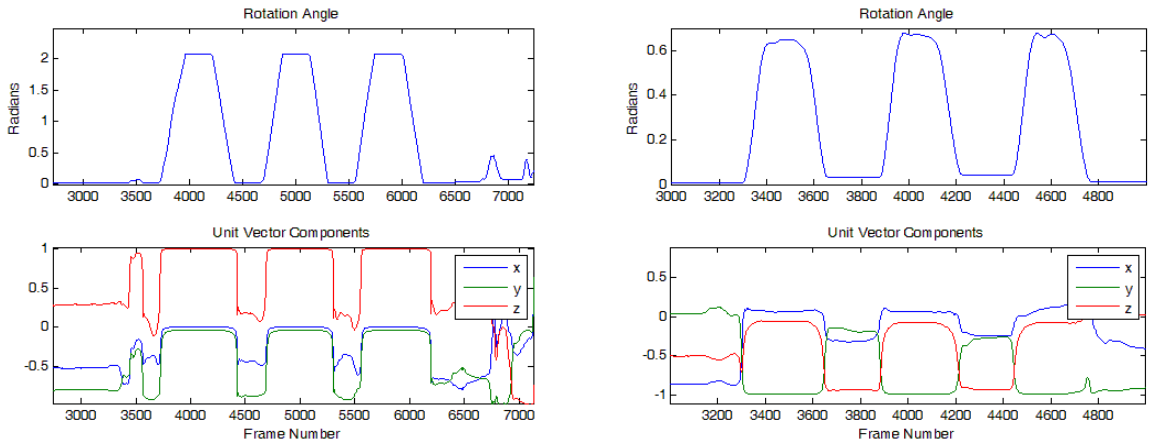

(a) **(b)**

Figure 25. Representative angle of rotation and unit vector components for (a) whole body rotation and (b) heel lift dynamic calibration motions of the foot MARG

The vertical axis of rotation from the whole body rotation dynamic calibration motion was defined as $\hat{v}_1$, and the joint axis of rotation from the heel lift (or squat) dynamic calibration motion was defined as $\hat{v}_2$. The heel lift dynamic calibration motion was used for foot and the squat dynamic calibration motion was used for the tibia. These vector components were used to defined the sensor to anatomical orientation matrix, ${}^{SEN}R_{SEG}$, for the foot and tibia segments. The z-axis was temporarily defined as the unit vector from the vertical axis of rotation (equation 27) and the y-axis was defined as the unit vector from the joint axis of rotation (equation 28). The x-axis was defined the cross product of the y- and z-axes (equation 29). To ensure the orientation matrix was orthogonal, the z-axis was then defined as the cross product of the x- and y-axes (equation 30). The 3 x 3 orientation matrix, ${}^{SEN}R_{SEG}$, defined the orientation of the segment's anatomical coorindate system with respect to the MARG coordinate system. It was composed of the set of three column vectors (equation 31).

$$\hat{z}_{TEMP} = \frac{{}^{SEN}\hat{v}_1}{\left|{}^{SEN}\hat{v}_1\right|} \tag{27}$$

$${}^{SEN}\hat{y}_{SEG} = \frac{{}^{SEN}\hat{v}_2}{\left|{}^{SEN}\hat{v}_2\right|} \tag{28}$$

$${}^{SEN}\hat{x}_{SEG} = {}^{SEN}\hat{y}_{SEG} \times \hat{z}_{TEMP} \tag{29}$$

$${}^{SEN}\hat{z}_{SEG} = {}^{SEN}\hat{x}_{SEG} \times {}^{SEN}\hat{y}_{SEG} \tag{30}$$

$${}^{SEN}R_{SEG} = \left[{}^{SEN}\hat{x}_{SEG}' \quad {}^{SEN}\hat{y}_{SEG}' \quad {}^{SEN}\hat{z}_{SEG}'\right] \tag{31}$$

Orientation matrices were defined for the foot, ${}^{SEN:foot}R_{SEG:foot}$, and tibia, ${}^{SEN:foot}R_{SEG:foot}$, and the static calibration pose was used to establish the initial ankle joint position. Orientation of the foot segment with respect to the tibia segment, ${}^{foot}R_{tib}$, was calculated using equation 32. Euler angle decomposition was used to calculate joint angles from the orientation matrix.

$${}^{foot}R_{tib} = {}^{SEN:foot}R^{-1}_{SEG:foot}\ {}^{SEN:tib}R_{SEG:tib} \tag{32}$$

Plantar flexion, inversion, and internal rotation angles at initial contact, peak during the landing phase, and overall angular displacement were identified using a custom Matlab script.

3.2.5.4 Initial Contact

Initial contact is typically identified using force platforms, but this equipment could not be used for the current study because they are contain ferrous material. The MARGs are sensitive to ferrous material and would result in erroneous data.[53] Additionally, initial contact had to be identified in the field and the force platforms could not be used with the synthetic field surface. Instead, initial contact was identified using linear accelerations of the instrumented equipment and marker trajectories of the video-based motion analysis system.

Initial contact for the instrumented equipment was based on a previously defined method.[68] Jasiewicz et al.[68] identified initial contact during normal gait using a linear accelerometer and angular velocity transducer (gyroscope). The vertical component, vertical when the foot is flat with the ground, of the foot accelerometer was used for analysis. Near vertical acceleration data and sagittal foot angle data were used to estimate initial contact. Initial contact was defined as local maximum of the near vertical acceleration that occurred 100 ms before and 100 ms after peak ankle dorsiflexion. The timing error between the linear acceleration method and foot switches was -11 ± 23 ms.

Linear acceleration and ankle plantar flexion / dorsiflexion data were used to identify initial contact of instrumented equipment (Figure 26). The acceleration component used was the z-axis which was vertical when the foot was flat with the ground. The MARG was inserted into the turf shoe with the z-axis oriented down (with gravity). Therefore, the local minimum of the vertical acceleration was used instead of local maximum acceleration as used by Jasiewicz et al.[68] The local minimum of the vertical acceleration that occurred after the ankle began to move into dorsiflexion was used to estimate initial contact. Initial contact is illustrated as the green circle in Figure 26.

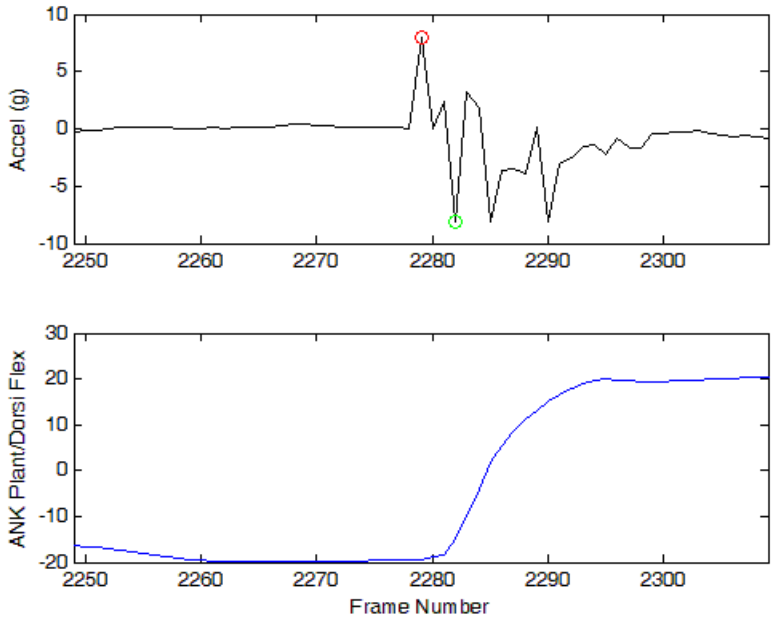

Figure 26. Initial contact estimation for instrumented equipment during a drop landing maneuver. Linear acceleration is plotted in the top frame and ankle plantar flexion (-) and dorsiflexion (+) in the bottom frame. Peak negative acceleration (green circle) is the estimated initial contact.

Initial contact for the video-based motion analysis system was based on a previously defined algorithm.[69, 70] Hreljac and Marshall[69] estimated heel strike and toe off during gait at self-selected speeds that ranged from slow to fast. Heel strike was estimated to occur at the local maximum in the vertical acceleration of the heel marker. The local maximum occurs when the derivative of acceleration (jerk) is equal to zero. Therefore, linear interpolation was used to estimate the actual time. The resulting error in heel strike as compared to a force platform was 4.5 ms. Hreljac and Stergiou[70] used the same algorithm to estimate heel strike and toe off using 2D marker displacement as compared to 3D in the previous study. A similar error of 4.5 ms was found. Linear interpolation was utilized because ground reaction force data was collected at higher sampling frequencies than marker data. In this study, data were collected at 256 Hz for

both systems therefore linear interpolation was not necessary. A limitation of this Hreljac and Marshall algorithm[69] was the assumption of a heel-strike gait pattern. The maneuvers performed in this study were landings and it was possible for participants to land in dorsiflexion (heel-first contact) and plantar flexion (toe-first contact). Using the heel marker to identify initial contact would incorrectly estimate initial contact if participants landed in plantar flexion. Therefore, the algorithm was applied to the heel and toe markers. The local maximum acceleration that occurred first was selected as initial contact. For example, vertical components of the right heel (RHEE) and right toe (RTOE) markers during a drop landing are shown in Figure 27. Position is shown in the top frame, acceleration in the middle frame, and jerk in the bottom frame. Initial contact is illustrated by magenta circles. In this trial, the participant landed in plantar flexion (toe-first).

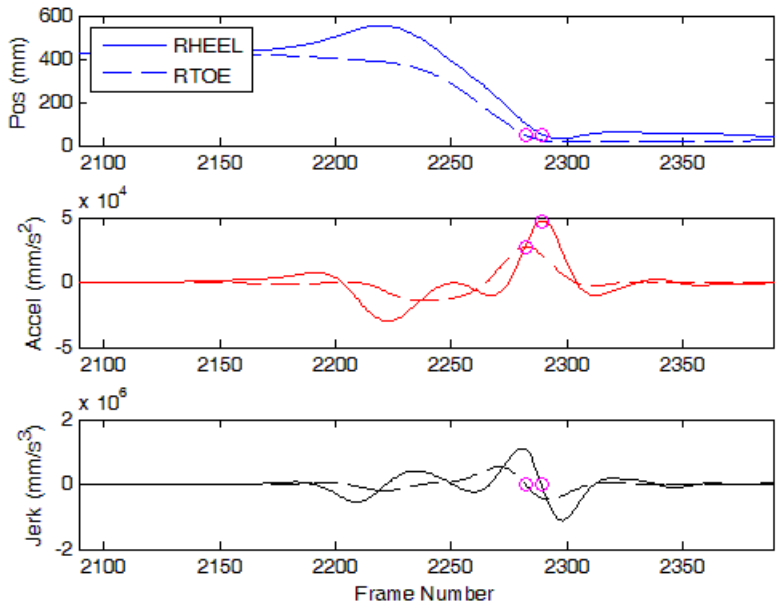

Figure 27. Initial contact estimation during drop landing maneuver. Vertical components of the right heel (RHEE) and right toe (RTOE) markers. Local maximum in the vertical component of acceleration were used to estimate initial contact as illustrated by the magenta circles.

3.2.6 Statistical Analysis

Intraclass correlation coefficients were used to calculate between-day reliability (ICC(2,1))[58] as shown in equation 33. Standard error of measurement (SEM) was calculated to obtain an absolute measure of the measurement error in degrees (equation 34).

$$ICC(2,1) = \frac{BMS - EMS}{BMS + (k-1)EMS + \frac{k(RMS - EMS)}{n}} \tag{33}$$

where BMS is the between-subjects mean square, EMS is the error mean square, RMS is the between-raters mean square, k is the number of raters, and n is the number of participants

$$SEM = SD\sqrt{1 - ICC} \tag{34}$$

where SD is the standard deviation and ICC is from equation 33

Concurrent criterion validity of the instrumented equipment was established by comparing ankle plantar flexion, inversion, and internal rotation angles measured simultaneously from the MARGs and the video-based motion analysis system. Pearson product-moment correlation coefficients, RMSE, and the Sprague and Geers (S&G) metric were used to quantify differences between MARG and video-based ankle joint kinematics. The three measures were used to assess concurrent criterion validity because they provide a comprehensive analysis of the

agreement. Correlation coefficients (equation 35) measure the level of the linear relationship between the two time histories. Root mean squared error (equation 36) takes the square root of the sum of the square difference between time histories, removing any cancelling effect of positive and negative differences.

$$r = \frac{n\sum MV - \left(\sum M\right)\left(\sum V\right)}{\sqrt{n\left(\sum M^2\right) - \left(\sum M\right)^2}\sqrt{n\left(\sum V^2\right) - \left(\sum V\right)^2}} \tag{35}$$

where M and V are MARG and video-based motion analysis data, respectively, and n is the number of pairs

$$RMSE = \sqrt{\frac{1}{n}\sum_{i=1}^{n}\left(M_i - V_i\right)^2} \tag{36}$$

where M and V are MARG and video-based motion analysis time history vectors at time step i, respectively, and n is the number of pairs

The S&G metric calculates magnitude error ($M_{S\&G}$) and phase error ($P_{S\&G}$) for the time histories. The magnitude and phase error are also combined to provide an overall error measure ($C_{S\&G}$) as shown in equations 37-42.[71, 72]

$$M_{S\&G} = \sqrt{\frac{\psi_{AA}}{\psi_{BB}} - 1} \tag{37}$$

$$P_{S\&G} = \frac{1}{\pi}\cos^{-1}\left(\frac{\psi_{AB}}{\sqrt{\psi_{AA}\psi_{BB}}}\right) \tag{38}$$

$$C_{S\&G} = \sqrt{M_{S\&G}^2 + P_{S\&G}^2} \tag{39}$$

where

$$\psi_{AA} = \frac{\sum_{i=1}^{n} M_i^2}{n} \tag{40}$$

$$\psi_{BB} = \frac{\sum_{i=1}^{n} V_i^2}{n} \tag{41}$$

$$\psi_{AB} = \frac{\sum_{i=1}^{n} M_i V_i}{n} \tag{42}$$

where M_i and V_i are MARG and video-based motion analysis time history vectors at time step i, respectively, of equal size n

Intraclass correlation coefficients were interpreted as poor (< 0.40), fair to good (0.40-0.75), and excellent (≥ 0.75) using Fleiss's criteria.[73] Correlation coefficients (r) were interpreted as moderate (0.65-0.74), good (0.75-0.84), very good (0.85-0.94), and excellent (0.95-1.00).[33, 45-47] All statistical analyses were performed using IBM SPSS Statistics, Version 20 (IBM Corporation, Armonk, NY, USA).

3.3 RESULTS

Seventeen healthy male soccer players were enrolled in the study. Three participants did not return for the second day of testing and data was lost on two participants. Therefore, data from 12 healthy male soccer players were used for analysis (Table 5). Representative data for laboratory and field maneuvers are provided in Appendix B.

Table 5. Participant demographics, mean ± standard deviation (n = 12)

Age (years)	Height (cm)	Weight (kg)	Leg Length (mm)	Knee Width (mm)	Ankle Width (mm)	Vertical Jump (cm)	Ball Height (cm)	Between Session Time (day)
26.3 ± 4.1	178.3 ± 7.2	78.5 ± 7.0	935.8 ± 71.5	103.6 ± 5.0	74.5 ± 3.1	52.1 ± 6.1	204.7 ± 9.0	8.7 ± 3.7

3.3.1 Reliability

3.3.1.1 Drop Landing Maneuver

Intraclass correlation coefficients ranged 0.380 – 0.969 for instrumented equipment, -0.247 – 0.899 for PIG, and -0.222 – 0.905 for mPIG (Table 6). Reliability statistics could not be calculated for time-to-peak internal rotation with the modified Plug-in Gait because there was zero variance. Standard error of measurement ranged 0.9 – 4.7° for initial contact, peak, and displacement (Table 6). Dorsiflexion was less than 5° for all angle variables and methods, and inversion was less than 3° for all angle variables and methods. Standard error of measurement ranged 27 – 102 ms for time-to-peak across all methods (Table 6).

3.3.1.2 Drop Jump Maneuver

Intraclass correlation coefficients ranged 0.072 – 0.887 for instrumented equipment, 0.059 – 0.867 for PIG, and 0.039 – 0.881 for mPIG (Table 7). Standard error of measurement ranged 0.9 – 7.7° for initial contact, peak, and displacement (Table 7). Dorsiflexion was less than 5° for initial contact for all methods and for peak for PIG and mPIG. Inversion was less than 3° for all variables and methods. Standard error of measurement ranged 21 – 142 ms for time-to-peak across all methods (Table 7).

3.3.1.3 Stop Jump Maneuver

Intraclass correlation coefficients ranged 0.058 – 0.558 for instrumented equipment, 0.286 – 0.789 for PIG, and -0.055 – 0.834 for mPIG (Table 8). Standard error of measurement ranged 0.9 – 13.1° for initial contact, peak, and displacement (Table 8). Dorsiflexion was only less than 5° for peak for all methods. Inversion was less than 3° for initial contact for PIG and mPIG, and for peak and displacement for all methods. Standard error of measurement ranged 33 – 151 ms for time-to-peak across all methods (Table 8).

3.3.1.4 Jump-Stop Cut Maneuver

Intraclass correlation coefficients ranged -0.175 – 0.907 for instrumented equipment, 0.397 – 0.896 for PIG, and 0.119 – 0.931 for mPIG (Table 9). Standard error of measurement ranged 1.0 – 10.1° for initial contact, peak, and displacement (Table 9). Dorsiflexion was less than 5° for initial contact and peak for all methods. Inversion was less than 3° for initial contact and displacement for all methods, and for peak for PIG and mPIG. Standard error of measurement ranged 30 – 134 ms for time-to-peak across all methods (Table 9).

3.3.1.5 Jump Header Soccer Maneuver

Intraclass correlation coefficients ranged -0.155 – 0.752 for instrumented equipment (Table 10). Standard error of measurement ranged 2.1 – 8.4° for initial contact, peak, and displacement (Table 10). Dorsiflexion was less than 5° for peak and inversion was less than 3° for displacement. Standard error of measurement ranged 0 – 62 ms for time-to-peak across all methods (Table 10).

3.3.1.6 Moving Header Soccer Maneuver

Intraclass correlation coefficients ranged -0.052 – 0.881 (Table 10). Standard error of measurement ranged 3.2 – 8.3° for initial contact, peak, and displacement (Table 10). Dorsiflexion was less than 5° for all variables, but was not less than 3° for any variables. Standard error of measurement ranged 15 – 37 ms for time-to-peak across all methods (Table 10).

3.3.1.7 Slalom Maneuver

Reliability statistics were not calculated for the slalom maneuver because the kinematics collected could not be used for analysis.

3.3.2 Concurrent Criterion Validity

Validity statistics for the instrumented equipment using PIG and mPIG as gold standards are shown in Tables 11 and 12. Sagittal plane data were highly correlated for PIG (r = 0.900 – 0.975) and mPIG (r = 0.925 – 0.979) methods for all maneuvers. The RMSE was less than 5° for drop landing, drop jump, and stop jump maneuvers for PIG and mPIG methods. The jump-stop cut

maneuver resulted in RMSE greater than 5° for PIG (RMSE = 3.59 – 4.21) and mPIG (RMSE = 3.70 – 4.17). The combined Sprague and Geers metric ($C_{S\&G}$) was lowest for the stop jump and was followed by drop jump, drop landing, and jump-stop cut. These results were similar for PIG and mPIG. However, the magnitude and phase errors did not follow a similar pattern across PIG and mPIG. The PIG method resulted in greater phase error for drop landing, drop jump, and stop jump maneuvers. Conversely, the mPIG method resulted in greater magnitude error for these maneuvers. The jump-stop cut maneuver resulted in similar findings of greater magnitude error as compared to phase error.

Frontal plane data were poorly correlated (r = -0.074 – 0.562) for PIG and mPIG methods for all maneuvers. Furthermore, RMSE was greater than 3° all maneuvers and methods, except for drop landing for the PIG method (RMSE = 2.86). The $C_{S\&G}$ was generally two times greater as compared to the sagittal plane.

Transverse plane data were poorly correlated for PIG and mPIG methods for all maneuvers. However the PIG method (r = 0.474 – 0.654) resulted in greater correlations compared to the mPIG method (r = -0.055 – -0.221). The RMSE was the greatest in the transverse plane (RMSE = 8.36° – 15.66°) and was similar between PIG and mPIG methods. The $C_{S\&G}$ for the PIG methods were similar to the frontal plane, which was approximately two times greater than the sagittal plane. The $C_{S\&G}$ for the mPIG method were similar across all maneuvers and were the highest combined errors. Magnitude error were lower as compared to phase errors for PIG and the opposite was found for the mPIG method.

Table 6. Reliability statistics for drop landing maneuver

		Initial Contact (°)				Peak (°)				Time-to-Peak (s)				Displacement (°)			
Method	Variable	ICC	95% CI		SEM	ICC	95% CI		SEM	ICC	95% CI		SEM	ICC	95% CI		SEM
Instrumented Equipment	Dorsiflexion	0.711	0.266	0.907	2.7	0.380	-0.174	0.765	3.9	0.693	0.070	0.910	0.051	0.518	-0.084	0.835	4.7
	Inversion	0.666	0.157	0.892	2.3	0.546	0.036	0.840	1.8	0.969	0.898	0.991	0.026	0.717	0.257	0.910	1.2
	Internal Rotation	0.761	0.348	0.925	3.3	0.761	0.348	0.925	3.3	-	-	-	-	0.890	0.667	0.967	3.0
Plug-in Gait	Dorsiflexion	0.743	0.251	0.922	2.8	0.822	0.487	0.945	2.2	0.899	0.699	0.970	0.028	0.809	0.417	0.943	2.9
	Inversion	0.812	0.467	0.942	0.9	0.674	0.217	0.892	1.7	-0.247	0.613	0.310	0.045	0.239	-0.384	0.703	1.7
	Internal Rotation	0.777	0.382	0.931	4.4	0.849	0.553	0.954	3.7	0.334	-0.311	0.754	0.102	0.608	0.092	0.868	3.5
Modified Plug-in Gait	Dorsiflexion	0.626	0.124	0.881	4.3	0.873	0.604	0.753	2.2	0.905	0.658	0.974	0.027	0.740	0.314	0.921	3.9
	Inversion	0.391	-0.283	0.794	1.7	-0.222	-0.801	0.443	1.5	0.098	-0.567	0.650	0.114	0.234	-0.436	0.720	1.4
	Internal Rotation	0.567	-0.022	0.862	1.8	0.841	0.512	0.955	0.9	0.616	0.107	0.877	0.063	0.096	-0.582	0.651	1.6

Table 7. Reliability statistics for drop jump maneuver

		Initial Contact (°)				Peak (°)				Time-to-Peak (s)				Displacement (°)			
Method	Variable	ICC	95% CI		SEM	ICC	95% CI		SEM	ICC	95% CI		SEM	ICC	95% CI		SEM
Instrumented Equipment	Dorsiflexion	0.755	0.354	0.923	2.6	0.072	-0.553	0.613	7.3	0.733	0.315	0.914	0.037	0.084	-0.400	0.584	6.0
	Inversion	0.741	0.314	0.918	1.5	0.487	-0.033	0.813	2.8	0.706	0.239	0.906	0.056	0.887	0.629	0.967	1.6
	Internal Rotation	0.788	0.392	0.935	3.5	0.648	0.138	0.885	5.2	0.397	-0.124	0.769	0.089	0.516	-0.015	0.828	6.9
Plug-in Gait	Dorsiflexion	0.782	0.412	0.932	2.8	0.638	0.115	0.882	2.6	0.780	0.395	0.931	0.034	0.459	-0.048	0.798	5.7
	Inversion	0.867	0.607	0.960	0.9	0.713	0.273	0.908	1.6	0.208	-0.345	0.674	0.103	0.397	-0.232	0.783	2.2
	Internal Rotation	0.837	0.523	0.951	4.3	0.596	0.035	0.866	7.7	0.059	-0.582	0.609	0.142	0.493	-0.121	0.825	6.6
Modified Plug-in Gait	Dorsiflexion	0.716	0.268	0.913	3.6	0.715	0.248	0.914	3.0	0.770	0.366	0.932	0.031	0.209	-0.324	0.683	7.5
	Inversion	0.415	-0.267	0.805	1.4	0.280	-0.407	0.744	1.4	0.219	-0.427	0.709	0.121	0.556	-0.056	0.859	1.4
	Internal Rotation	0.881	0.615	0.967	1.3	0.857	0.571	0.959	1.6	0.039	-0.612	0.616	0.127	0.697	0.183	0.909	2.1

Table 8. Reliability statistics for stop jump maneuver

		Initial Contact (°)				Peak (°)				Time-to-Peak (s)				Displacement (°)			
Method	Variable	ICC	95% CI		SEM	ICC	95% CI		SEM	ICC	95% CI		SEM	ICC	95% CI		SEM
Instrumented Equipment	Dorsiflexion	0.284	-0.376	0.732	7.1	0.251	-0.307	0.698	4.1	0.506	-0.002	0.821	0.051	0.241	-0.373	0.703	12.7
	Inversion	0.058	-0.482	0.584	3.4	0.269	-0.301	0.710	3.1	0.421	-0.110	0.782	0.103	0.438	-0.115	0.794	2.7
	Internal Rotation	0.558	-0.023	0.851	5.9	0.074	-0.550	0.614	11.0	0.329	-0.224	0.739	0.151	0.136	-0.457	0.642	10.7
Plug-in Gait	Dorsiflexion	0.506	-0.100	0.831	6.4	0.398	-0.247	0.785	3.2	0.621	0.134	0.872	0.035	0.286	-0.306	0.723	11.4
	Inversion	0.789	0.409	0.935	0.9	0.730	0.319	0.913	1.4	0.649	0.182	0.882	0.062	0.602	0.107	0.864	1.6
	Internal Rotation	0.699	0.236	0.903	4.1	0.535	-0.009	0.838	6.6	0.380	-0.261	0.776	0.140	0.605	0.120	0.865	5.5
Modified Plug-in Gait	Dorsiflexion	-0.055	-0.713	0.565	8.1	0.714	0.237	0.914	2.8	0.652	0.158	0.891	0.033	0.286	-0.356	0.741	13.1
	Inversion	0.302	-0.185	0.724	2.1	0.052	-0.510	0.602	1.6	0.228	-0.214	0.672	0.127	0.340	-0.206	0.754	1.4
	Internal Rotation	0.453	-0.133	0.813	2.5	0.834	0.492	0.952	1.4	0.196	-0.290	0.666	0.100	0.768	0.329	0.932	1.2

Table 9. Reliability statistics for jump-stop cut maneuver

		Initial Contact (°)				Peak (°)				Time-to-Peak (s)				Displacement (°)			
Method	Variable	ICC	95% CI		SEM	ICC	95% CI		SEM	ICC	95% CI		SEM	ICC	95% CI		SEM
Instrumented Equipment	Dorsiflexion	0.675	0.222	0.893	4.4	0.844	0.536	0.953	2.8	0.645	0.158	0.882	0.036	0.220	-0.388	0.691	10.7
	Inversion	0.907	0.719	0.972	1.9	0.609	0.089	0.869	3.2	0.706	0.257	0.905	0.039	0.484	-0.041	0.813	2.6
	Internal Rotation	0.579	0.009	0.860	5.9	0.186	-0.471	0.681	8.5	-0.175	-0.697	0.432	0.134	0.269	-0.361	0.720	6.8
Plug-in Gait	Dorsiflexion	0.896	0.684	0.969	2.8	0.686	0.209	0.899	1.6	0.746	0.339	0.919	0.031	0.600	0.055	0.867	7.3
	Inversion	0.783	0.396	0.933	1.0	0.765	0.373	0.926	1.2	0.511	-0.093	0.832	0.050	0.552	0.050	0.842	1.1
	Internal Rotation	0.741	0.328	0.917	4.2	0.576	0.079	0.853	5.2	0.397	-0.223	0.782	0.117	0.573	0.076	0.851	3.3
Modified Plug-in Gait	Dorsiflexion	0.931	0.765	0.981	2.5	0.496	-0.127	0.835	2.4	0.730	0.278	0.919	0.030	0.461	-0.183	0.822	9.4
	Inversion	0.367	-0.301	0.783	1.6	0.354	-0.322	0.778	1.9	0.367	-0.269	0.779	0.044	0.624	0.048	0.884	2.1
	Internal Rotation	0.855	0.546	0.959	1.8	0.765	0.301	0.929	1.7	0.119	-0.577	0.666	0.080	0.427	-0.224	0.807	1.4

Table 10. Reliability statistics for field maneuvers

		Initial Contact (°)				Peak (°)				Time-to-Peak (s)				Displacement (°)			
Maneuver	Variable	ICC	95% CI		SEM	ICC	95% CI		SEM	ICC	95% CI		SEM	ICC	95% CI		SEM
Header	Dorsiflexion	0.535	0.030	0.834	2.2	0.145	-0.483	0.654	6.2	0.384	-0.245	0.776	0.062	-0.155	-0.627	0.425	6.4
	Inversion	0.498	-0.013	0.818	4.5	0.542	0.037	0.838	4.4	0.752	0.332	0.922	0.039	0.378	-0.140	0.759	2.1
	Internal Rotation	0.253	-0.386	0.713	8.4	0.265	-0.376	0.719	8.3	0.007	-0.547	0.558	0.000	0.525	-0.076	0.838	5.2
Moving Header	Dorsiflexion	0.564	-0.009	0.853	4.7	0.648	0.168	0.883	3.6	0.642	0.116	0.883	0.020	0.563	0.025	0.850	4.1
	Inversion	0.767	0.361	0.927	3.3	0.305	-0.320	0.737	4.6	0.543	-0.015	0.843	0.037	0.730	0.295	0.914	3.2
	Internal Rotation	-0.052	-0.659	0.536	8.3	0.660	0.146	0.890	7.1	0.881	0.486	0.941	0.015	0.674	0.177	0.895	8.0
Slalom	Dorsiflexion																
	Inversion																
	Internal Rotation																

Table 11. Validity statistics for instrumented equipment and Plug-in Gait method

Maneuver	Angle	Correlation Coeff			RMSE			Msg			Psg			Csg		
Drop Landing	Plantar / dorsiflexion	0.935	±	0.072	3.59	±	1.30	0.080	±	0.151	0.142	±	0.069	0.211	±	0.106
	Eversion / inversion	0.327	±	0.417	2.86	±	1.18	-0.284	±	0.420	0.335	±	0.130	0.619	±	0.181
	Internal / external rotation	0.545	±	0.182	8.36	±	2.82	-0.094	±	0.501	0.295	±	0.125	0.569	±	0.214
Drop Jump	Plantar / dorsiflexion	0.975	±	0.015	4.18	±	1.67	0.060	±	0.174	0.090	±	0.027	0.158	±	0.133
	Eversion / inversion	-0.074	±	0.452	4.76	±	1.17	-0.434	±	0.451	0.426	±	0.139	0.705	±	0.195
	Internal / external rotation	0.637	±	0.170	10.32	±	3.00	-0.133	±	0.505	0.285	±	0.102	0.521	±	0.283
Stop Jump	Plantar / dorsiflexion	0.973	±	0.019	4.21	±	1.77	0.070	±	0.167	0.088	±	0.028	0.155	±	0.133
	Eversion / inversion	-0.164	±	0.415	5.18	±	1.26	-0.457	±	0.321	0.456	±	0.138	0.684	±	0.151
	Internal / external rotation	0.654	±	0.145	10.37	±	3.67	-0.124	±	0.420	0.288	±	0.127	0.485	±	0.223
Jump Stop Cut	Plantar / dorsiflexion	0.900	±	0.068	7.47	±	3.04	0.242	±	0.243	0.134	±	0.065	0.312	±	0.211
	Eversion / inversion	-0.089	±	0.242	5.07	±	1.66	-0.270	±	0.405	0.365	±	0.152	0.560	±	0.190
	Internal / external rotation	0.474	±	0.229	10.57	±	3.32	-0.071	±	0.385	0.212	±	0.111	0.411	±	0.191

Table 12. Validity statistics for instrumented equipment and modified Plug-in Gait method

Maneuver	Angle	Correlation Coeff			RMSE			Msg			Psg			Csg		
Drop Landing	Plantar / dorsiflexion	0.953	±	0.030	3.70	±	1.15	0.192	±	0.220	0.116	±	0.056	0.287	±	0.134
	Eversion / inversion	0.376	±	0.332	3.38	±	1.45	-0.204	±	0.357	0.406	±	0.142	0.616	±	0.162
	Internal / external rotation	-0.082	±	0.491	9.01	±	2.44	-0.694	±	0.207	0.417	±	0.169	0.832	±	0.205
Drop Jump	Plantar / dorsiflexion	0.979	±	0.011	4.17	±	1.44	0.159	±	0.132	0.079	±	0.023	0.192	±	0.114
	Eversion / inversion	0.562	±	0.278	3.76	±	0.93	-0.400	±	0.243	0.308	±	0.148	0.570	±	0.111
	Internal / external rotation	-0.055	±	0.407	11.46	±	2.08	-0.678	±	0.224	0.429	±	0.109	0.818	±	0.194
Stop Jump	Plantar / dorsiflexion	0.977	±	0.015	4.17	±	1.25	0.157	±	0.112	0.077	±	0.024	0.183	±	0.102
	Eversion / inversion	0.394	±	0.310	3.85	±	0.94	-0.277	±	0.222	0.301	±	0.112	0.480	±	0.129
	Internal / external rotation	-0.128	±	0.462	11.83	±	1.74	-0.665	±	0.198	0.462	±	0.109	0.826	±	0.160
Jump Stop Cut	Plantar / dorsiflexion	0.925	±	0.036	8.52	±	3.94	0.370	±	0.254	0.122	±	0.058	0.403	±	0.241
	Eversion / inversion	0.508	±	0.376	4.62	±	1.46	0.052	±	0.262	0.322	±	0.163	0.448	±	0.165
	Internal / external rotation	-0.221	±	0.263	15.66	±	3.67	-0.714	±	0.203	0.464	±	0.164	0.892	±	0.148

3.4 DISCUSSION

The purpose of this study was to establish the reliability and validity of a kinematic assessment using instrumented equipment during athletic maneuvers. It was hypothesized the instrumented equipment would have good test-retest reliability (ICC > 0.80) and standard error of measurement $\leq$ 5° for plantar flexion/dorsiflexion and $\leq$ 3° for inversion/eversion. Ankle joint kinematics collected by the instrumented equipment were hypothesized to be valid with excellent correlation coefficients ($r \geq 0.95$) and root mean squared errors $\leq$ 5° for plantar flexion/dorsiflexion and $\leq$ 3° for inversion/eversion as compared to a video-based motion analysis system. The instrumented equipment resulted in poor to excellent reliability and very good to excellent validity for drop landing and drop jump maneuvers, poor to fair reliability and excellent validity for the stop jump maneuver, and poor to excellent reliability and very good validity for the jump-stop cut maneuver. Soccer-specific field maneuvers resulted in poor to good reliability.

3.4.1 Reliability

Intraclass correlation coefficients ranged from poor to good. The hypothesis of good test-retest reliability was not supported for the instrumented equipment because the majority of ICC were less than 0.80 (Tables 6-9). While most variables were not greater than 0.80, ICC were fair to good[73] and similar to PIG results. Only one study was identified that calculated test-retest reliability statistics for ankle joint kinematics. Cloete and Scheffer[29] used coefficient of multiple

correlations to assess reliability and found excellent reliability of all planes of motion for the ankle (CMC = 0.872 – 0.976). Participants performed a gait task and similar results were found for the knee and hip. No studies were identified that collected ankle joint kinematics using an inertial based motion analysis system during similar athletic maneuvers. The landing impact that occurs during the athletic maneuvers performed in this study would be expected to increase motion artifact and possibly reduce test-retest reliability. One study was identified that collected ankle joint kinematics during similar athletic maneuver for a video-based motion analysis system. Ford et al.[74] calculated between-session ICC for longitudinal studies designs. Participants performed a drop jump maneuver from a 31 cm box approximately seven weeks apart (6.7 ± 1.4 weeks). Reliability statistics were calculated for angles at initial contact, peak angle during the first landing phase, and total excursion. The results of this study were compared to Ford et al[74] (Table 13) and were found to be similar for PIG across all variables. Instrumented equipment were similar for dorsiflexion and inversion at initial contact, but lower for dorsiflexion peak and displacement. Overall, angles at initial contact were more reliable for the instrumented equipment than peak angle and displacement. This is likely due to the landing impact that occurred after initial contact.

Table 13. Test-retest reliability during drop jump maneuver compared to Ford et al., 2007[74]

	Dorsiflexion			Inversion		
Method	Initial Contact	Peak	Displacement	Initial Contact	Peak	Displacement
Instrumented Equipment	0.755	0.072	0.084	0.741	0.487	0.887
Plug-in Gait	0.782	0.638	0.459	0.867	0.713	0.397
Modified Plug-in Gait	0.716	0.715	0.209	0.415	0.280	0.556
Ford et al.[74]*	0.922	0.584	0.826	0.835	0.754	0.489

* ICC (3,1)

Generally, drop landing and drop jump maneuvers resulted in the best ICCs, followed by jump-stop cut and stop jump maneuvers. The stop jump maneuver resulted in poor reliability statistics compared to the other maneuvers. Poor reliability was found for the instrumented equipment and the PIG method. A possible explanation for poor reliability of the stop jump maneuver is ankle landing strategy. Akins et al. identified that some participants land in plantar flexion and others in dorsiflexion.[75] Landing in plantar flexion results in a negative value and dorsiflexion a positive value. Positive and negative values for ankle flexion angle in the reliability calculation may have resulted in the poor reliability statistics.

Field maneuvers failed to support the hypothesis of ICC > 0.80, resulting in lower ICC as compared to laboratory maneuvers. The jump header soccer maneuver resulted in fair to good ICC for initial contact and poor ICC for peak and displacement in the sagittal plane. The frontal plane resulted in fair to good ICC for initial contact, peak, and time-to-peak; and poor ICC for displacement. The moving header soccer maneuver resulted in fair to good ICC for all variables in sagittal and frontal planes. This was the first study to establish reliability statistics on these maneuvers. Butler et al.[62] performed a soccer heading maneuver similar to the moving header maneuver, but no reliability statistics were reported for the maneuver. The slalom maneuver was select because it is commonly performed in soccer practices to increase speed and agility. Unfortunately, consistent measurements of ankle joint kinematics were not obtained. Participants sprinted to a cone and then performed a plant-and-cut maneuver on the test leg. The preceding sprint caused data to drift and was likely due to the sensor fusion algorithm. The gradient descent algorithm does not utilize zero-velocity updates.[67] Zero-velocity detecting algorithms have been used in gait studies to identify when the sensor is stationary[76] and may have allowed for better slalom data.

Standard error of measurement was calculated to provide an absolute measure of the measurement error. It was hypothesized that SEM would less than 5° for dorsiflexion and the hypothesis was partially supported. For drop landing and moving header maneuvers, initial contact, peak, and displacement were less than 5°. For drop jump, jump-stop cut, and jump header maneuvers, SEM was less than 5° for initial contact, but peak and displacement were not. Only peak angle resulted in SEM less than 5° for stop jump, initial contact and displacement were greater than 5°. The higher SEM is likely due to the poor ICC values (ICC = 0.072 – 0.145). Standard error of measurement for ankle joint kinematics was not identified in the literature.

3.4.2 Validity and Sensor Accuracy

The instrumented equipment collected valid and accurate data in the sagittal plane. Excellent correlations ($r > 0.95$) were hypothesized and found for the drop jump and stop jump maneuvers. Very good correlations ($r > 0.90$) were found for the drop landing and jump-stop cut maneuvers. Frontal and transverse plane data were not valid ($r = -0.22 – 0.65$). Limited validity data is available in the literature and has only been computed for gait[32, 33, 35] and stair ascent/descent.[31] Good sagittal plane correlations were identified in the literature and ranged 0.93 – 0.98.[31, 33, 35] Conversely, Cloete and Scheffer[32] found poor sagittal plane correlations ($r = 0.08 – 0.17$) during gait. The authors attributed the poor correlations to differences in the calculation of rotation axes and poor sensor securement to the foot. In this study, the axes of rotation for were calculated using a function method.[34] For the sagittal plane, participants performed closed-chain heel lifts which results in the axis of rotation being approximately through the malleoli. The axis of

rotation for the PIG and mPIG methods is established using the lateral and medial malleoli which likely contributed to the good correlations in this study.

Frontal and transverse planes did not results in valid data which differ from previous studies.[33, 35] Picerno et al.[35] did not report validity statistics by plane of motion or joint, but found correlations greater than 0.942 during gait. Similarly, Ferrari et al.[33] found correlations of 0.98 for the frontal plane and 0.68 for the transverse plane. Bergmann et al.[31] did not collect frontal and transverse plane kinematics, only sagittal plane. The results of this study followed a similar pattern of the knee and hip kinematics of Cloete and Scheffer.[32] They found valid sagittal plane data (r = 0.92 – 0.94), but frontal and transverse plane data were not valid (r = 0.26 – 0.72). The authors did not provide explanations for the difference between the planes of motion.

The instrumented equipment accurately measured sagittal plane angles for the drop landing, drop jump, and stop jump maneuvers (RMSE < 5.0°); sagittal plane data during the jump-stop cut maneuver were not (RMSE = 7.5 – 8.5). Results of accurate sagittal plane angle data are similar to previous studies measuring sensor accuracy for ankle joint kinematics. Errors in sagittal plane measures of previous studies range 0.3° – 4.5°,[31, 34-36] excluding Cloete and Scheffer[29] who found RMSE = 11.6°. Frontal and transverse planes were not accurate for any maneuver (RMSE > 3.0°) except for the frontal plane during drop landing (RMSE = 2.9°). These results are in contrast to O'Donovan et al.[34] and Picerno et al.[35] who found good sensor accuracy (RMSE < 3.0°) for the frontal and transverse planes.

Possible reasons for not finding valid and accurate senor data in the frontal and transverse planes include smaller range of motion during the maneuvers, greater sensitivity to impact accelerations, and axis of rotation estimation. Anatomically, ankle range of motion in the frontal plane is smaller compared to the sagittal plane, approximately 60° versus 70°, respectively.[77]

During landing maneuvers, differences in the range of motion is greater with approximately 50° in the sagittal plane and 10° in the frontal plane.[14] The smaller motion that occurs during the jumping and landing maneuvers performed in this study may not be large enough to be measured with the instrumented equipment. The impact experienced by the sensors during the landing phase of the maneuvers may also introduce too much noise, resulting in erroneous data. No previous studies were identified that measured ankle joint kinematics during jumping and landing maneuvers. While the closed-chain heel lift provided a good axis of rotation for the sagittal plane, differences in how the axes of rotation are calculated may have attributed to invalid data. The axis of rotation for the transverse plane was determined using a full body rotation. O'Donovan et al.[34] used this method to define the longitudinal axis of the whole body and therefore the vertical axes of the tibia and foot. Care was taken during data collection to ensure participants were standing in the anatomical neutral position, but this may not have been the most appropriate approach for the vertical axis. The frontal plane axis of rotation was the cross product of the sagittal and transverse axes of rotation.

To the author's knowledge, this was the first human kinematic study to use the Sprague and Geers metric for validity. Based on the results of this study, the metric may be a useful tool for future studies. Sagittal plane kinematics for the drop landing, drop jump, and stop jump were valid and accurate. Reviewing $C_{S\&G}$ values (Tables 11-12), values less than 0.30 resulted in valid and accurate measures. More research using this metric as a validation tool for human motion analysis is needed, but appears promising. The main benefit of this metric is that magnitude and phase are quantified independently and then combined into a single score.

Reliable and valid ankle joint kinematics were collected in the sagittal plane using the instrumented equipment for laboratory and field maneuvers. Drop landing and drop jump

maneuvers resulted in poor to excellent reliability and very good to excellent validity. The stop jump maneuver resulted in poor to fair reliability and excellent validity. The reduced reliability measures are likely due to the changes in ankle landing strategy between trials and/or sessions.[75] The jump-stop cut maneuver resulted in poor to excellent reliability and very good validity. Field maneuvers resulted with poor to good reliability.

4.0 IDENTIFICATION OF LABORATORY MANEUVERS THAT ELICIT GAME-LIKE DEMANDS

The purpose of this study was to identify laboratory maneuvers that elicit game-like demands. Ankle joint kinematics collected in the field were compared to ankle joint kinematics collected in the laboratory during athletic maneuvers of varied demand. It was hypothesized that ankle joint kinematics would be similar between the landing phase of the jump header and drop landing maneuver at a platform height of 20 cm, between the landing phase of the moving header and stop jump at 40% of the participant's height, and between the cutting phase of the slalom course and jump-stop cutting maneuver at 40% of the participant's height.

4.1 INTRODUCTION

Identification of laboratory maneuvers that elicit game-like demands required data to be collected in the laboratory and in the field. Limited information was available in the literature and no studies were identified comparing human kinematics under both conditions. A reason for limited studies comparing laboratory and field data is the lack of portable instrumentation. Instrumentation capable of measuring and recording human kinematics in the field would increase content validity of athletic maneuvers used in sport medicine research laboratories and provide a vital tool for injury prevention research. Instrumented shin guards and soccer shoes

were developed to measure reliable and valid ankle joint kinematics (Chapters 2-3) because ankle sprains were the most common injury among collegiate soccer athletes.[1, 2] Athletes that experience these injuries have recurrent sprains due to ankle instability,[6, 7] incur proprioceptive deficits,[8-10] and are at greater risk of ankle osteoarthritis.[11, 12] To prevent ankle sprain injuries, the mechanisms of non-contact injuries must first be identified.

4.1.1 Mechanisms of Non-Contact Ankle Sprain Injuries

The mechanisms of non-contact ankle sprain injuries were reviewed to determine the type of simulated athletic maneuvers to be collected in the laboratory and soccer-specific maneuvers to be collected in the field. Non-contact ankle sprain injuries accounted for 31-79% of ankle sprain injuries in soccer players and the most common mechanisms of non-contact ankle sprain injuries were landing, twisting/turning, and running.[78-81] Woods et al. tracked ankle sprain injuries of 91 English professional soccer clubs over two competitive seasons. Non-contact ankle sprain injuries accounted for 39% of injuries and player-to-player contact accounted for 56% of injuries. Mechanisms of non-contact ankle sprain injuries included landing (35%), twisting/turning (31%), and running (11%). Similar rates of non-contact ankle sprain injuries were found for Icelandic elite male soccer clubs (31%)[79] and higher rates in English youth (9 – 18 years) of the English Football Association (48%).[80] Cloke et al.[80] found similar mechanisms of non-contact ankle sprain injuries, but were reported as a percentage of all ankle sprain injuries (not as a percentage of non-contact injuries). The mechanisms included running (11%), twisting/turning (10%), and landing (8%). Greater rates of non-contact ankle sprain injuries were identified for Greek professional players (71%)[81] Fousekis et al.[81] prospectively tracked 100

players for one competitive season and 17 players experienced non-contact ankle sprain injuries. The mechanisms of injury were landing (77%) and cutting (23%).

4.1.2 Review of Laboratory Maneuvers for Examining Ankle Injuries

Biomechanical studies use athletic maneuvers in laboratories to simulate actions associated with mechanisms of injury. Landing and twisting/turning have been identified as the common mechanisms of non-contact ankle sprain injuries.[78-81] Common athletic maneuvers used to simulate landing include drop landing,[50, 82, 83] drop jump,[84-86] and stop jump maneuvers.[87-89] Twisting/turning is commonly simulated using a side-step cutting maneuver.[90-92] Methodological variations in drop landing, drop jump, stop jump, and side-step cutting maneuvers were reviewed to identify appropriate demands to vary. Soccer-specific biomechanical studies were also reviewed to identify appropriate field maneuvers.

The drop landing maneuver is performed with participants standing on an elevated platform and dropping down with one or both feet. Participants typically land on force platforms and the landing phase of the maneuver is used for analysis. The drop landing is commonly used in sports medicine research because it requires the lower extremity to decelerate the body upon landing.[83] The drop jump maneuver is similar to the drop landing. Participants stand on an elevated platform, drop down, and then immediately perform a maximal vertical jump. The drop jump maneuver is also commonly used because it requires the lower extremity to decelerate the body upon landing and is immediately followed by a change of direction.[88, 93, 94] Platform heights for drop landings[43, 50, 82, 83, 95-98] ranged 20 to 80 cm (Table 14). The most frequent height was 60 cm although a few studies used multiple platform heights.[43, 96, 97] Platform heights for drop

jumps[74, 84-86, 99-102] ranged 15 to 50 cm (Table 15). The most frequent height was 30-31 cm and two studies used multiple platform heights.[100, 101]

Investigators have demonstrated that platform height significantly alters landing biomechanics. Santello et al.[97] used the drop landing maneuver and found drop height significantly altered ground reaction forces and joint kinematics. Platform heights were 20, 40, 60, and 80 cm. Peak vertical ground reaction forces significantly increased with drop height and time-to-peak vertical ground reaction force significantly decreased. Joint kinematics were reported at initial contact, peak after landing, and time-to-peak joint angle. Knee flexion angle decreased significantly at 80 cm as compared to 20 cm. Ankle and hip flexion angles at initial contact decreased with drop height, but were not significant. Peak knee and hip flexion angles significantly increased with drop height and no differences were found for the ankle. Time-to-peak ankle and hip flexion angles significantly increased at 80 cm as compared to 20 cm. Moran et al.[100, 101] found similar findings using the drop jump maneuver. Increased platform height significantly decreased knee flexion at initial contact, significantly increased knee flexion displacement, and did not alter peak knee flexion angle.[100, 101] Platform heights were 30 and 50 cm[100] and 15, 30, and 45 cm.[100] These results demonstrate that platform height differences of 15 to 20 cm are able to elicit changes in joint kinematics. Therefore, platform heights of 20, 40, and 60 cm were selected as the varied demand for the drop landing and drop jump maneuvers in this study.

The stop jump maneuver consists of an approach, landing, takeoff, and jump direction. It places the lower extremity under similar demands as the drop jump maneuver: deceleration and change of direction.[88, 93, 94] The stop jump provides greater specificity with athletes as compared to the drop jump because athletes generally do not drop or jump from elevated heights. The stop

jump simulates a basketball rebound, volleyball spike, or similar plant-and-jump athletic maneuver. Of the methodologies reviewed,[87-89, 103-109] approach varied greatly, landing and takeoff were the same, and jump directions differed (Table 16). All stop jump variations required two-footed landings and takeoffs, and performed vertical jump directions. Variations in jump direction included forwards and backwards,[87, 104] and left and right.[107]

The stop jump approach consisted of three types: defined number of steps;[104, 105, 108] upper limit of steps;[87, 89, 103, 106, 109] and a jump distance of 40% of the participant's height.[88, 107] The defined number of steps were 3 or 4 steps and the upper limit of steps allowed up to 3, 4, or 5 approach steps. Interestingly, approach type varied within research groups which makes it difficult to identify an objective method to vary demand. Approach was also defined as a jump distance of 40% of the participant's height. A broad jump was performed from the 40% jump distance exposing participants to the same demand. A justification for selecting 40% was not provided,[88, 107] but is a moderate jump that all athletes can perform. No kinematic studies were identified comparing different approach types or jump distances. A defined jump distance as a function of the participant's height exposes participants to a similar demand and is easily varied. Therefore, jump distances of 20, 40, and 60% of the participant's height were selected as the varied demand for the stop jump maneuver in this study.

The side-step cutting maneuver consists of an approach distance, approach speed, cut angle, and post-cut instructions. The maneuver exposes the lower extremity to deceleration, change of direction, and twisting/turning.[110, 111] With respect to specificity, the side-step cut is similar to the stop jump because athletes commonly perform plant-and-cut movements to avoid defenders. Several studies were identified and methodologies reviewed (Table 17).[90-92, 110, 112-130] Approach distance ranged 3.0 to 8.0 m[91, 92, 113, 117, 120-122, 124, 128, 130] and was not specified in all

studies. Approach speed varied from 3.0 to 7.0 m/s with the majority of studies allowing the speed to vary 1.0 to 1.5 m/s. Timing gates were the most common methods of controlling approach speed. A cut angle of 45° was most common with a few studies using 30° and/or 60° cut angles.[110, 115, 116, 124] Post-cut instructions were not provided in most studies. While the effect of post-cut instructions on the side-step cut maneuver are unknown, the current study included instructions to ensure participants completed the maneuver similarly and also allow future researcher to recreate the maneuver. Post-cut instructions reported were exiting the cut with a speed of 4.5-5.5 m/s, [118] run a specific distance[90, 127, 129] or number of steps,[119] and simply run.[128]

Three studies did not use the standard running approach, but used a broad jump from level ground[90, 129] and jump from an elevated platform.[127] Ford et al.[90] developed a jump-stop cut maneuver that likely reduces the variability of using an approach speed range. Participants stood 40 cm from force platforms in an athletic ready position. The athletic ready position required participants to stand with a knee flexion angle of 45° ± 5° for 4 seconds and then perform the jump-stop cut maneuver. Participants jumped forward to the force platform using both feet, performed the side-step cut at a 45° cut angle with one foot, and ran past a marker 2.5 m away. This maneuver was also performed by Miranda et al.,[129] but an initial jump distance of approximately 1 m was used. Similar to the stop jump maneuver, no studies were identified comparing different approach types or jump distances. Jump distances defined as a percentage of participant height places a similar demand on each participant. Therefore, the jump-stop cut maneuver was selected over the traditional side-step cut maneuver with an approach speed. Jump distances of 20, 40, and 60% of the participant's height were selected as the varied demand for the jump-stop cut maneuver in this study.

4.1.3 Review of Soccer-Specific Field Maneuvers

The literature was reviewed to identify biomechanical studies analyzing joint kinematics of soccer-specific maneuvers. Studies analyzing kicking biomechanics were excluded. One study was identified that performed a soccer-specific jump heading maneuver. Butler et al.[62] developed a jump heading maneuver where participants performed a modified stop jump maneuver that included striking a soccer ball with their head. Participants performed a broad jump from 50% of their height (measured to the center of the force platforms), landed with each foot on separate force platforms, and immediately jumped and struck the soccer ball with their head. The soccer ball was placed at height equal to 50% of the participant's maximum vertical jump height. No instructions were provided on heading or landing technique.

Due to the lack of kinematic analyses of soccer-specific maneuvers, other methods were used to identify soccer-specific maneuvers. Soccer players, soccer training manuals, and soccer training websites were consulted; resulting in two landing maneuvers and one cutting maneuver. The two landing maneuvers are taught in sequence to learn proper heading technique. Players progress from a static jump header to a dynamic moving header maneuver. The jump header[63] is a stationary maneuver for players to focus on header technique. The moving header maneuver[63] is performed similar to the jump header, but includes a three step approach. Typically, a coach or teammate tosses the soccer ball towards the player and the player jumps and heads the ball back. Tossing the ball introduces variability which can be reduced by hanging the ball from a string. The cutting maneuver selected was a slalom course.[64] A slalom course is a timed event that consists of sprinting and cutting between cones as fast as possible. Eils et al.[64] developed a slalom course using three side-step cuts with each leg. Participants began at a starting line, sprinted to a cone where a side-step cutting maneuver was performed, and continued through the

course performing cuts at each cone. These soccer-specific field maneuvers are game-like training exercises used by soccer coaches and are familiar to players. Furthermore, these maneuvers incorporate the most prevalent mechanisms of non-contact ankle sprain injuries.

The purpose of this study was to identify laboratory maneuvers that elicit game-like demands. Ankle joint kinematics collected in the field were compared to ankle joint kinematics collected in the laboratory during athletic maneuvers of varied demand. It was hypothesized that ankle joint kinematics would be similar between the landing phase of the jump header and drop landing maneuver at a platform height of 20 cm, between the landing phase of the moving header and stop jump at 40% of the participant's height, and between the cutting phase of the slalom course and jump-stop cutting maneuver at 40% of the participant's height.

Table 14. Review of drop landing maneuver. Age reported in mean (SD). (-) denotes information was not provided.

Author	Gender	Age (years)	Population	Legs	Platform Height (cm)	Platform Distance (cm)
Santello et al., 2001[97]	Male (n=7) Female (n=1)	All: 21.2 (1.1)	Physically active students	Two	20, 40, 60, 80	-
Huston et al., 2001[96]	Male (n=10) Female (n=10)	All: 28 (5)	Not provided	Two	20, 40, 60	-
Lephart et al., 2002[83]	Male (n=15) Female (n=15)	M: 21.3 (1.6) F: 19.3 (1.2)	M: recreational athletes F: NCAA DI athletes	One	20	11
Decker et al., 2003[50]	Male (n=12) Female (n=9)	M: 28.3 (3.9) F: 26.4 (4.5)	Recreational athletes	Two	60	-
Kernozek et al., 2005[82]	Male (n=15) Female (n=15)	M: 24.5 (2.3) F: 23.6 (1.8)	Recreational athletes	Two	60	-
Blackburn & Padua, 2008[95]	Male (n=20) Female (n=20)	All: 21.5 (1.9)	Physically active	Two	60	-
Sell et al., 2010[98]	Male (n=70)	28.8 (7.1)	Soldiers	Two	50	-
Tran et al., 2010[43]	Male (n=6) Female (n=4)	-	-	Two	30, 40, 50	-

Table 15. Review of drop jump maneuver. Age reported in mean (SD). (-) denotes information was not provided.

Author	Gender	Age (years)	Population	Legs	Platform Height (cm)	Platform Distance (cm)	Jump Direction
Hewett et al., 2005[85]	Female (n=205)	16.1 (1.7)	Soccer, basketball, and volleyball	Two	31	-	Max vertical
Moran & Marshall, 2006[100]	Male (n=15)	21.4 (1.5)	Physically active	Two	30, 50	-	Max vertical
McLean et al., 2007[86]	Male (n=39) Female (n=39)	M: 20.7 (1.3) F: 20.8 (0.8)	NCAA DI basketball, soccer, and volleyball	Two	50	-	Max vertical
Chappell & Limpivasti, 2008[84]	Female (n=33)	19.0 (1.2)	NCAA DI basketball and soccer	Two	31	-	Max vertical
Moran et al., 2009[101]	Female (n=15)	20.9 (1.1)	Competitive soccer	Two	15, 30, 45	-	Max vertical
Shultz et al., 2009[102]	Male (n=39) Female (n=39)	M: 22.6 (2.6) F: 22.2 (2.9)	Not provided	Two	45	10	Max vertical
Ford et al., 2010[74]	Male (n=50) Female (n=265)	Range of mean ages: 12.3-16.1	Competitive sports	Two	31	-	Max vertical
Dowling et al., 2011[99]	Male (n=20) Female (n=18)	26.9 (4.3)	Recreational athletes	Two	36	-	Max vertical

Table 16. Review of stop jump maneuver. Age reported in mean (SD). (-) denotes information was not provided.

Author	Gender	Age (years)	Population	Approach	Landing	Takeoff	Jump Direction
Chappell et al., 2002[87]	Male (n=10) Female (n=10)	M: 23.4 (1.1) F: 21.0 (1.7)	Recreational athlete	Up to 3 steps	Two-footed	Two-footed	Forward, vertical, backward
Yu et al., 2004[103]	Male (n=12) Female (n=12)	M: 26 (2.5) F: 26.0 (2.6)	Recreational athlete	Up to 5 steps	Two-footed	Two-footed	Vertical
Chappell et la., 2005[104]	Male (n=10) Female (n=10)	M: 23.7 (0.8) F: 21.7 (2.1)	Recreational athlete	3 steps	Two-footed	Two-footed	Forward, vertical, backward
Yu et al., 2005[105]	Male (n=30) Female (n=30)	Range 11-16	Recreational soccer	4 steps	Two-footed	Two-footed	Vertical
Yu et al., 2006[89]	Male (n=30) Female (n=30)	M: 22.4 (1.6) F: 22.1 (1.4)	College students	Up to 5 steps	Two-footed	Two-footed	Vertical
Sell et al., 2006[88]	Male (n=18) Female (n=17)	M: 16.4 (1.4) F: 15.9 (1.1)	High school basketball	40% of height	Two-footed	Two-footed	Vertical, left, right
Chappell et al., 2007[106]	Male (n=17) Female (n=19)	M: 22.6 (2.2) F: 22.3 (2.2)	Recreational athlete	2- to 3-steps	Two-footed	Two-footed	Vertical
Sell et al., 2007[107]	Male (n=19) Female (n=17)	M: 16.3 (1.5) F: 15.9 (1.1)	High school basketball	40% of height	Two-footed	Two-footed	Vertical
Herman et al., 2008[108]	Female (n=66) Intervention (n=39) Control (n=35)	-	Recreational athlete	4 steps	Two-footed	Two-footed	Vertical
Wang et al., 2011[109]	Male (n=10)	21.1 (2.2)	Elite university volleyball	Up to 3 steps	Two-footed	Two-footed	Vertical

Table 17. Review of side-step cut maneuvers. Age reported in mean (SD). (-) denotes information was not provided.

Author	Gender	Age	Population	Approach Distance (m)	Approach Speed (m/s)	Cut Angle (°)	Post Cut Instructions
McLean et al., 1999[112]	Male (n=16) Female (n=14)	M: 19.4 (2.2) F: 19.1 (1.8)	High performance athletes	-	5.5-7.0	35-60	-
Simonsen et al., 2000[114]	Female (n=6)	21 (18-23)	Elite handball	2 steps	Run	-	-
Colby et al., 2000[113]	Male (n=9) Female (n=6)	All: 22.2 (1.7)	Recreational athlete	8.0	3/4 game speed	45	-
Besier et al. 2001[110, 115] Besier et al. 2003[116]	Male (n=11)	21.3 (3.4)	Soccer	-	3.0	30, 60	-
McLean et al., 2004[117]	Male (n=8) Female (n=8)	M: 21.4 (3.2) F: 23.3 (3.8)	-	3.0	4.5-5.5	30-40	-
McLean et al., 2004[91]	Male (n=10) Female (n=10)	M: 20.2 (1.9) F: 21.1 (3.0)	NCAA DI basketball	3.0	4.5-5.5	30-40	-
Pollard et al., 2004[118]	Male (n=12) Female (n=12)	M: 19.7 (1.5) F: 19.3 (1.1)	Collegiate soccer	-	5.5-6.5	45	4.5-5.5 m/s exit speed
Ford et al., 2005[90]	Male (n=54) Female (n=72)	M: 14.5 (2.2) F: 14.3 (1.9)	Middle and high school basketball	0.4	Jump	45	Run past marker 2.5m away
McLean et al., 2005[119]	Male (n=10) Female (n=10)	M: 20.2 (1.9) F: 21.1 (3.0)	NCAA DI basketball	-	4.5-5.5	35-55	~5 steps required after cut
Sigward et al., 2006[121] Pollard et al., 2007[122]	Male (n=15) Female (n=15)	M: 19.6 (1.9) F: 19.4 (1.5)	NCAA DI/DII soccer	5.0	5.5-7.0	45	-
Dayakidis et al., 2006[120]	Male FAI (n=15) Control (n=15)	FAI: 25.0 (5.0) CTRL: 23.9 (3.8)	Greek Division 2 or 3 basketball	7.0	5.0 (0.2)	45	-
Beaulieu et al., 2008[123]	Male (n=15) Female (n=15)	F: 21.1 (3.6) M: 22.9 (3.7)	Elite soccer		4.0-5.0	45	-

Table 17. Continued

Author	Gender	Age	Population	Approach Distance (m)	Approach Speed (m/s)	Cut Angle (°)	Post Cut Instructions
Hanson et al., 2008[124]	Male (n=20) Female (n=20)	M: 19.4 (1.4) F: 19.8 (1.1)	NCAA DI soccer	3.0	3.0	60	-
Fedie et al., 2010[126]	Male (n=19) Female (n=19)	M: 19.9 (1.6) F: 20.7 (1.8)	NCAA DIII basketball	-	4.5	35-60	-
Dowling et al., 2010[125]	Male (n=11) Female (n=11)	All: 23.6 (2.7)	Recreational athlete	-	Run	30	-
DiStefano et al., 2011[127]	Male (n=38) Female (n=27)	All: 10 (1.0)	Youth soccer	Box*	-	60	Run 2-3 m
Kristianslund et al., 2012[128]	Female (n=123)	22.5 (7.0)	Norwegian Division 1 Handball	6.0	-	30	Run
Sigward et al., 2012[92]	Male (n=76) Female (n=80)	Range: 9-23	Club or collegiate soccer	7.0	4-5.5	45	-
Stearns and Pollard., 2013[130]	Female ACLR (n=12) Control (n=12)	 ACLR: 23.7 (1.9) Control: 21.3 (1.2)	Soccer	5.0	5.5-7.0	45	-
Miranda et al., 2013[129]	Control (n=10, 5M/5F) ACLR (n=10, 4M/6F)	Control: 25.2 (1.6) ACLR: 27.0 (1.7)	Recreational athlete	~1.0	Jump	45	Jog past marker 2.5 m away

* 30 cm box placed 50% of participants height from edge for force platform

4.2 METHODS

4.2.1 Participants

Fourteen healthy male soccer players were recruited and enrolled in the study. Inclusion criteria for participants were no history of injury or joint instability of the ankle. Additionally, all participants engaged in organized, competitive soccer matches a minimum of once a week and participated in physical activity for a minimum of 30 minutes, 3 times per week. Participants were excluded if they had a recent (3 months) lower extremity musculoskeletal injury that could affect their performance of the maneuvers, history of an allergy to adhesive tape, major ligamentous injury or surgery of the knee or ankle, concussion or mild head injury within the previous year, or any neurological, balance, metabolic, cardiovascular, or pulmonary disorder. Data was lost for two participants. Therefore, data from 12 healthy male soccer players were used for analysis (age = 26.3 ± 4.1 years, height = 178.3 ± 7.2 cm, mass = 78.5 ± 7.0 kg).

4.2.2 Subject Recruitment

Subjects were recruited using flyers posted throughout the Universities of the greater Pittsburgh region. Subjects that telephoned in response to the recruitment flyers were screened for inclusion-exclusion criteria. Those eligible for the study were enrolled into the study and scheduled for testing. Written informed consent approved by the University of Pittsburgh Institutional Review Board was obtained prior to participation.

4.2.3 Instrumentation

Soccer turf shoes and shin guards were instrumented with magnetic angular rate and gravity sensors (MARG). The MARGs contained a 3D linear accelerometer (±8 g), 3D angular rate sensor (gyroscope) (±2000 $°s^{-1}$), and 3D magnetometer (±8.1 G) to measure ankle joint kinematics at 256 Hz (x-IMU, x-io Technologies Limited, United Kingdom). The MARGs were integrated into the soccer equipment and ankle joint kinematics were collected data at 256 Hz. A Vertec Vertical Jump tester (Sports Imports, Columbus, OH, USA) was used to measure vertical jump height.

4.2.4 Procedures

4.2.4.1 Laboratory Testing

Participants performed a five minute warm-up on a stationary bicycle at a self-selected pace and then performed a maximum vertical jump test. Standing reach height was measured with participants reaching the highest point with their feet flat on the ground. Three maximal two-footed jumps were performed and the highest point reached was measured. Maximum vertical jump height was calculated as the difference between the maximum height reached and the standing reach height. Maximum vertical jump height was used to determine the soccer ball height during the jump header and moving header maneuvers in the field. Soccer ball height was 50% of the participant's maximum vertical jump height.[62]

Participants then performed the athletic maneuvers of varied demand: drop landing; drop jump; stop jump; and jump-stop cut maneuver (Figure 22, Chapter 3). The drop landing maneuver (Figure 22a, Chapter 3) was performed from 20, 40, and 60 cm platforms. Participants

dropped with both feet and landed on the ground with both feet. The drop jump maneuver (Figure 22b, Chapter 3) was the same as the drop landing maneuver, except participants performed a maximal vertical jump immediately after the landing. The stop-jump maneuver (Figure 22c, Chapter 3) was a two-footed jump from 20, 40, and 60% of the participant's height to a marked landing location. Immediately after landing with both feet, participants performed a two-footed vertical jump for maximum height. The jump-stop cut maneuver (Figure 22b, Chapter 3) was a 2-footed jump from 20, 40, and 60% of the participant's height to a marked landing location, followed by a one-footed 45° cutting maneuver and run past a cone placed 2.5 m away. Limb dominance was determined by asking participants which leg they used to maximally kick a ball. All maneuvers were described and demonstrated prior to data collection. Participants were allowed to perform practices trials and three trials were collected for data analysis. Participants rested for 60 seconds in between maneuvers and trials to prevent fatigue.

4.2.4.2 Field Testing

Ankle joint kinematics were collected during three soccer-specific maneuvers in the field: jump header; moving header; and slalom course (Figure 23, Chapter 3). For header maneuvers, participants were provided instructions on header technique. Participants were asked to maintain a stiff neck by keeping their neck muscles tight and to bend at the waist when striking the ball. Prior to striking the ball, participants extended the torso backward and then flexed the torso forwards to strike the ball. No instructions were provided on landing technique. For the jump header maneuver[63] (Figure 23a, Chapter 3), participants performed a vertical jump, struck the ball with their forehead, and landed with both feet. The landing phase of this maneuver was used for analysis. For the moving header maneuver[63] (Figure 23b, Chapter 3), participants took three forward steps, jumped vertically, struck the ball with their forehead, and landed with both feet.

The landing phase prior to striking the ball was used for analysis. The slalom course[64] (Figures 23c & 24, Chapter 3) was setup using three cones. The first cone was the start line, the second cone was the location of the plant-and-cut maneuver, and third cone was the finish line. Participants sprinted from the start line to the second cone placed as shown in Figure 24, Chapter 3. Participants performed a plant-and-cut maneuver and sprinted to the finish line. The plant-and-cut maneuver was used for analysis. Participants performed practices trials and three trials were collected for data analysis. Participants rested for 60 seconds in between maneuvers and trials to prevent fatigue.

4.2.5 Data Reduction

Data from the two MARGs were synchronized using a trigger. The trigger was a programmable microcontroller that produced a synchronization pulse of two square waves at 1 Hz. The synchronization pulse was recorded with the auxiliary port (analog-in) of the MARGs. After data collection, data were synchronized by aligning the pulses.

Ankle joint kinematics were calculated using a functional approach[34] and is detailed in Chapter 3. Briefly, orientation of both MARGs was calculated using the gradient descent algorithm.[67] After the instrumented equipment was attached to the participant, a static calibration pose (T-pose) was used to determine initial sensor-to-sensor orientation and was followed by dynamic calibration motions. Dynamic calibration motions were used to establish an orientation matrix to transform from the MARG's coordinate system to the segment's anatomical coordinate system.[34] Three dynamic calibration motions were performed: whole body rotation; heel lifts; and squat. Orientation of the foot anatomical matrix with respect to the tibia anatomical matrix

was calculated for each time point. Euler angle decomposition[44] was then used to calculate joint angles.

Initial contact was identified using linear accelerations measured with the foot accelerometer. This method is detailed in Chapter 3 and was based on a previously defined method.[68] The local minimum of the vertical acceleration that occurred after the ankle began to move into dorsiflexion estimated initial contact. Plantar flexion at initial contact, peak dorsiflexion during the landing phase, and angular displacement in the sagittal plane were identified using a custom Matlab script.

4.2.6 Statistical Analysis

Normality of dependent variables was assessed using the Shapiro-Wilk test. Data were not normally distributed therefore nonparametric tests were used. The related-samples Friedman one-way analysis of variance by ranks test was used to compare field and laboratory ankle joint kinematic data. The independent variable was experimental condition and had four levels: field; demand 1; demand 2; and demand 3 (Table 18). Dependent variables were plantar flexion angles at initial contact, peak angle during the landing or cutting phase, and overall angular displacement during the landing or cutting phase (Table 18). Post-hoc analyses were performed as necessary using the Wilcoxon signed-ranks test. Alpha was set at 0.05 for all statistical analyses. All statistical analyses were performed using IBM SPSS Statistics, Version 20.

Table 18. Independent and dependent variables for the drop landing maneuver

	Field	Laboratory		
Dependent Variable	Jump Header	20 cm	40 cm	60 cm
Plantar flexion at initial contact				
Peak dorsiflexion				
Time-to-peak plantar flexion				
Sagittal plane angular displacement				

4.3 RESULTS

Representative data for laboratory and field maneuvers are provided in Appendix B.

4.3.1 Drop Landing Maneuver

The analysis of variance identified significant differences for plantar flexion at initial contact, peak dorsiflexion, and angular displacement ($p \leq 0.001$, Table 19). The post-hoc analysis identified significant differences between platform height and the jump header maneuver. Plantar flexion at initial contact was significantly less for 20 and 40 cm ($p \leq 0.015$) as compared to the jump header, and 60 cm was similar ($p = 0.239$, Figure 28a). Peak dorsiflexion was significantly less for 20 cm ($p = 0.019$) and similar for 40 and 60 cm ($p \geq 0.136$), Figure 28b). Angular displacement in the sagittal plane was significantly less for 20 and 40 cm ($p \leq 0.012$) and was similar for 60 cm ($p = 0.754$, Figure 28d). No significant differences were identified for time-to-peak dorsiflexion ($p = 0.150$).

The post-hoc analysis also identified significant differences between platform heights (Table 20). Plantar flexion at initial contact significantly increased with platform height with significant differences between all heights ($p \leq 0.012$, Figure 28a). Peak dorsiflexion

significantly increased with platform height with significant increases between 20 and 40 cm ($p = 0.003$) and between 20 and 60 cm ($p = 0.005$, Figure 28b). Angular displacement increased with platform height and was significant between all platform heights ($p \leq 0.006$, Figure 28d).

4.3.2 Drop Jump Maneuver

Significant differences were identified for plantar flexion at initial contact, peak dorsiflexion, and time-to-peak dorsiflexion ($p \leq 0.027$, Table 19). Plantar flexion at initial contact was significantly less for drop jumps at 20 and 40 cm ($p \leq 0.005$) and was similar to the jump header for 60 cm ($p = 0.117$, Figure 29a). Peak dorsiflexion was significantly greater for all drop jumps as compared to the jump header ($p \leq 0.041$, Figure 29b). Time-to-peak dorsiflexion was significantly greater for 20 and 40 cm ($p \leq 0.012$) and was similar for 60 cm ($p = 0.255$, Figure 29c). No significant differences were identified for angular displacement ($p = 0.107$).

Similar to the drop landing maneuver, plantar flexion at initial contact significantly increased with platform height with significant differences between all heights ($p \leq 0.002$, Figure 29a). Time-to-peak dorsiflexion significantly decreased with platform height between 20 and 60 cm ($p = 0.023$, Figure 29c). Platform height had no effect on peak dorsiflexion or angular displacement.

4.3.3 Stop Jump Maneuver

Significant differences between the stop jump and moving header maneuver were identified for time-to-peak dorsiflexion and angular displacement ($p \leq 0.004$, Table 19 and Figure 30). Time-to-peak dorsiflexion was significantly greater for all stop jump distances ($p \leq 0.006$) as compared

to the moving header maneuver (Figure 30c). Angular displacement was significantly less at 40 and 60% jump distances ($p \leq 0.019$) and was similar at 20% ($p = 0.136$, Figure 30d).

The post-hoc analysis identified one significant difference with increased jump distance. Angular displacement in the sagittal plane significantly decreased between 20 and 40% jump distances ($p = 0.028$, Figure 30d). Jump distance had no effect on plantar flexion at initial contact, peak dorsiflexion, or time-to-peak dorsiflexion.

4.3.4 Jump-Stop Cut Maneuver

Comparisons between slalom and jump-stop cut maneuvers were not performed because the kinematics collected during the slalom course were erroneous and could not be used for data analysis. Participants sprinted to a cone and then performed a plant-and-cut maneuver on the test leg. The preceding sprint caused data to drift and was likely due to the sensor fusion algorithm.

Table 19. Ankle joint kinematics for field and laboratory maneuvers (n = 12). Field data was compared to laboratory data of varied demand using the related-sample Friedman two-way analysis of variance and Wilcoxon signed-ranks test (Post-Hoc) as necessary.

Drop landing														Post-Hoc*	
Dependent Variable	Jump Header			20 cm			40 cm			60 cm			p-value	20cm	40cm	60cm
Plantar flexion at initial contact (°)	19.8	±	3.1	11.9	±	6.3	16.8	±	5.3	18.4	±	5.3	**≤ 0.001**	**0.003**	**0.015**	0.239
Peak dorsiflexion (°)	21.0	±	2.7	17.6	±	3.7	21.7	±	3.9	22.8	±	3.8	**0.001**	**0.019**	0.480	0.136
Time-to-peak dorsiflexion (s)	0.14	±	0.04	0.16	±	0.09	0.19	±	0.06	0.20	±	0.07	0.150	-	-	-
Sagittal angular displacement (°)	40.8	±	3.7	29.5	±	5.7	38.5	±	5.3	41.2	±	6.6	**≤ 0.001**	**0.002**	**0.012**	0.754

Drop jump														Post-Hoc	
Dependent Variable	Jump Header			20 cm			40 cm			60 cm			p-value	20cm	40cm	60cm
Plantar flexion at initial contact (°)	19.8	±	3.1	7.1	±	6.0	15.3	±	6.1	17.7	±	6.0	**≤ 0.001**	**0.002**	**0.005**	0.117
Peak dorsiflexion (°)	21.0	±	2.7	23.1	±	4.0	23.6	±	3.3	23.9	±	3.8	**0.010**	**0.041**	**0.023**	**0.041**
Time-to-peak dorsiflexion (s)	0.14	±	0.04	0.23	±	0.09	0.20	±	0.06	0.18	±	0.08	**0.027**	**0.012**	**0.005**	0.255
Sagittal angular displacement (°)	40.8	±	3.7	41.6	±	17.0	47.4	±	14.1	46.7	±	11.2	0.107	-	-	-

Stop jump														Post-Hoc	
Dependent Variable	Moving Header			20%			40%			60%			p-value	20%	40%	60%
Plantar flexion at initial contact (°)	0.9	±	6.0	1.7	±	6.3	4.3	±	9.1	4.0	±	7.4	0.296	-	-	-
Peak dorsiflexion (°)	19.1	±	6.4	23.0	±	2.8	22.5	±	2.7	21.6	±	2.6	0.098	-	-	-
Time-to-peak dorsiflexion (s)	0.14	±	0.04	0.21	±	0.04	0.22	±	0.05	0.23	±	0.05	**0.002**	**0.006**	**0.006**	**0.003**
Sagittal angular displacement (°)	56.7	±	6.0	50.3	±	13.7	44.0	±	14.2	45.6	±	14.3	**0.004**	0.136	**0.012**	**0.019**

Significant findings are bolded

* Post-hoc comparison to field data

Table 20. Effect of platform height and jump distance on dependent variables

Drop landing	Friedman	20-40	20-60	40-60
Plantar flexion at initial contact (°)	**≤ 0.001**	**0.002**	**0.002**	**0.012**
Peak dorsiflexion (°)	**0.001**	**0.003**	**0.005**	0.084
Time-to-peak dorsiflexion (s)	0.150	-	-	-
Sagittal angular displacement (°)	**≤ 0.001**	**0.002**	**0.002**	**0.006**

Drop jump	Friedman	20-40	20-60	40-60
Plantar flexion at initial contact (°)	**≤ 0.001**	**0.002**	**0.002**	**0.002**
Peak dorsiflexion (°)	**0.010**	0.480	0.347	0.433
Time-to-peak dorsiflexion (s)	**0.027**	0.239	**0.023**	0.388
Sagittal angular displacement (°)	0.107	-	-	-

Stop jump	Friedman	20-40	20-60	40-60
Plantar flexion at initial contact (°)	0.296	-	-	-
Peak dorsiflexion (°)	0.098	-	-	-
Time-to-peak dorsiflexion (s)	**0.002**	0.108	0.092	0.505
Sagittal angular displacement (°)	**0.004**	**0.028**	0.117	0.695

Significant findings are bolded

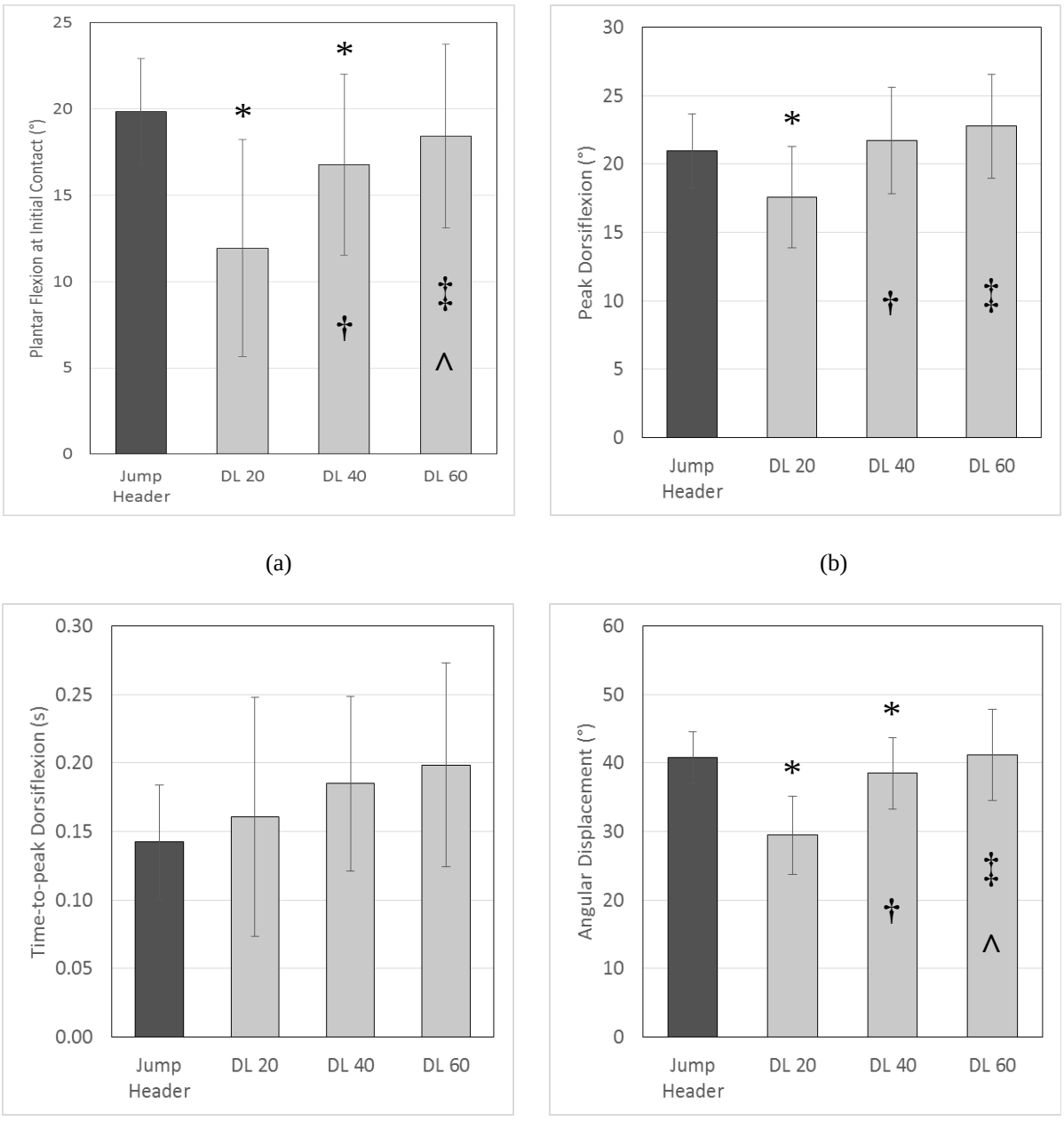

Figure 28. Comparison between jump header and drop landing maneuvers. (a) Plantar flexion angle at initial contact, (b) Peak dorsiflexion angle during landing phase, (c) Time-to-peak dorsiflexion angle, (d) Angular displacement during maneuver. * Significant difference as compared to jump header, significant difference between: † 20 cm and 40 cm, ‡ 20 cm and 60 cm, ^ 40 cm and 60 cm

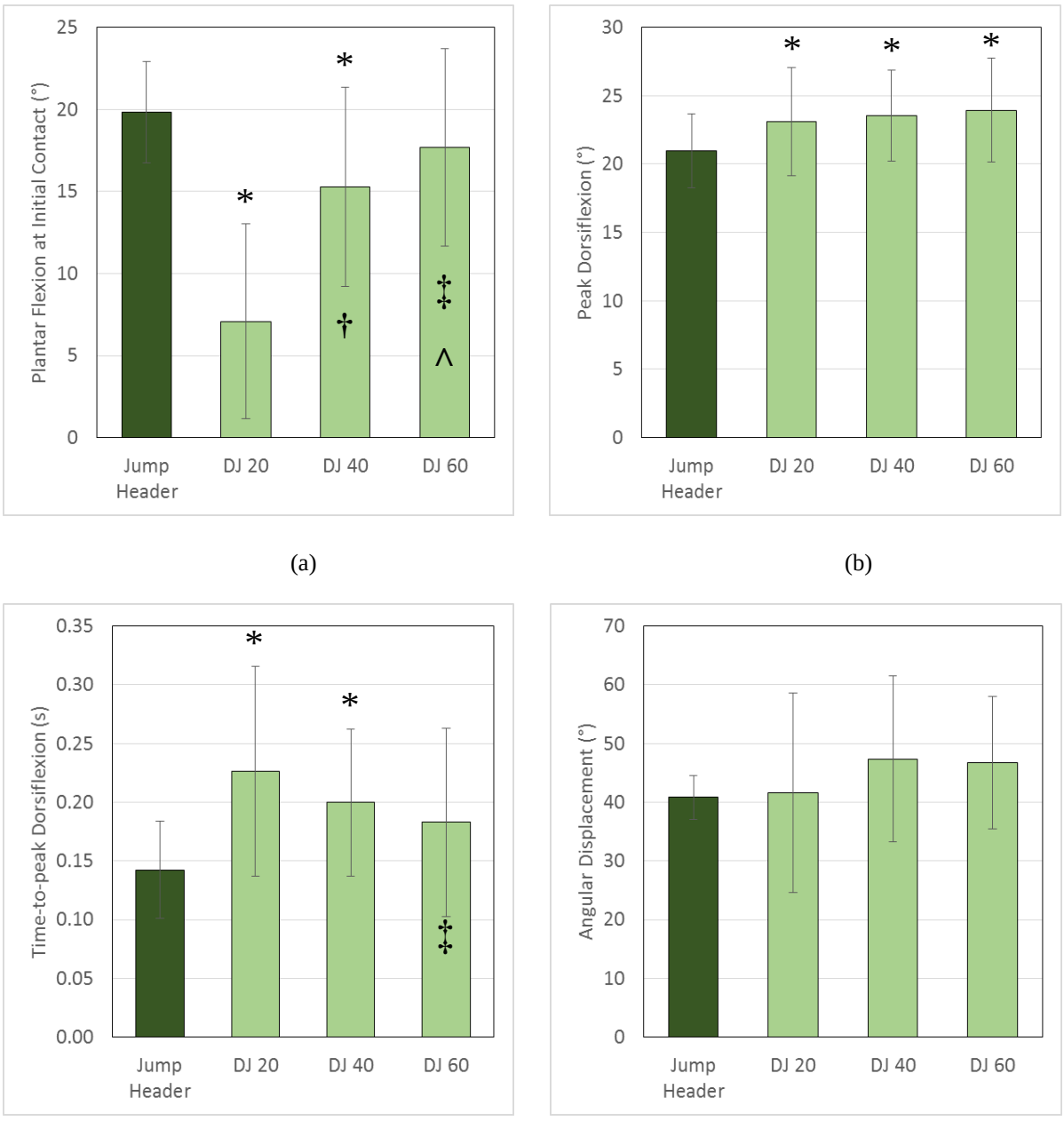

Figure 29. Comparison between jump header and drop jump maneuvers. (a) Plantar flexion angle at initial contact, (b) Peak dorsiflexion angle during landing phase, (c) Time-to-peak dorsiflexion angle, (d) Angular displacement during maneuver. * Significant difference as compared to jump header, significant difference between: † 20 cm and 40 cm, ‡ 20 cm and 60 cm, ^ 40 cm and 60 cm

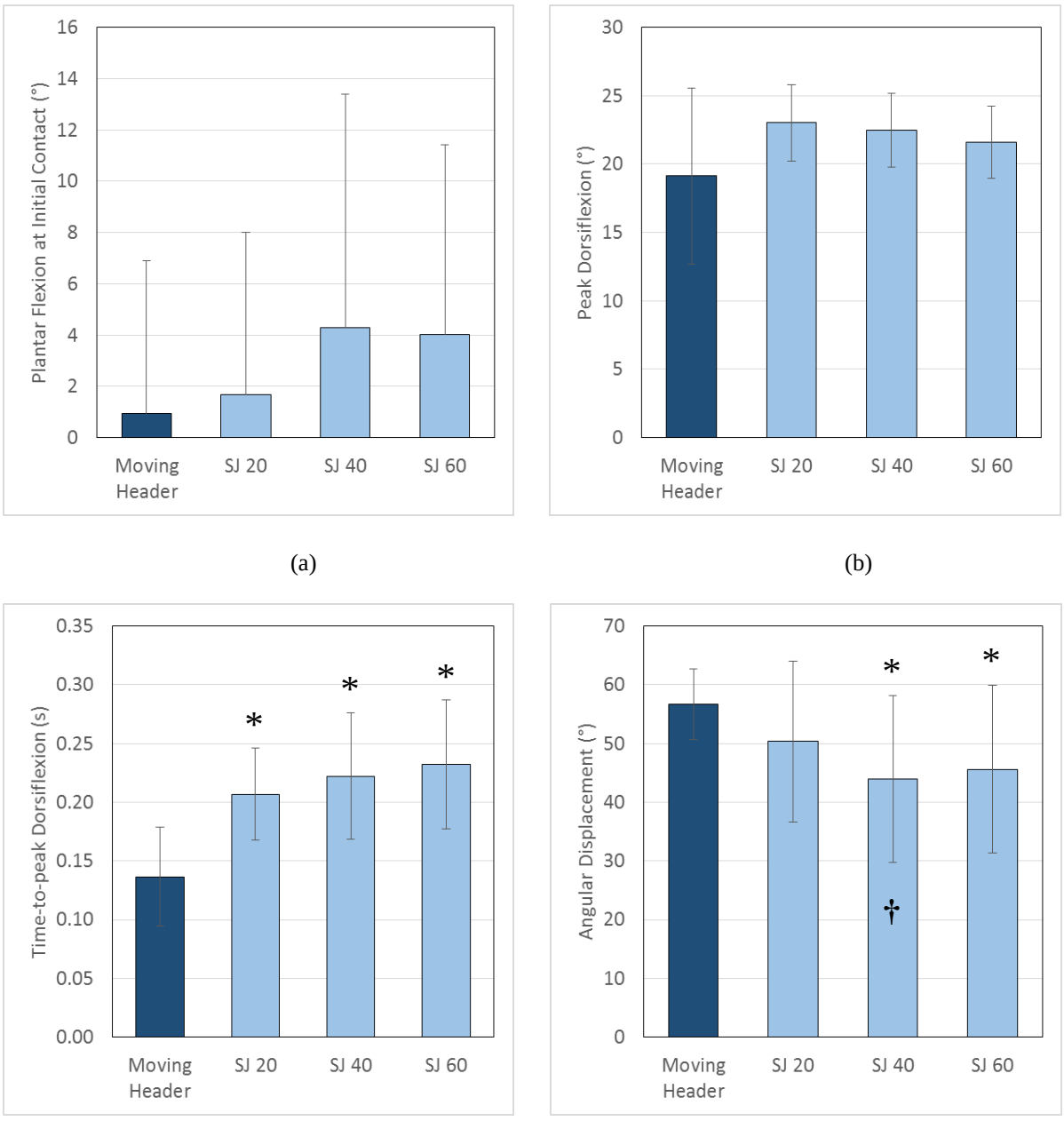

Figure 30. Comparison between moving header and stop jump maneuvers. (a) Plantar flexion angle at initial contact, (b) Peak dorsiflexion angle during landing phase, (c) Time-to-peak dorsiflexion angle, (d) Angular displacement during maneuver. * Significant difference as compared to moving header, significant difference between: † 20% and 40%

4.4 DISCUSSION

The purpose of this study was to identify laboratory maneuvers that elicit game-like demands. Ankle joint kinematics collected in the field were compared to ankle joint kinematics collected in the laboratory during athletic maneuvers of varied demand. It was hypothesized that ankle joint kinematics would be similar between the landing phase of the jump header and drop landing maneuver at a platform height of 20 cm, between the landing phase of the moving header and stop jump at 40% of the participant's height, and between the cutting phase of the slalom course and jump-stop cutting maneuver at 40% of the participant's height. Drop landing and drop jump maneuvers from a platform height of 60 cm elicited a similar response to the jump header field maneuver. A jump distance recommendation for the stop jump and jump-stop cut maneuvers was not warranted. Increased jump distance did not significantly alter landing biomechanics for the stop jump maneuver and slalom field data was not able to be processed. The instrumented equipment allowed this study to be the first to compare human kinematic data collecting in the laboratory and field.

Similarities were identified between the jump header and drop landing from the 60 cm platform height for all variables: plantar flexion at initial contact; peak dorsiflexion; time-to-peak dorsiflexion; and angular displacement in the sagittal plane. Significant differences were identified for the 20 cm platform height for all variables except time-to-peak dorsiflexion, and results for 40 cm were mixed. These results do not support the hypothesis that the drop landing maneuver from the 20 cm platform height and jump header maneuver are similar. Instead, the results suggest the 60 cm platform height should be used to simulate a soccer-specific jump header maneuver.

Plantar flexion at initial contact and peak dorsiflexion increased significantly with platform height. Santello et al.[97] found no significant differences in plantar flexion at initial contact or peak dorsiflexion with platform height. These differences are likely because the participants of Santello et al.[97] performed the landing barefoot as compared to shod in this study. Dropping barefoot from an elevated platform height may result in a protective mechanism to reduce foot pain. Previous studies have found kinematic[131] and kinetic[132] differences in landing biomechanics when landing barefoot as compared to shod. Time-to-peak dorsiflexion increased with platform height, but no significant differences were identified which are similar to previous results.[97] Three studies were identified that used multiple platform heights for the drop landing maneuver, but only Santello et al.[97] reported ankle joint kinematics. Huston et al.[96] reported changes in knee kinematics and Tran et al.[43] reported changes in tibial accelerations and ground reaction forces.

The drop jump from the 60 cm platform and jump header resulted in similar plantar flexion at initial contact, time-to-peak dorsiflexion, and angular displacement. Jump header peak dorsiflexion was significantly different from all platform heights. Similar to the drop landing, drop jumps from a 60 cm platform height elicited a similar demand as the jump header maneuver. Ankle joint kinematics during the drop jump maneuver were similar to those reported by McLean et al.[86] at a 50 cm platform height.

Comparing drop landing and drop jump maneuvers results from this study reveals that plantar flexion at initial contact was similar between maneuvers and increased significantly with platform height. However, all other variables responded differently. Peak dorsiflexion and angular displacement both increased significantly with platform height for the drop landing, but did not change for the drop jump. For the drop jump, it appears that participants performed the

maximum vertical jump the same regardless of platform height. Conversely, participants attenuated the impact for drop landings as shown with increased peak dorsiflexion and angular displacement. Time-to-peak dorsiflexion was similar for the drop landing and significantly decreased for the drop jump. While time-to-peak decreased significantly, a decrease of 5 ms (23 vs 18 ms) may not be clinically significant.

Few significant differences were identified between the stop jump and moving header maneuver. Time-to-peak dorsiflexion was significantly greater in the laboratory for all jump distances and angular displacement was significantly less at 40 and 60% jump distances. Plantar flexion at initial contact and peak dorsiflexion were similar across all jump distances. These results did not support the hypothesis of the stop jump at 40% jump distance elicited a similar demand as the moving header. The post-hoc analysis revealed that jump distance did not significantly alter ankle joint kinematics. The only significant finding was a significant decrease in angular displacement between 20 and 40% jump distances. The lack of significant differences between jump distances suggests that increased jump distance did not change the demand required by the participants to perform the maneuver. Increased jump distance was expected to significantly alter ankle biomechanics because Sell et al.[133] identified that peak posterior ground reaction forces increased significantly with jump distance. Participants performed a stop jump maneuver at jump distances of 20, 40, 60, and 80% of the participant's height, but joint kinematics were not reported. Therefore, a recommendation for jump distance to elicit demands similar to the moving header cannot be made. Based on feedback from participants, the 20% jump distance was awkward and most preferred the 40% jump distance.

The instrumented soccer equipment allowed ankle joint kinematics to be compared between field and laboratory maneuvers. Drop landing and drop jump maneuvers from a 60 cm

platform elicited a similar response to the jump header maneuver. A jump distance recommendation for the stop jump maneuver is not warranted because jump distance did not significantly alter landing biomechanics for the stop jump maneuver.

5.0 LIMITATIONS

Limitations of this study include motion artifact, different methods of initial contact estimation, erroneous slalom data, and the lack of altered landing biomechanics with increased jump distance for the stop jump maneuver. Motion artifact and initial contact estimation may have affected ankle joint kinematic data measured using the instrumented equipment. Erroneous slalom data and the lack of altered landing biomechanics for the stop jump maneuver were unexpected and did not allow comparisons to be made between laboratory and field data.

Motion artifact is common in human movement motion analysis[134, 135] and the greater size of the inertial sensors as compared to retro-reflective markers may have introduced additional motion artifact. To reduce motion artifact in this study, the tibia MARG was secured to the medial surface of the tibia with a double-sided adhesive disc. The medial surface of the tibia provided a flat surface with minimal soft tissue. The shin guard was placed over the MARG and both were secured to the leg with a knee-high soccer sock, elastic strap, and underwrap. The shin guards were designed to have ample space so to not contact the MARG during data collection. However, there was a possibility that movement of the shin guard may have introduced artifact into the signal. The foot MARG was placed into the sole of the soccer turf shoe. The insole was placed over the MARG and then participants put on the shoes. When participants wore the instrumented turf shoe the foot MARG could be felt under their arch, but did not limit their performance. While the weight of the participants was expected to keep the

MARG in place, there was a possibility that artifact could be introduced into the signal if the MARG popped out of the sole of the shoe. Participants did not mentioned movement of shin guards or MARGs during data collection. There was a possibility that motion artifact introduced errors into the orientation measurement of the MARG and ultimately affected ankle joint kinematic measurements. In Chapter 2, angles at initial contact resulted in better reliability measures as compared to peak angle and angular displacement. The impact at landing may have introduced motion artifact and may explain the lower reliability measures.

Initial contact of the foot with the ground was estimated differently for the instrumented equipment and video-based motion analysis system. Both algorithms were based on previously defined methods and used linear acceleration. The instrumented equipment used the change in linear acceleration of the foot MARG and the video-based motion analysis system used the change in linear acceleration of marker trajectories. It is possible the systems identified different initial contacts which would have affected the time point for joint kinematics and resulted in different angles.

The slalom maneuver was selected because it is commonly used by soccer players to increase speed and agility. Unfortunately, consistent measurements of ankle joint kinematics were not obtained. Participants sprinted to a cone and then performed a plant-and-cut maneuver on the test leg. The preceding sprint caused data to drift and was likely due to the sensor fusion algorithm. The gradient descent algorithm does not utilize zero-velocity updates.[67] Zero-velocity detecting algorithms have been used in gait studies to identify when the sensor is stationary[76] and may have allowed for better slalom data. Without slalom data, a recommendation of a jump distance that elicited a game-like demand for the jump-stop cut maneuver was not possible.

Increased jump distance for the stop jump maneuver did not significantly alter ankle joint kinematics. The post-hoc analysis identified one significant difference which was a decrease in angular displacement between 20% and 40% jump distances. The lack of significant differences suggests that jump distance did not change the demand required by the participants to perform the maneuver. No previous studies were identified that performed the stop jump maneuver using different approaches. Increased jump distance was expected to significantly alter ankle biomechanics because Sell et al.[133] found that peak posterior ground reaction forces increased significantly with jump distance; joint kinematics were not reported in the study. Similar results across jump distance did not allow a recommendation of a jump distance that elicited a game-like demand for the stop jump maneuver.

6.0 CONCLUSIONS AND FUTURE WORK

Instrumented soccer equipment was development (Chapter 2) and used to collect ankle joint kinematics in the laboratory and in the field. The instrumented equipment collected reliable and valid ankle joint kinematics in the sagittal plane during common sports medicine laboratory maneuvers and soccer-specific field maneuvers (Chapter 3). Drop landing and drop jump maneuvers resulted in poor to excellent reliability and very good to excellent validity. The stop jump maneuver resulted in poor to fair reliability and excellent validity. The reduced reliability measures are likely due to the changes in ankle landing strategy between trials and/or sessions.[75] The jump-stop cut maneuver resulted in poor to excellent reliability and very good validity. Soccer-specific field maneuvers resulted with poor to good reliability.

Few studies were available that assessed reliability and validity for inertial based motion analysis systems to measure ankle joint kinematics. Of the studies identified, none performed athletic maneuvers such as running, jumping, or landing. Furthermore, few reliability and validity studies using video-based motion analysis systems reported ankle joint kinematics. Injury prevention research has focused on knee and hip biomechanics and ankle biomechanics are rarely reported. As a distal joint to the knee, the ankle is an important link the kinetic chain. Akins et al.[75] found that the ankle landing strategy during the stop jump maneuver altered knee joint resultant forces. Individuals landing in plantar flexion had increased proximal tibia anterior

shear force, which is a direct loading mechanism of the anterior cruciate ligament.[107] Future research should measure and report ankle joint kinematics.

To the author's knowledge, this was the first human kinematic study to use the Sprague and Geers metric for validity. The main benefit of this metric is that magnitude and phase are quantified independently and then combined into a single score ($C_{S\&G}$). Based on the results of this study, $C_{S\&G}$ values less than 0.30 resulted in valid and accurate measures. More research using this metric as a validation tool for human motion analysis is needed, but appears promising.

The instrumented soccer equipment allowed ankle joint kinematics to be compared between laboratory and field maneuvers (Chapter 4). The results provided justification for selecting platform heights for drop landing and drop jump maneuvers, but not jump distances for stop jump and jump-stop cut maneuvers. Drop landing and drop jump maneuvers from a platform height of 60 cm elicited a similar response to the jump header field maneuver. A jump distance recommendation for the stop jump and jump-stop cut maneuvers was not warranted. Increased jump distance did not significantly alter landing biomechanics for the stop jump maneuver and slalom field data were not able to be processed.

Future research should investigate alternate sensor fusion algorithms to improve kinematic measurements. The gradient descent algorithm was selected for this study because it was developed specifically with the x-IMU device and performed better than a Kalman-based algorithm.[67] However, this algorithm did not perform well for the slalom maneuver. Improved algorithms may allow the instrumented equipment to collect real-time athlete data during competitive soccer matches and possibly record an actual injury event.

The instrumented equipment could be used in future studies as a field-friendly injury prevention tool. Joint kinematics could be collected in the field during pre-season athlete screenings. Biomechanical variables from the analysis could be used to prospectively identify risk factors of ankle injuries. Electromyography could also be incorporated to measure muscle activation patterns. The analog-in feature of the x-IMU's auxiliary port would allow activation patterns of four muscles to be measured. However, the maximum sampling frequency of the x-IMU is 512 Hz and a minimum of 800-1000 Hz is recommended for electromyography.[136]

APPENDIX A

CONFIRMATION OF FREQUENCY RESPONSE COMPUTATION

The frequency response of the MARG resulted in a typical first-order magnitude response and an atypical phase lead response. Due to atypical phase response, the frequency response computation was confirmed. White noise was used as the input signal and the output signal was created by filtering the input signal with a low-pass filter. The results of the computation were compared with the frequency response of the low-pass filter. The Matlab code used is provided below.

The input signal was defined as array of 10,000 samples of white noise generated using the randn Matlab function. A digital 1st order low-pass butterworth filter with a 10 Hz cut-off frequency was designed and used to filter the input signal. The filtered signal was defined as the output signal, both signals are plotted in Figure 31a. The frequency response computation was used to create the magnitude and phase responses (Figure 31b). The frequency response of the digital filter was also created using the freqz Matlab function and plotted with the calculated responses (Figure 31b). The resulting frequency responses were very similar, confirming the frequency response computation used in this study.

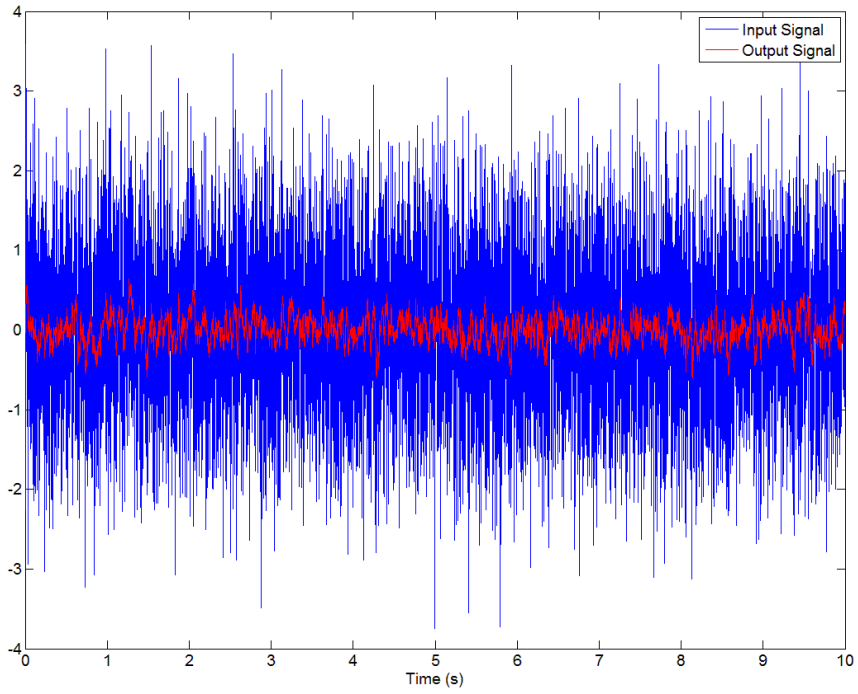

(a)

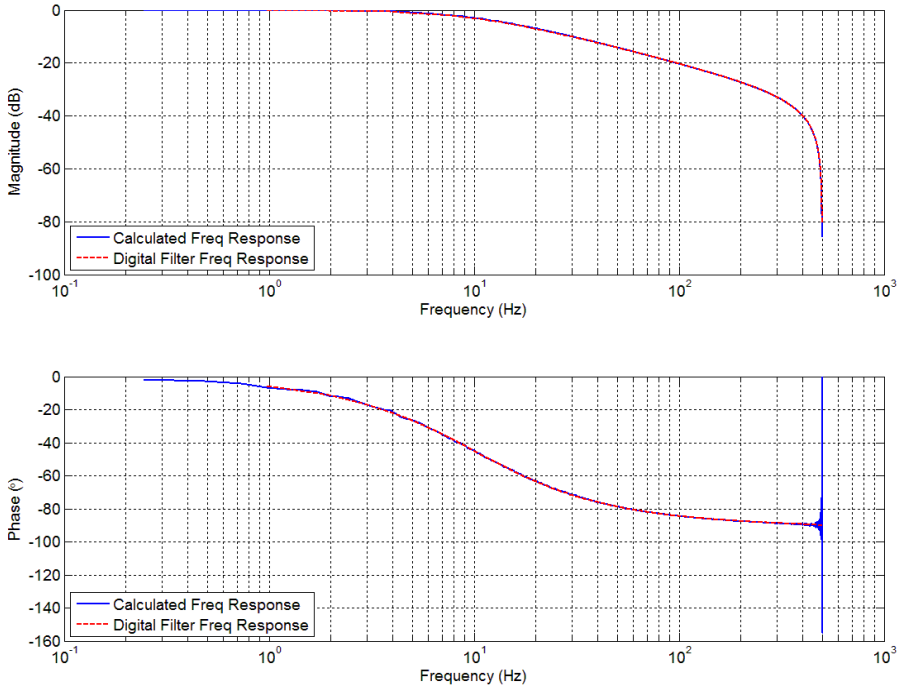

(b)

Figure 31. Confirmation of frequency response computation. (a) White noise input signal and filtered output signals (b) Calculated frequency response and digital filter frequency response

```
% Confirmation of the frequency response computation
% Jon Akins

clear;clc

Fs = 1000;            % Sampling frequency
wn = randn(10000,1);  % input signal

% Time
t = (0:1/Fs:(length(wn)-1)/Fs)';

% Filter input signal white noise data
Fc = 10;
[b,a] = butter(1, Fc/(Fs/2),'low');
wnFilt = filter(b,a,wn);  % output

% Freq response of filter
[H,W] = freqz(b,a,[],Fs);

% Plot of input and output signals
figure()
plot(t,wn); hold on
plot(t,wnFilt,'r')
legend('Input Signal','Output Signal')
xlabel('Time (s)','FontSize',14)
set(gca,'FontSize',14)

% Estimate transfer function using time series data
[EstH, EstF] = tfestimate(wn,wnFilt,[],[],[],Fs);

% Plot of frequency responses
figure()
subplot(2,1,1)
semilogx(EstF, 20*log10(abs(EstH)),'b-','LineWidth',2)
xlabel('Frequency (Hz)','FontSize',14)
ylabel('Magnitude (dB)','FontSize',14)
set(gca,'FontSize',14)
grid on; hold on
subplot(2,1,1); semilogx(W,20*log10(abs(H)),'r--','LineWidth',2);
legend('Calculated Freq Response','Digital Filter Freq Response',...
       'Location','SouthWest')

subplot(2,1,2)
semilogx(EstF, unwrap((angle(EstH)))*180/pi, 'b-','LineWidth',2)
xlabel('Frequency (Hz)','FontSize',14)
ylabel('Phase (\circ)','FontSize',14)
set(gca,'FontSize',14)
ylim([-100 100])
grid on; hold on
subplot(2,1,2); semilogx(W,unwrap((angle(H)))*180/pi,'r--','LineWidth',2);
legend('Calculated Freq Response','Digital Filter Freq Response',...
       'Location','SouthWest')
```

APPENDIX B

REPRESENTATIVE DATA FOR LABORATORY AND FIELD MANEUVERS

Representative data for laboratory and field maneuvers are shown in Figures 32 – 38. The black circles represent angles at initial contact, the magenta circles represent maximum angle during the landing phase, and the cyan circles represent minimum angles during the landing phase.

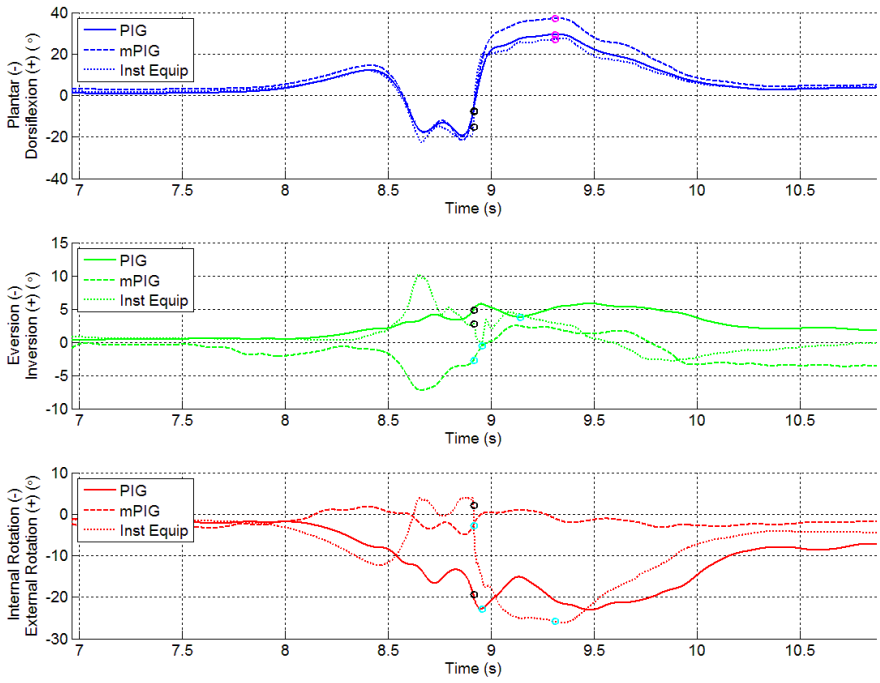

Figure 32. Representative drop landing data from the 40 cm platform

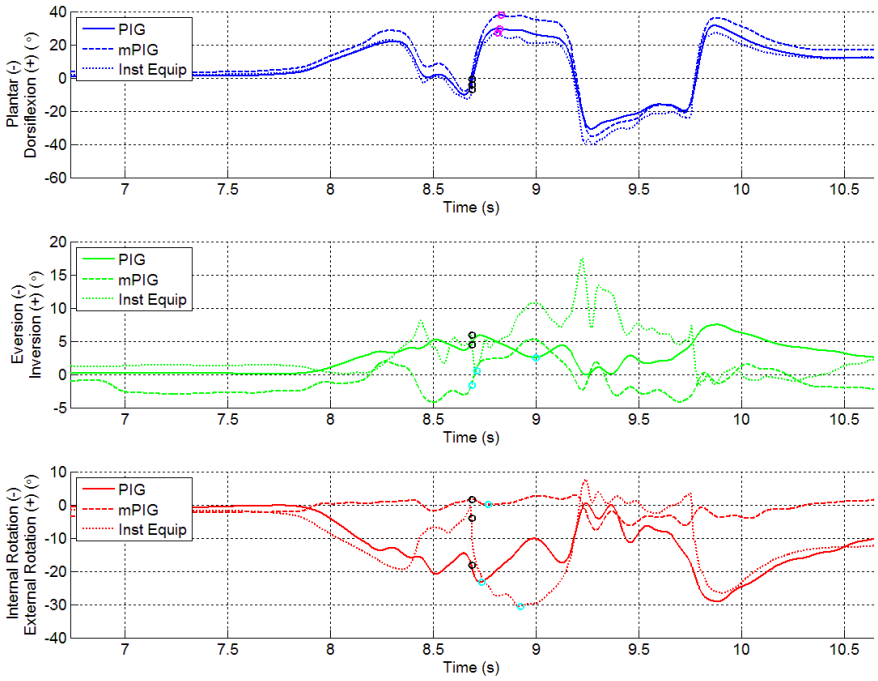

Figure 33. Representative drop jump data from the 40 cm platform

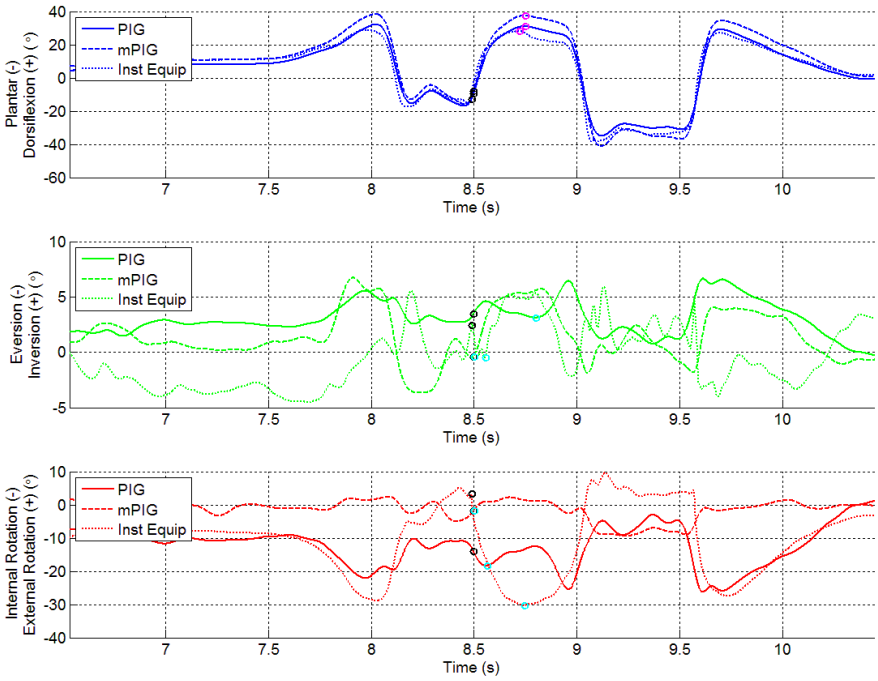

Figure 34. Representative stop jump data from 40% of the participant's height

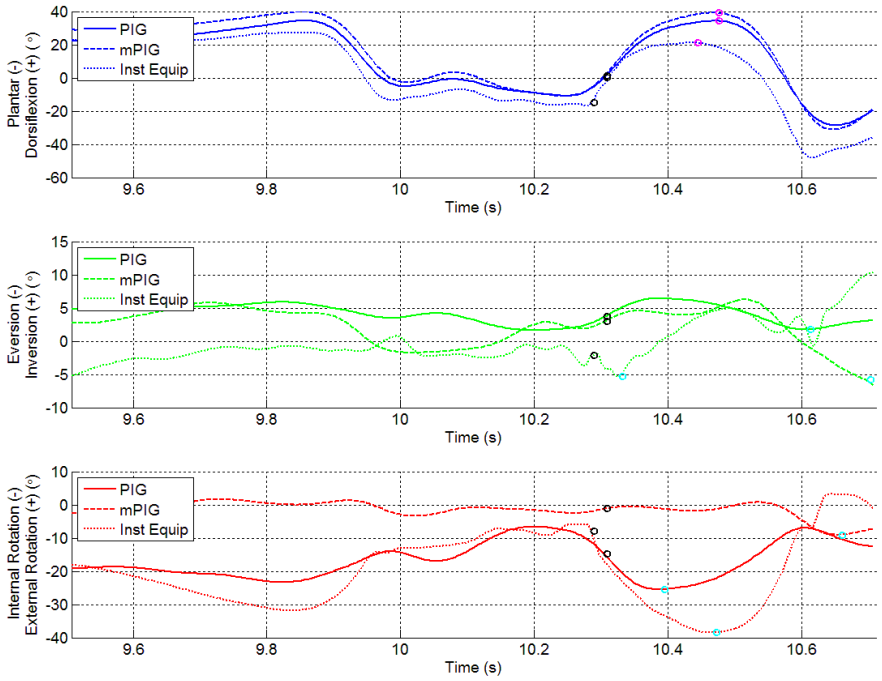

Figure 35. Representative jump-stop jump data from 40% of the participant's height

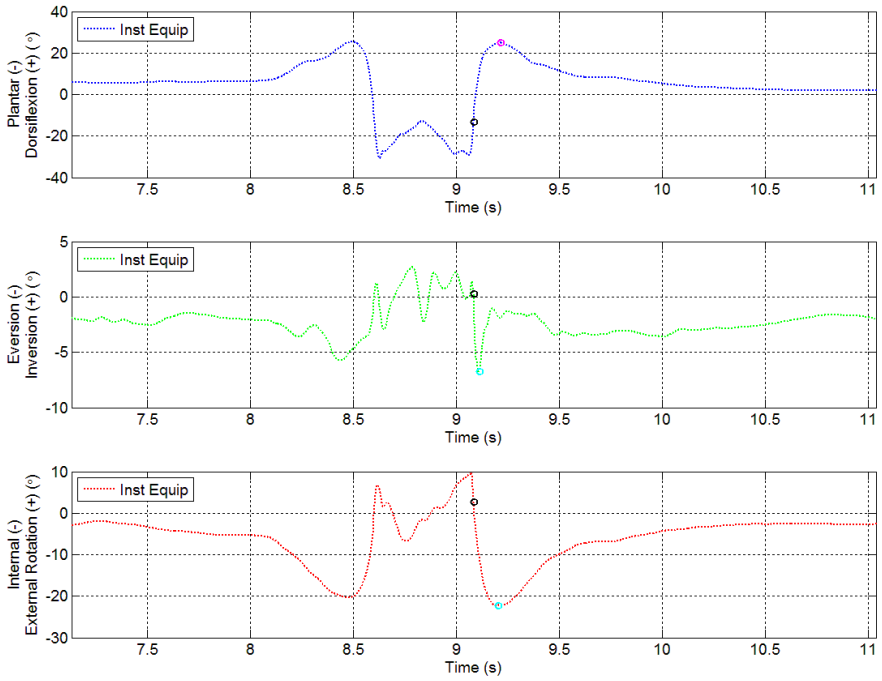

Figure 36. Representative jump header data

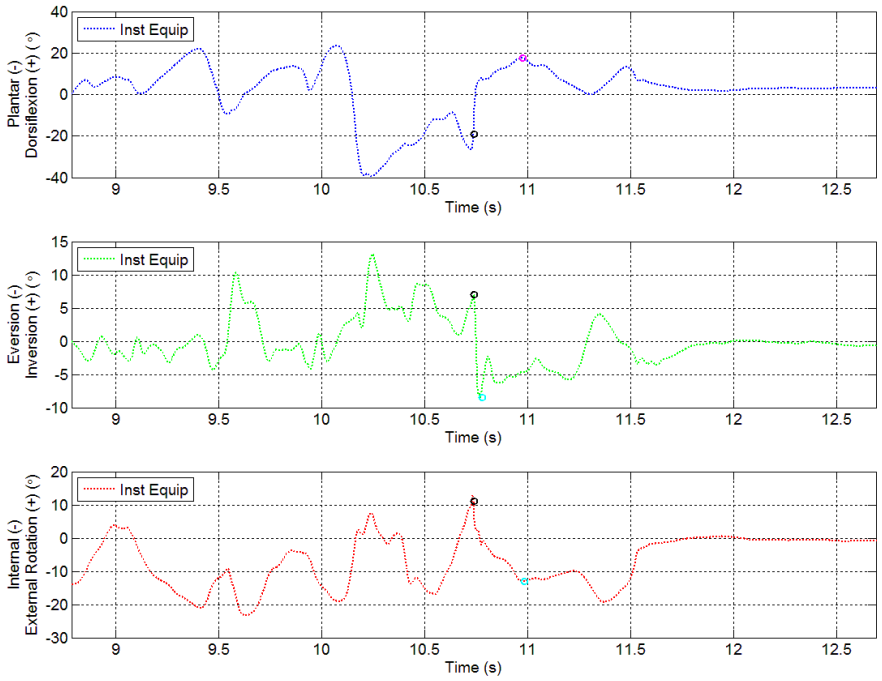

Figure 37. Representative moving header data

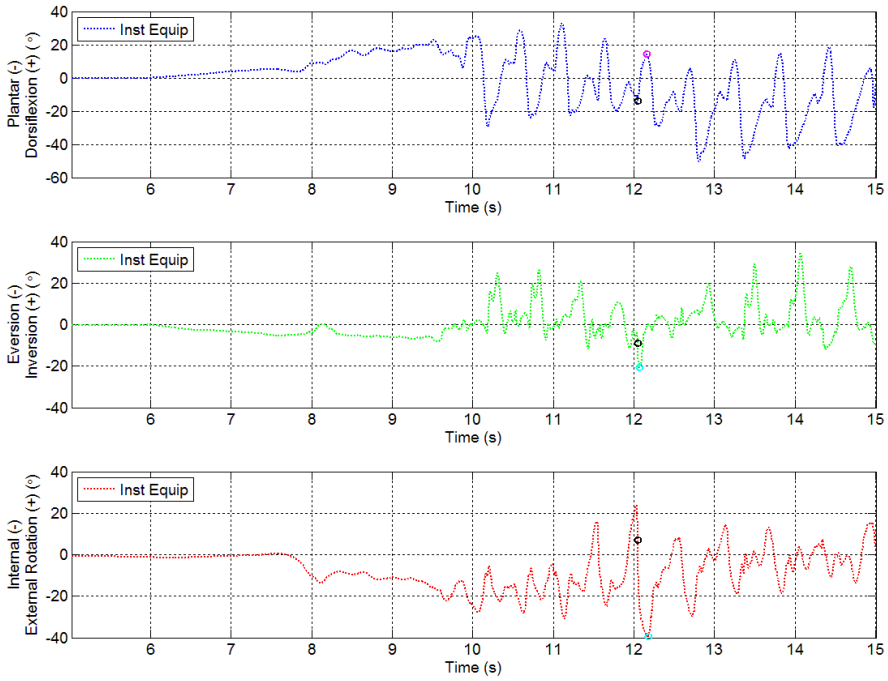

Figure 38. Representative slalom data

BIBLIOGRAPHY

1.Agel J, Evans T, Dick R, Putukian M, Marshall S. Descriptive epidemiology of collegiate men's soccer injuries: National Collegiate Athletic Association Injury Surveillance System, 1988-1989 through 2002-2003. J Athl Train. 2007;42(2):270-7.

2.Dick R, Putukian M, Agel J, Evans T, Marshall S. Descriptive epidemiology of collegiate women's soccer injuries: National Collegiate Athletic Association Injury Surveillance System, 1988-1989 through 2002-2003. J Athl Train. 2007;42(2):278-85.

3.Garrick JG. The frequency of injury, mechanism of injury, and epidemiology of ankle sprains. Am J Sports Med. 1977;5(6):241-2.

4.Mack R. Ankle injuries in athletics. Clin Sports Med. 1982;1(1):71-84.

5.Messina DF, Farney WC, DeLee JC. The incidence of injury in Texas high school basketball. Am J Sports Med. 1999;27(3):294-9.

6.Ekstrand J, Gillquist J. Soccer injuries and their mechanisms: a prospective study. Med Sci Sports Exerc. 1983;15(3):267-70.

7.Yeung M, Chan KM, So C, Yuan W. An epidemiological survey on ankle sprain. Br J Sports Med. 1994;28(2):112-6.

8.Gross MT. Effects of recurrent lateral ankle sprains on active and passive judgments of joint position. Phys Ther. 1987;67(10):1505-9.

9.Löfvenberg R, Kärrholm J, Sundelin G, Ahlgren O. Prolonged reaction time in patients with chronic lateral instability of the ankle. Am J Sports Med. 1995;23(4):414-7.

10.Ryan L. Mechanical stability, muscle strength and proprioception in the functionally unstable ankle. Aust J Physiother. 1994;40:41-7.

11.Hintermann B, Boss A, Schäfer D. Arthroscopic findings in patients with chronic ankle instability. Am J Sports Med. 2002;30(3):402-9.

12.Valderrabano V, Hintermann B, Horisberger M, Fung TS. Ligamentous posttraumatic ankle osteoarthritis. Am J Sports Med. 2006;34(4):612-20.

13.Hootman JM, Dick R, Agel J. Epidemiology of collegiate injuries for 15 sports: summary and recommendations for injury prevention initiatives. J Athl Train. 2007;42(2):311-9.

14.Brown CN, Padua D, Marshall SW, Guskiewicz K. Individuals with mechanical ankle instability exhibit different motion patterns than those with functional ankle instability and ankle sprain copers. Clin Biomech (Bristol, Avon). 2008;23(6):822-31.

15.Brown CN, Padua DA, Marshall SW, Guskiewicz KM. Variability of motion in individuals with mechanical or functional ankle instability during a stop jump maneuver. Clin Biomech (Bristol, Avon). 2009;24(9):762-8.

16.Caulfield BM, Garrett M. Functional instability of the ankle: differences in patterns of ankle and knee movement prior to and post landing in a single leg jump. Int J Sports Med. 2002;23(1):64-8.

17.Delahunt E, Monaghan K, Caulfield B. Ankle function during hopping in subjects with functional instability of the ankle joint. Scand J Med Sci Sports. 2007;17(6):641-8.

18.Drewes LK, McKeon PO, Paolini G, Riley P, Kerrigan DC, Ingersoll CD, et al. Altered ankle kinematics and shank-rear-foot coupling in those with chronic ankle instability. J Sport Rehabil. 2009;18(3):375-88.

19.Lin CF, Chen CY, Lin CW. Dynamic ankle control in athletes with ankle instability during sports maneuvers. Am J Sports Med. 2011;39(9):2007-15.

20.Monaghan K, Delahunt E, Caulfield B. Ankle function during gait in patients with chronic ankle instability compared to controls. Clin Biomech (Bristol, Avon). 2006;21(2):168-74.

21.Demeritt KM, Shultz SJ, Docherty CL, Gansneder BM, Perrin DH. Chronic ankle instability does not affect lower extremity functional performance. J Athl Train. 2002;37(4):507-11S.

22.Bertucci W, Grappe F, Groslambert A. Laboratory versus outdoor cycling conditions: differences in pedaling biomechanics. J Appl Biomech. 2007;23(2):87-92.

23.Jones AM, Doust JH. A 1% treadmill grade most accurately reflects the energetic cost of outdoor running. J Sports Sci. 1996;14:321-7.

24.Chan YY, Fong DTP, Chung MML, Li WJ, Liao WH, Yung PSH, et al. Identification of ankle sprain motion from common sporting activities by dorsal foot kinematics data. J Biomech. 2010;43(10):1965-9.

25.Kidder SM, Abuzzahab Jr F, Harris G, Johnson J. A system for the analysis of foot and ankle kinematics during gait. IEEE Trans Rehabil Eng. 1996;4(1):25-32.

26.Fong DTP, Hong Y, Shima Y, Krosshaug T, Yung PSH, Chan KM. Biomechanics of supination ankle sprain. Am J Sports Med. 2009;37(4):822-7.

27.Kristianslund E, Bahr R, Krosshaug T. Kinematics and kinetics of an accidental lateral ankle sprain. J Biomech. 2011;doi: 10.1016/j.biomech.2011.07.014.

28.Mok KM, Fong DTP, Krosshaug T, Engebretsen L, Hung ASL, Yung PSH, et al. Kinematics analysis of ankle inversion ligamentous sprain injuries in sports. Am J Sports Med. 2011;39(7):1548-52.

29.Cloete T, Scheffer C. Repeatability of an off-the-shelf, full body inertial motion capture system during clinical gait analysis. Conf Proc IEEE Eng Med Biol Soc; Buenos Aires, Argentina. 2010. p. 5125-8.

30.Mariani B, Hoskovec C, Rochat S, Büla C, Penders J, Aminian K. 3D gait assessment in young and elderly subjects using foot-worn inertial sensors. J Biomech. 2010;43(15):2999-3006.

31.Bergmann JH, Mayagoitia RE, Smith IC. A portable system for collecting anatomical joint angles during stair ascent: a comparison with an optical tracking device. Dynamic Medicine. 2009;8(1):3.

32.Cloete T, Scheffer C. Benchmarking of a full-body inertial motion capture system for clinical gait analysis. Conf Proc IEEE Eng Med Biol Soc; Vancouver, British Columbia, Canada. 2008. p. 4579-82.

33.Ferrari A, Cutti AG, Garofalo P, Raggi M, Heijboer M, Cappello A, et al. First in vivo assessment of "Outwalk": a novel protocol for clinical gait analysis based on inertial and magnetic sensors. Med Biol Eng Comput. 2010;48(1):1-15.

34.O'Donovan KJ, Kamnik R, O'Keeffe DT, Lyons GM. An inertial and magnetic sensor based technique for joint angle measurement. J Biomech. 2007;40(12):2604-11.

35.Picerno P, Cereatti A, Cappozzo A. Joint kinematics estimate using wearable inertial and magnetic sensing modules. Gait Posture. 2008;28(4):588-95.

36.Young D, D'Orey S, Opperman R, Hainley C, Newman D. Estimation of lower limb joint angles during walking using extended kalman filtering. IFMBE Proceedings; Singapore. 2010. p. 1319-22.

37.Cuesta-Vargas AI, Galan-Mercant A, Williams JM. The use of inertial sensors system for human motion analysis. Phys Ther Rev. 2010;15(6):462-73.

38.Fong DT, Chan YY. The use of wearable inertial motion sensors in human lower limb biomechanics studies: a systematic review. Sensors (Basel). 2010;10(12):11556-65.

39.Roetenberg D, Luinge H, Slycke P. Xsens MVN: Full 6DOF human motion tracking using miniature inertial sensors: Xsens Technologies; 2009 [cited 2011 September 15]. Available from: http://www.xsens.com/images/stories/PDF/MVN_white_paper.pdf.

40.Cutti AG, Ferrari A, Garofalo P, Raggi M, Cappello A. 'Outwalk': a protocol for clinical gait analysis based on inertial and magnetic sensors. Med Biol Eng Comput. 2010;48(1):17-25.

41.Elvin NG, Elvin AA, Arnoczky SP. Correlation between ground reaction force and tibial acceleration in vertical jumping. J Appl Biomech. 2007;23(3):180-9.

42.Elvin NG, Elvin AA, Arnoczky SP, Torry MR. The correlation of segment accelerations and impact forces with knee angle in jump landing. J Appl Biomech. 2007;23(3):203-12.

43.Tran J, Netto K, Aisbett B, Gastin P. Validation of accelerometer data for measuring impacts during jumping and landing tasks. 28th International Conference on Biomechanics in Sports; Konstanz, Germany. 2010. p. 1-4.

44.Winter DA. Biomechanics and motor control of human movement. 3rd ed. Hoboken, NJ: John Wiley & Sons Inc; 2005.

45.Garofalo P, Cutti AG, Filippi MV, Cavazza S, Ferrari A, Cappello A, et al. Inter-operator reliability and prediction bands of a novel protocol to measure the coordinated movements of shoulder-girdle and humerus in clinical settings. Med Biol Eng Comput. 2009;47(5):475-86.

46.Kadaba M, Ramakrishnan H, Wootten M, Gainey J, Gorton G, Cochran G. Repeatability of kinematic, kinetic, and electromyographic data in normal adult gait. J Orthop Res. 1989;7(6):849-60.

47.Yavuzer G, Oken O, Elhan A, Stam HJ. Repeatability of lower limb three-dimensional kinematics in patients with stroke. Gait Posture. 2008;27(1):31-5.

48.Cockcroft SJ. An evaluation of inertial motion capture technology for use in the analysis and optimization of road cycling kinematics [Thesis]: University of Stellenbosch; 2011.

49.Kwakkel S, Godha S, Lachapelle G. Foot and ankle kinematics during gait using foot mounted inertial system. ION NTM San Diego CA. 2007.

50.Decker MJ, Torry MR, Wyland DJ, Sterett WI, Richard Steadman J. Gender differences in lower extremity kinematics, kinetics and energy absorption during landing. Clin Biomech (Bristol, Avon). 2003;18(7):662-9.

51.Cortes N, Onate J, Abrantes J, Gagen L, Dowling E, Van Lunen B. Effects of gender and foot-landing techniques on lower extremity kinematics during drop-jump landings. J Appl Biomech. 2007;23(4):289-99.

52.Schot P, Dufek J. Landing performance, part I: kinematic, kinetic, and neuromuscular aspects. Med Exerc Nutr Health. 1993;2:69-83.

53.De Vries W, Veeger H, Baten C, Van Der Helm F. Magnetic distortion in motion labs, implications for validating inertial magnetic sensors. Gait Posture. 2009;29(4):535-41.

54.Innovative Sports Training I. The MotionMonitor Software User's Guide. 2006.

55.Goodvin C, Park EJ, Huang K, Sakaki K. Development of a real-time three-dimensional spinal motion measurement system for clinical practice. Med Biol Eng Comput. 2006;44(12):1061-75.

56.Neter J, Wasserman W, Kutner M. Applied linear statistical models: regression, analysis or variance, and experimental designs. 2nd ed. Homewood, IL: Irwin; 1985.

57.Winer BJ, Brown DR, Michels KM. Statistical principles in experimental design. 2nd ed. New York: McGraw-Hill; 1971.

58.Portney LG, Watkins MP. Foundations of clinical research: Applications to practice. Upper Saddle River, NJ: Prentice Hall; 2000.

59.Shrout PE, Fleiss JL. Intraclass correlations: uses in assessing rater reliability. Psychol Bull. 1979;86(2):420-8.

60.Geers T. An objective error measure for the comparison of calculated and measured transient response histories. Shock and Vibration Information Center The Shock and Vibration Bull 54, Pt 2 p 99-108(SEE N 85-18388 09-39). 1984.

61.Faul F, Erdfelder E, Lang AG, Buchner A. G* Power 3: A flexible statistical power analysis program for the social, behavioral, and biomedical sciences. Behav Res Methods. 2007;39(2):175-91.

62.Butler RJ, Willson JD, Fowler D, Queen RM. Gender Differences in Landing Mechanics Vary Depending on the Type of Landing. Clin J Sport Med. 2013;23(1):52-7.

63.eHowSports. Soccer Tips: Heading Drills for Soccer 2010 [cited 2011 December, 11]. Available from: http://www.youtube.com/watch?v=QK19XTJuDvY.

64.Eils E, Streyl M, Linnenbecker S, Thorwesten L, Volker K, Rosenbaum D. Characteristic plantar pressure distribution patterns during soccer-specific movements. Am J Sports Med. 2004;32(1):140-5.

65.Vicon Motion Systems. Plug-In Gait Model Details. Centennial, CO: Vicon Motion Systems; 2012.

66.Brown RG, Hwang PYC. Introduction to random signals and applied Kalman filtering: John Wiley & Sons; 1997.

67.Madgwick SOH, Harrison AJL, Vaidyanathan R, editors. Estimation of IMU and MARG orientation using a gradient descent algorithm. IEEE International Conference on Rehabilitation Robotics; 2011; Zurich, Switzerland.

68.Jasiewicz JM, Allum JHJ, Middleton JW, Barriskill A, Condie P, Purcell B, et al. Gait event detection using linear accelerometers or angular velocity transducers in able-bodied and spinal-cord injured individuals. Gait Posture. 2006;24(4):502-9.

69.Hreljac A, Marshall RN. Algorithms to determine event timing during normal walking using kinematic data. J Biomech. 2000;33(6):783-6.

70.Hreljac A, Stergiou N. Phase determination during normal running using kinematic data. Med Biol Eng Comput. 2000;38(5):503-6.

71.Geers TL. An objective error measure for the comparison of calculated and measured transient response histories. Shock and Vibration Information Center The Shock and Vibration Bull 54, Pt 2 p 99-108(SEE N 85-18388 09-39). 1984.

72.Schwer LE. Validation metrics for response histories: perspectives and case studies. Engineering with Computers. 2007;23(4):295-309.

73.Fleiss JL. Design and analysis of clinical experiments. New York, NY: Wiley; 1985.

74.Ford KR, Shapiro R, Myer GD, van den Bogert AJ, Hewett TE. Longitudinal sex differences during landing in knee abduction in young athletes. Med Biol Eng Comput. 2010;42(10):1923-31.

75.Akins JS, McGinn MA, Heebner NR, Sell TC, Lephart SM, editors. Ankle landing strategy during a vertical stop-jump maneuver alters knee joint resultant forces (abstract). American Society of Biomechanics Annual Meeting; 2013; Omaha, NE.

76.Skog I, Handel P, Nilsson J-O, Rantakokko J. Zero-velocity detection—An algorithm evaluation. IEEE Trans Biomed Eng. 2010;57(11):2657-66.

77.Porter RS, Sharp M. The Merck Manual: For Health Care Professionals: Merck Research Laboratories; 2006.

78.Woods C, Hawkins R, Hulse M, Hodson A. The football association medical research programme: an audit of injuries in professional football: an analysis of ankle sprains. Br J Sports Med. 2003;37(3):233-8.

79.Arnason A, Gudmundsson A, Dahl H, Johannsson E. Soccer injuries in Iceland. Scand J Med Sci Sports. 1996;6(1):40-5.

80.Cloke DJ, Spencer S, Hodson A, Deehan D. The epidemiology of ankle injuries occurring in English Football Association academies. Br J Sports Med. 2009;43(14):1119-25.

81.Fousekis K, Tsepis E, Vagenas G. Intrinsic Risk Factors of Noncontact Ankle Sprains in Soccer A Prospective Study on 100 Professional Players. Am J Sports Med. 2012;40(8):1842-50.

82.Kernozek TW, Torry MR, Van Hoof H, Cowley H, Tanner S. Gender differences in frontal and sagittal plane biomechanics during drop landings. Med Sci Sports Exerc. 2005;37(6):1003-12.

83.Lephart SM, Ferris CM, Riemann BL, Myers JB, Fu FH. Gender differences in strength and lower extremity kinematics during landing. Clin Orthop Relat Res. 2002;401:162-9.

84.Chappell JD, Limpisvasti O. Effect of a neuromuscular training program on the kinetics and kinematics of jumping tasks. Am J Sports Med. 2008;36(6):1081-6.

85.Hewett TE, Myer GD, Ford KR, Heidt RS, Colosimo AJ, McLean SG, et al. Biomechanical measures of neuromuscular control and valgus loading of the knee predict anterior cruciate ligament injury risk in female athletes. Am J Sports Med. 2005;33(4):492-501.

86.McLean SG, Felin RE, Suedekum N, Calabrese G, Passerallo A, Joy S. Impact of fatigue on gender-based high-risk landing strategies. Med Sci Sports Exerc. 2007;39(3):502-14.

87.Chappell JD, Yu B, Kirkendall DT, Garrett WE. A comparison of knee kinetics between male and female recreational athletes in stop-jump tasks. Am J Sports Med. 2002;30(2):261-7.

88.Sell TC, Ferris CM, Abt JP, Tsai YS, Myers JB, Fu FH, et al. The effect of direction and reaction on the neuromuscular and biomechanical characteristics of the knee during tasks that simulate the noncontact anterior cruciate ligament injury mechanism. Am J Sports Med. 2006;34(1):43-54.

89.Yu B, Lin CF, Garrett WE. Lower extremity biomechanics during the landing of a stop-jump task. Clin Biomech (Bristol, Avon). 2006;21(3):297-305.

90.Ford KR, Myer GD, Toms HE, Hewett TE. Gender differences in the kinematics of unanticipated cutting in young athletes. Med Sci Sports Exerc. 2005;37(1):124-9.

91.McLean SG, Huang X, Su A, van den Bogert AJ. Sagittal plane biomechanics cannot injure the ACL during sidestep cutting. Clin Biomech (Bristol, Avon). 2004;19(8):828-38.

92.Sigward SM, Pollard CD, Havens KL, Powers CM. Influence of Sex and Maturation on Knee Mechanics during Side-Step Cutting. Med Sci Sports Exerc. 2012;44(8):1497-503.

93.Boden BP, Dean GS, Feagin J, Garrett W. Mechanisms of anterior cruciate ligament injury. Orthopedics. 2000;23(6):573-8.

94.Olsen O-E, Myklebust G, Engebretsen L, Bahr R. Injury mechanisms for anterior cruciate ligament injuries in team handball a systematic video analysis. Am J Sports Med. 2004;32(4):1002-12.

95.Blackburn JT, Padua DA. Influence of trunk flexion on hip and knee joint kinematics during a controlled drop landing. Clin Biomech (Bristol, Avon). 2008;23(3):313-9.

96.Huston LJ, Vibert B, Ashton-Miller JA, Wojtys EM. Gender differences in knee angle when landing from a drop-jump. Am J Knee Surg. 2001;14(4):215-20.

97.Santello M, McDonagh MJN, Challis JH. Visual and non-visual control of landing movements in humans. J Physiol. 2001;537(1):313-27.

98.Sell TC, Chu Y, Abt JP, Nagai T, Deluzio J, McGrail MA, et al. Minimal additional weight of combat equipment alters air assault soldiers landing biomechanics. Mil Med. 2010;175(1):41-7.

99.Dowling AV, Favre J, Andriacchi TP. A wearable system to assess risk for anterior cruciate ligament injury during jump landing: measurements of temporal events, jump height, and sagittal plane kinematics. J Biomech Eng. 2011;133(7):071008-1-7.

100.Moran A, Marshall BM. Effect of fatigue on tibial impact accelerations and knee kinematics in drop jumps. Med Sci Sports Exerc. 2006;38(10):1836-42.

101.Moran KA, Clarke M, Reilly F, Wallace ES, Brabazon D, Marshall B. Does endurance fatigue increase the risk of injury when performing drop jumps? J Strength Cond Res. 2009;23(5):1448-55.

102.Shultz SJ, Nguyen AD, Leonard MD, Schmitz RJ. Thigh strength and activation as predictors of knee biomechanics during a drop jump task. Med Sci Sports Exerc. 2009;41(4):857-66.

103.Yu B, Herman D, Preston J, Lu W, Kirkendall DT, Garrett WE. Immediate effects of a knee brace with a constraint to knee extension on knee kinematics and ground reaction forces in a stop-jump task. Am J Sports Med. 2004;32(5):1136-43.

104.Chappell JD, Herman DC, Knight BS, Kirkendall DT, Garrett WE, Yu B. Effect of fatigue on knee kinetics and kinematics in stop-jump tasks. Am J Sports Med. 2005;33(7):1022-9.

105.Yu B, McClure SB, Onate JA, Guskiewicz KM, Kirkendall DT, Garrett WE. Age and gender effects on lower extremity kinematics of youth soccer players in a stop-jump task. Am J Sports Med. 2005;33(9):1356-64.

106.Chappell JD, Creighton RA, Giuliani C, Yu B, Garrett WE. Kinematics and electromyography of landing preparation in vertical stop-jump. Am J Sports Med. 2007;35(2):235-41.

107.Sell TC, Ferris CM, Abt JP, Tsai YS, Myers JB, Fu FH, et al. Predictors of proximal tibia anterior shear force during a vertical stop-jump. J Orthop Res. 2007;25(12):1589-97.

108.Herman DC, Weinhold PS, Guskiewicz KM, Garrett WE, Yu B, Padua DA. The effects of strength training on the lower extremity biomechanics of female recreational athletes during a stop-jump task. Am J Sports Med. 2008;36(4):733-40.

109.Wang LI. The lower extremity biomechanics of single-and double-leg stop-jump tasks. J Sports Sci Med. 2011;10:151-6.

110.Besier TF, Lloyd DG, Cochrane JL, Ackland TR. External loading of the knee joint during running and cutting maneuvers. Med Sci Sports Exerc. 2001;33(7):1168-75.

111.Cross MJ, Gibbs NJ, Bryant GJ. An analysis of the sidestep cutting manoeuvre. Am J Sports Med. 1989;17(3):363-6.

112.McLean SG, Neal RJ, Myers PT, Walters MR. Knee joint kinematics during the sidestep cutting maneuver: potential for injury in women. Med Sci Sports Exerc. 1999;31(7):959-68.

113.Colby S, Francisco A, Yu B, Kirkendall D, Finch M, Garrett W. Electromyographic and kinematic analysis of cutting maneuvers. Am J Sports Med. 2000;28(2):234-40.

114.Simonsen EB, Magnusson S, Bencke J, Naesborg H, Havkrog M, Ebstrup J, et al. Can the hamstring muscles protect the anterior cruciate ligament during a side-cutting maneuver? Scand J Med Sci Sports. 2000;10(2):78-84.

115.Besier TF, Lloyd DG, Ackland TR, Cochrane JL. Anticipatory effects on knee joint loading during running and cutting maneuvers. Med Sci Sports Exerc. 2001;33(7):1176-81.

116.Besier TF, Llyod DG, Ackland TR. Muscle activation strategies at the knee during running and cutting maneuvers. Med Sci Sports Exerc. 2003;35(1):119-27.

117.McLean SG, Lipfert SW, Van Den Bogert AJ. Effect of gender and defensive opponent on the biomechanics of sidestep cutting. Med Sci Sports Exerc. 2004;36(6):1008-16.

118.Pollard CD, Davis IMC, Hamill J. Influence of gender on hip and knee mechanics during a randomly cued cutting maneuver. Clin Biomech (Bristol, Avon). 2004;19(10):1022-31.

119.McLean SG, Huang X, van den Bogert AJ. Association between lower extremity posture at contact and peak knee valgus moment during sidestepping: implications for ACL injury. Clin Biomech (Bristol, Avon). 2005;20(8):863-70.

120.Dayakidis MK, Boudolos K. Ground reaction force data in functional ankle instability during two cutting movements. Clin Biomech (Bristol, Avon). 2006;21(4):405-11.

121.Sigward SM, Powers CM. The influence of gender on knee kinematics, kinetics and muscle activation patterns during side-step cutting. Clin Biomech (Bristol, Avon). 2006;21(1):41-8.

122.Pollard CD, Sigward SM, Powers CM. Gender differences in hip joint kinematics and kinetics during side-step cutting maneuver. Clin J Sport Med. 2007;17(1):38-42.

123.Beaulieu ML, Lamontagne M, Xu L. Gender differences in time-frequency EMG analysis of unanticipated cutting maneuvers. Med Sci Sports Exerc. 2008;40(10):1795-804.

124.Hanson AM, Padua DA, Blackburn JT, Prentice WE, Hirth CJ. Muscle activation during side-step cutting maneuvers in male and female soccer athletes. J Athl Train. 2008;43(2):133-43.

125.Dowling AV, Corazza S, Chaudhari AM, Andriacchi TP. Shoe-Surface Friction Influences Movement Strategies During a Sidestep Cutting Task Implications for Anterior Cruciate Ligament Injury Risk. Am J Sports Med. 2010;38(3):478-85.

126.Fedie R, Carlstedt K, Willson JD, Kernozek TW. Effect of attending to a ball during a side-cut maneuver on lower extremity biomechanics in male and female athletes. Sports Biomech. 2010;9(3):165-77.

127.DiStefano LJ, Blackburn JT, Marshall SW, Guskiewicz KM, Garrett WE, Padua DA. Effects of an age-specific anterior cruciate ligament injury prevention program on lower extremity biomechanics in children. Am J Sports Med. 2011;39(5):949-57.

128.Kristianslund E, Faul O, Bahr R, Myklebust G, Krosshaug T. Sidestep cutting technique and knee abduction loading: implications for ACL prevention exercises. Br J Sports Med. 2012. Epub 20 December 2012.

129.Miranda DL, Fadale PD, Hulstyn MJ, Shalvoy RM, Machan JT, Fleming BC. Knee Biomechanics during a Jump-Cut Maneuver: Effects of Gender and ACL Surgery. Med Sci Sports Exerc. 2013;45(5):942-51.

130.Stearns KM, Pollard CD. Abnormal Frontal Plane Knee Mechanics During Sidestep Cutting in Female Soccer Athletes After Anterior Cruciate Ligament Reconstruction and Return to Sport. Am J Sports Med. 2013. Epub February 20.

131.Webster KE, Kinmont CJ, Payne R, Feller JA. Biomechanical differences in landing with and without shoe wear after anterior cruciate ligament reconstruction. Clinical Biomechanics. 2004;19(9):978-81.

132.Fong Yan A, Sinclair PJ, Hiller C, Wegener C, Smith RM. Impact attenuation during weight bearing activities in barefoot vs. shod conditions: A systematic review. Gait Posture. 2012. Epub 11 December 2012.

133.Sell TC, Akins JS, A.R. O, Lephart SM. Relationship between tibial acceleration and proximal anterior tibia shear force across increasing jump distance (in review). J Appl Biomech. 2013.

134.Leardini A, Chiari L, Della Croce U, Cappozzo A. Human movement analysis using stereophotogrammetry. Part 3. Soft tissue artifact assessment and compensation. Gait Posture. 2005;21(2):212-25.

135.Lucchetti L, Cappozzo A, Cappello A, Croce UD. Skin movement artefact assessment and compensation in the estimation of knee-joint kinematics. J Biomech. 1998;31(11):977-84.

136.Merletti R. Standards for reporting EMG data. J Electromyogr Kinesiol. 1999;9(1):III-IV.